Effects of Defects Made by Automated Fibre Placement Process on Carbon/Epoxy Composite Structures.

Vincent Cadran

A thesis submitted in partial satisfaction of the requirements for the degree of

Master of Engineering.

Department of Mechanical Engineering

McGill University

July 30th, 2019

« The McGill Structures and Composite Materials Laboratory explores the design of composite materials and their structures "From Start to Finish". Design optimization helps to achieve the final goal: a successfully designed composite structure. »

Professor Larry LESSARD

McGill

"Stay Hungry, Stay Foolish."

Steve Jobs.

To my mom, dad, and brother,

ABSTRACT

Manufacturers use Automated Fibre Placement (AFP) as a fabrication process for large and complex composite parts. An AFP machine consists of a computer-controlled robotic arm with a head at the end capable of constant placement of uncured pre-impregnated carbon fibres grouped together to form bands called tows. AFP shows great potential to transition from hand layup to an automated technique [1, 2] with a lot of flexibility in terms of fibres orientation, stacking sequence, thickness and allows fibres to be used in double curvature regions. Fibre path scheme is dictated by both part geometry and steering capability to ensure good quality parts. There is a joint effort from engineers of different fields – design, manufacturing, stress – to govern the AFP process, but this method also creates defects which undermine the structural performance of the part [3, 4]. Primary defects observed by the aerospace industry are mis-aligned tows also referred as steered tows: combinations of both side-to-side gaps and overlaps.

Corresponding detection methods are labor intensive and time consuming [5]. Proposed in this Thesis is an investigation on the effects of steered tows defects on the mechanical performance of composite structures made with AFP techniques. By varying the orientation, size and number of steered tows defects embedded in carbon-epoxy laminates, their mechanical effects have been examined experimentally in static tension, static compression and cyclic fatigue, and also numerically via Finite-Element Model (FEM) for both static tension and compression. Certification of composite structures remains a challenge because this material is difficult to repair and its performance is difficult to predict.

Locally, gaps reduce axial stiffness of laminates without much effect on the global stiffness. Gap density has a linear effect on laminate stiffness while orientation and location have a non-linear effect on laminate stiffness [6]. Overlaps induce waviness on adjacent plies – extra material due to shifted tows – which does not have significant changes on stiffness [7, 8]. Overlaps can locally improve strength of laminates. Combinations of both side-to-side gaps

and overlaps show strong out-of-plane waviness influence, making laminate strength prediction much more difficult to assess. In this thesis is used microscopic observations of cured specimens to study the post-cure, post-compaction real geometry of embedded defects and to qualitatively assess the effects of through-the-thickness waviness on the mechanical performance of defects.

Side-to-side half gap / half overlap defects are embedded in laminate structures and tested. Compression is found to be much more critical than tension. Defects embedded at 45° and 90° behave similarly, they have the largest knockdown factors. From a microscopic analysis, the real post-cure defect geometry is used in a Finite-Element (FE) model on Abaqus Software to predict the performance of specimens with defects in both static tension and compression. This ply-by-ply FE model assumes that the defects have only an effect on the plies in which they are embedded in the first place while the other plies stay intact. The comparison between experimental results and simulations shows that the FE Model is too conservative when defects are oriented in 0° along the length of the specimens and not conservative when defects are oriented in 45° and 90°. This suggests the assumption was wrong and that the plies without embedded defects also suffer damage from out-of-plane waviness.

ABRÉGÉ

Les industriels utilisent le placement de fibres automatisé (abrégé AFP pour « Automated Fibre Placement ») comme moyen de production de pièces de grandes dimensions à géométries complexes en matériaux composites. Une machine AFP consiste en un bras articulé robotisé contrôlé par ordinateur qui est capable de régulièrement déposer des bandes de fibres de carbone pré-imprégnées d'époxy. Un groupe élémentaire de fibres est appelé un « tow ». Les techniques AFP ont un grand potentiel pour assurer la transition du placement manuel de fibres vers des techniques automatisées [1, 2]. La qualité de la pièce finie fabriquée en composites dépend grandement du chemin suivi lors du placement de fibres sur un moule. Ce chemin est dicté à la fois par des contraintes géométriques et les capacités de direction/rotation du robot. Des ingénieurs de différents domaines – design, calculs structurels et production – mettent leurs efforts en commun pour contrôler les techniques AFP. Cependant, ces méthodes de production induisent des défauts qui peuvent avoir des effets sur les performances mécaniques d'une pièce en composites [3, 4]. Les défauts les plus couramment rencontrés sont issus de mauvais alignement des fibres aussi appelé « tow steering »: combinaison de gaps et overlaps côte à côte.

Les méthodes de détection des défauts sont couteuses en temps et en argent [5]. Cette thèse se propose d'investiguer les effets des défauts de type « tow steering » sur les performances mécaniques de pièces composites fabriquées avec les techniques AFP. En faisant varier l'orientation, la taille et le nombre de défauts introduits dans des coupons, les effets mécaniques sont étudiés expérimentalement en tension statique, compression statique et en fatigue – cycles de tension/compression – ainsi que numériquement au travers de simulations en éléments finis pour les tests en tension statique et compression statique. La certification de structures en matériaux composites constitue un défi car ces matériaux sont difficiles à réparer et leurs performances sont difficiles à prédire.

Localement, les gaps réduisent la rigidité du laminé du fait de l'absence de fibres sans pour autant changer la rigidité moyenne globale. La densité de gaps a un effet linéaire sur la rigidité des laminés alors que leur orientation et localisation ont des effets non linéaires [6]. Les overlaps induisent des ondulations des plis adjacents dues à la présence de surplus de matériau. Ces ondulations n'ont pas d'influences importantes sur la rigidité mais davantage sur la résistance aux efforts [7, 8]. La combinaison de gaps et overlaps côte à côte introduit des ondulations hors plans importantes rendant la prédiction de performances mécaniques des laminés encore plus difficile.

Des défauts de type « tow steering » c'est à dire des gaps et overlaps côte à côte sont introduits dans des laminés et testés. La résistance à la compression a été trouvée beaucoup plus critique que la résistance à la tension. Les défauts à 45° et 90° de la direction de chargement ont des comportements similaires et leurs facteurs de réduction sont les plus grands. À partir d'une analyse microscopique, la géométrie réelle des gaps et overlaps est modélisée en éléments finis sur le logiciel commercial Abaqus. Ce modèle est sensé prédire les performances mécaniques de laminés avec défauts en tension statique et compression statique. La modélisation pli par pli est basée sur l'hypothèse que les défauts ont seulement un effet sur les plis dans lesquels ils ont été introduits lors de la production alors que les autres plis restent intacts. La comparaison entre les données expérimentales et les résultats de simulations montrent que le modèle est trop conservatif quand les défauts sont orientés à 0° et pas conservatif quand les plis sont à 45° et 90°. Cela signifie que l'hypothèse n'est pas correcte et que les plis fabriqués sans défauts sont affectés par les gaps et overlaps.

ACKNOWLEDGEMENTS

First and foremost, I would like to thank my Master supervisor Professor Larry Lessard for his mentorship and vast invaluable expertise from which I have learned how to become a better engineer. I will forever be grateful to Professor Lessard who made my dream Canadian adventure come true in a world-renowned university, changing my life for the better. I value beyond just academics this relationship built on trust and hard work. I cannot be more grateful to my parents and brother for their love and support at all times during these years far from home. I would not have made it this far without their encouragement in every step of my life.

Second, I would like to express my great appreciation to the members of the excellent Structures and Composite Materials Laboratory. I would especially like to acknowledge the feedback and rich scientific advice from Nicolas Krumenacker, Swaroop Visweswaraiah and Valentin Romanov, as well as Daniel Del Rossi who initiated this Thesis research project, with whom I became close friends. Thanks to Matteo Putt and Pranshul Thakur for their hard work.

Third, I wish to acknowledge Bell Helicopter for their financial support and their guidance at every step of the project. Notably, Maxime Lapalme, Pier-Alexandre Pelletier and Sébastien Duval who helped to make these ideas come to fruition. I wish to thank the National Research Council Canada and especially Marc Palardy-Sim for the recommendation and the access to the equipment. Sincere thanks to Polytechnique Montréal, notably Professor Martin Lévesque, Isabelle Nowlan and Kambiz Chizari whose help on the mechanical testing was vital. Thanks to Lingyu Yue for his technical skills on the use of Digital Image Correlation systems.

Finally, I am forever grateful for the amazing people I had the chance to meet in Montréal, for the life-long friendships who contributed to this journey and beyond, and especially for my girlfriend Catherine and her treasured love during the last intense moments of my Masters.

DECLARATION OF AUTHORSHIP

The research presented in this Thesis and its write-up is entirely the work of the Author with the only exceptions being the following experimental activities.

The Author and Daniel Del Rossi [4], a former Master student at McGill University, built the experimental test plan together, presented in section § 3. Test plan . Manufacturing presented in section § 4.1 Manufacturing was done at National Research Council (NRC) Canada facilities by Daniel Del Rossi with the help of Matteo Putt, an undergraduate student doing an internship during the summer of 2018. Daniel and Matteo went to the facilities and worked with the technicians in every step of the manufacturing. This was a paid contract to NRC.

§ 7.1 Tensile Tests were done with the help of Daniel Del Rossi [4]. The Author performed all compression and fatigue testing by himself. Tests were done at Polytechnique Montréal. This was a paid contract to the laboratory of mechanical engineering under the supervision of Professor Martin Lévesque, with the help of Isabelle Nowlan, lab manager, and Kambiz Chizari, lab technician.

The Author emphasizes that the Finite-Element model presented in this Thesis section § 6 Modelling and the following § 7 Results and discussion have completely been developed independently to the work presented by Daniel in [4].

All pictures present in this Thesis have been taken by the Author with the exception of those Figures with the legend referencing Daniel's Thesis [4].

Financial support was given by the National Science and Engineering Research Council of Canada and by Bell Helicopter. Maxime Lapalme and Pier-Alexandre from Bell Helicopter were supervising and guiding the progress of the project.

Bell Helicopter

“

Bell Helicopter is an industry-leading producer of commercial and military, manned and unmanned vertical-lift aircraft and the pioneer of the revolutionary tiltrotor aircraft. Among other projects, Bell is exploring new opportunities in the future of air transportation with electric and hybrid VTOL aircraft.

”

Bell [9]

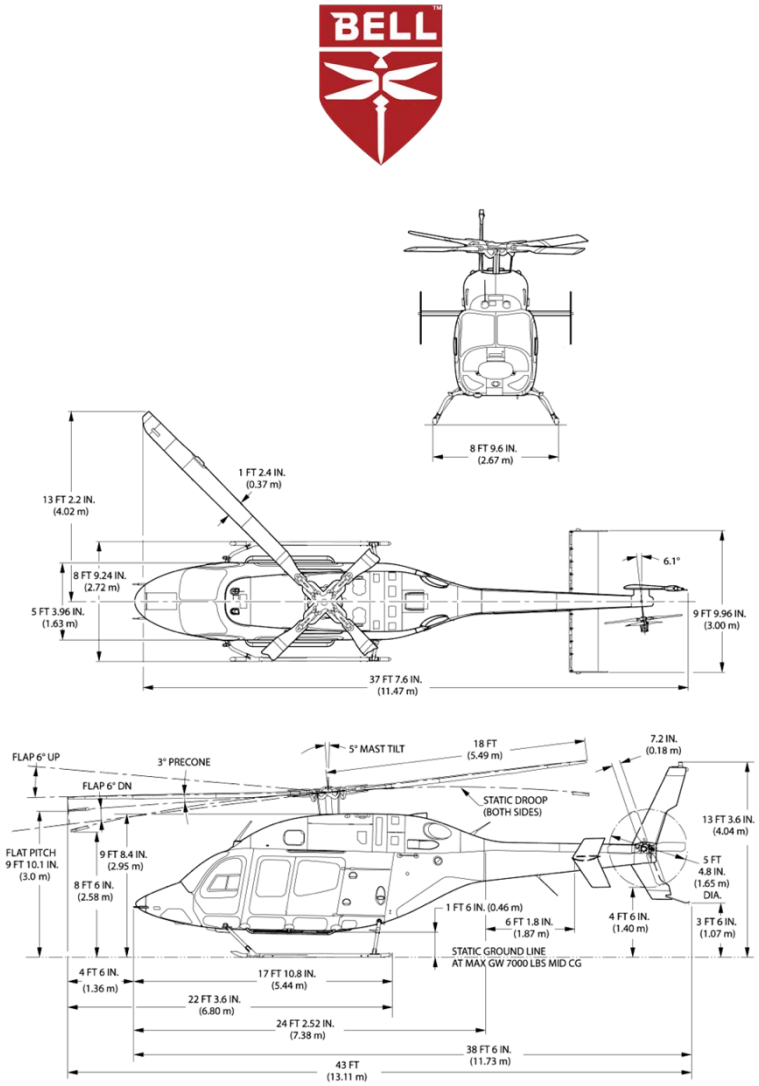

Figure 1 Bell 429 - 27% made of composite materials[1]

[1] https://drawingdatabase.com/bell-429-globalranger/

TABLE OF CONTENT

FIGURES

TABLES

EQUATIONS

1. INTRODUCTION

1.1. Composite Materials

The past few decades have seen outstanding advances in the development of composite materials and their structural applications. Composite materials are making their way into several aspects of our society. Companies from a wide range of industries show great interest in adapting their techniques to integrate composite materials in their products. Because they are hybrid heterogeneous materials, they can be difficult to characterize. Aircraft manufacturers have already made a lot of effort to increase the performance of their planes and helicopters toward lighter and stronger fuselages. Composite materials gather several mechanical properties that are a perfect match for this type of application. As shown on Shabby diagrams for material selection in Figure 2, composite materials have a high stiffness-to-weight ratio, much higher than those of conventional metals. Other interesting properties inherent to composites are good damping capabilities which could reduce vibrations and noise of aircrafts, as well as increased impact and corrosion resistance.

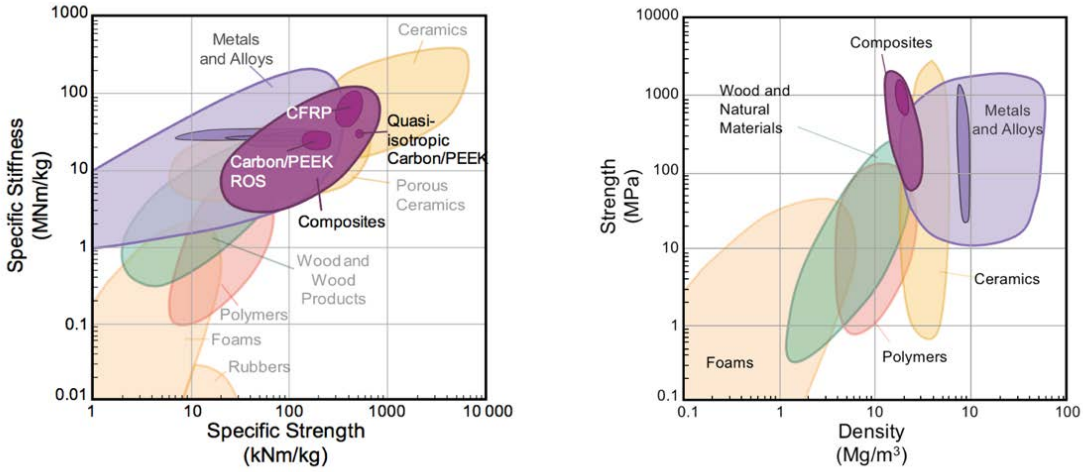

Figure 2 Material selection charts [10, 11]

A composite material is composed of stiff and strong fibres in a softer and weaker matrix, providing interesting combinations of stiffness, strength and toughness. To provide

strengthening, fibre concentration must be maximized. They must be strong enough to transmit loads from fibre to fibre but the interfaces must be weak enough to deflect crack and to enable crack bridging. Continuous fibres are very efficient but they can be more difficult to process and arrange. Short fibre composites are easier to process, but aspect ratio must be above a critical value to obtain good mechanical performance.

A basic structure in composite materials is called a laminate. It is made of a stack of several layers called plies defined by their fibre orientation. To obtain an isotropic behavior, a layup should be made of several plies oriented in different directions. The norm to describe a laminate is to write between brackets the orientation of each plies from the bottom to the top of the structure. Most laminates are symmetric and balanced, which respectively means there is the same number of plies above and below the middle plane, and that there is the same number of plies of plus and minus orientation in the laminate. For example, a layup denoted as $[45/90_2/0]_s$ can be rewritten as [45/90/90/0/0/90/90/45]. The index S means symmetric and the index 2 means the sequence is repeated. An example of a stack composed of 3 oriented plies is shown in Figure 3: Fibres are represented with dark lines and matrix is in grey.

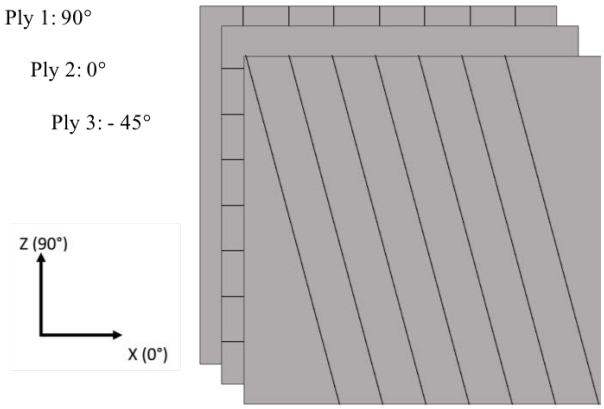

Figure 3 Stack of 3 composite plies

Once a laminate has been laid down, it has to be cured, in or out of autoclave, upon at least atmospheric pressure to increase compaction of the plies together. An autoclave is a big pressurized oven, see Figure 4 Autoclave of American Airlines' composite repair shop

Figure 4 Autoclave of American Airlines' composite repair shop [2]

Today's state of the art of composite materials shows that they are not suitable for every application. For instance, the SpaceX's Mars starship rocket unveiled in 2019 will be made of steel. This rocket's structure will have to deal with extreme temperatures and mechanical forces at stake during each take-off and landing both on Earth and on Mars which also leads to the necessity to perfectly understand the material fatigue behavior. The choice of a material is also very dependent on the costs of development and production, on the capability to reach high production yields, and on sustainability issues raised due to the emergence of a global awareness. Even if composite materials have been studied since the 1950's, a lot of work still has to be done to develop material and techniques to meet both industries required production rates and certification norms from aviation agencies.

1.2. Aeronautic Industry Objectives

The new Airbus A350 is composed of more than 50% of carbon fibres, Safran Leap engine uses composite fan blades and Bell Helicopter is developing new primary and secondary

[2] https://www.mro-network.com/

structures in advanced composite materials. Those structures have different sizes, from large cylinders of 60 feet long by 40 feet wide to small and complex shaped components. Many more applications can find good use of the high performance of composite materials but improvements first have to be made on the cost effectiveness of manufacturing composite materials. Automation is a way to go forward.

Material suppliers and aircraft manufacturers work hand in hand to develop promising techniques for fast manufacturing. Automated Tape Laying (ATL) and Automated Fibre Placement (AFP) are the two main automated technologies that are employed today to manufacture advanced composite laminates from unidirectional (referred as UD) pre-impregnated fibres – simply referred as "prepreg". More importantly, both ATL and AFP manufacturing techniques can improve layup quality and reduce material waste.

Figure 5 AFP machine laying down fibres on a mould at STELIA Aerospace [3]

1.3. ATL/AFP Manufacturing Techniques

ATL and AFP machines are computer-controlled robot arms with a tape placement head at the end to lay down composite prepreg on a mold. ATL is employed to deliver wide prepreg

[3] https://www.compositesworld.com/

tape onto a surface. The composite prepreg is applied using pressure by a roller onto the mold to decrease void content and heating in order to increase the tackiness. Hot torches, laser, and infrared irradiation techniques are used to heat the tape. Once a path is achieved, the robot cuts the tape and restarts the process at another location. The layup operation during AFP is similar to that of ATL. The AFP systems only differ from ATL in the width of the material that is laid down [12]. Despite the change in material form, the prepreg tape or tows are either stored ahead in a creel – cold – cabinet or directly on the head. An AFP head delivers several tows in a single sequence. Tows form a tape, while a sequence of tapes makes a ply. Presently, AFP machines deliver up to 32 tows in parallel [1]. Each tow is individually managed and can be cut separately which increases the steering capability. Layup speed, temperature and tow tension are controlled during layup. Productivity is a function of the number and width of tows which are directly determined by the complexity of the shape: feasible geometries depend on material properties and machine steering capability. Figure 6 is a schematic of an AFP/ATL typical fibre placement head and Figure 7 shows a real picture of an AFP head.

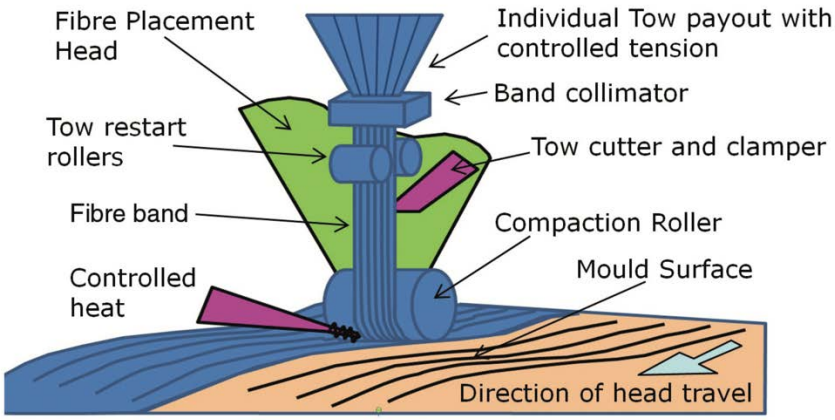

Figure 6 Automated Fibre Placement (AFP) head [13]

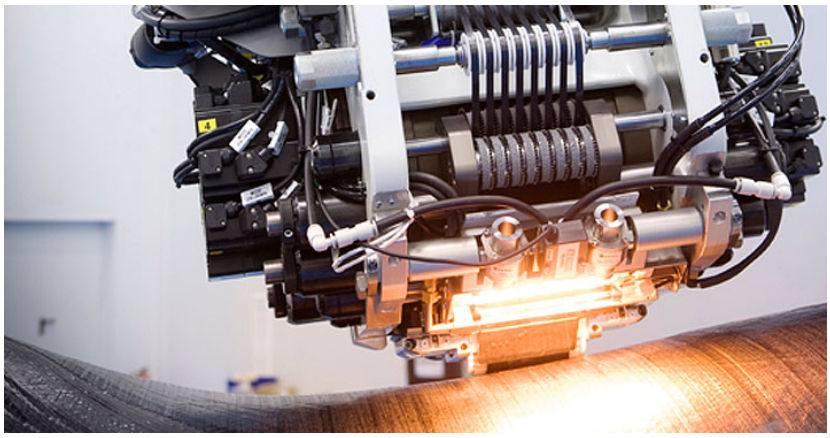

Figure 7 AFP head machine by M-Torres [4]

Reviews of ATL processes by Grimshaw [14] and Evans [15] show the pros and cons of different machines available with industrial objectives in sight. In 2001, Grimshaw [14] showed the material waste of an ATL layup is a function of the part size from 30% for small parts down to 2% for large structures. Automated manufacturing processes can achieve much higher production rates and better waste management than with manual layup[16, 17]. Postier [18] reported that ATL is capable of achieving 65% reduction in layup time and an additional reduction in material wastage rates for certain components. Since each tow is individually clamped, cut, and restarted, it is supposed with AFP to improve layup over surfaces with double-curvature, improve productivity and reduce materials waste [1].

Specifications	ATL Method	AFP Method	Conventional Methods
Material scrap	Low	Low	High
Labour costs	Low	Low	High
Repeatability	High	High	Low
Accuracy	High	High	Low
Productivity	High	High	Low
Cost effective	Yes	Yes	No
Material types	Wide tapes	Narrow tows	Wide tapes
Lay-up speed	Very high	Relatively high	Very high
Components' geometry	Large components	Curved & contoured surfaces	Large components

Figure 8 Comparison between ATL, AFP and hand layup [19]

[4] https://www.mtorres.es

Several industries are interested in the end product quality achieved by the ATL and AFP process especially due to their reliability and economic improvements. Since the 1970s and the arrival of ATL as the first automated process, manual tape layup has progressively been replaced. ATL is particularly productive for simple flat components while AFP will have more benefits in the production of more complex structures. ATL and AFP also include waste management technologies and these new technologies also have seen the linear and rotational lay down speeds increase up to 2m/s and 10kg/h of prepreg. Since the 1980s, AFP has gained maturity. Both ATL and AFP are robust processes that are now facing slower technical improvements rates. New technologies still under development are coming from brand new concepts Continuous Tow Steering (CTS) machines which can achieve very small steering radii, smaller than those made by available AFP machines [20, 21].

1.4. AFP Features

AFP robots are not perfect. They may create defects in some areas which end up being embedded in the laminate, see Figure 9. These flaws may appear due to several reasons [1, 3, 22-24].

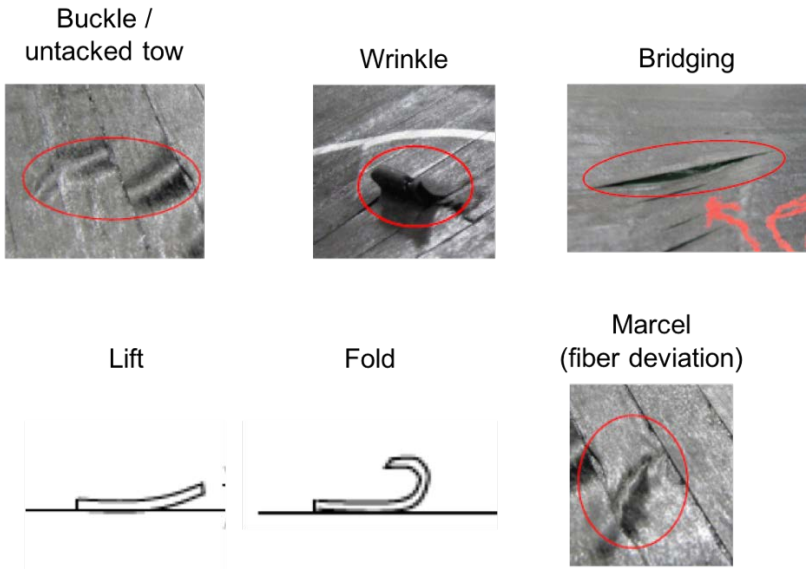

Figure 9 Examples of defects made by AFP techniques [25]

First, the material feeding the head of the robot can have twisted tows or rich resin regions creating bulks in the layup. Secondly, the AFP lay down process cannot precisely follow highly curved shapes due to steering limits and precision issues. Tows can be misaligned due to the lack of precision of the process, creating gaps – rich resin regions - and overlaps – high fibre content. It typically scales up with the amount of steering. AFP manufacturing techniques are also very interesting to make Variable Stiffness Panels (VSP) where fibres follow curved paths. These panels present enhanced buckling resistance and first-ply failure behavior [26, 27]. However most of the panels manufactured by AFP techniques are straight-fibres laminates because VSP are complex and the mismatch between different fibre orientations on a single layer can cause a knockdown in mechanical performance, as studied by Falco [26] and Fayazbakhsh [8, 28, 29]. Two layup strategies appear: full overlap or full gap dropping methods (plus any percentage in between), as shown in Figure 10.

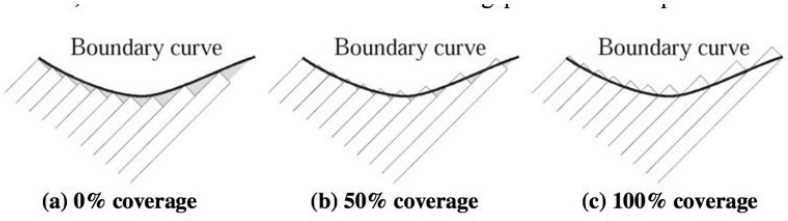

Figure 10 Tow-drop location strategies [1]

Finally, manufacturing parameters such as compaction, tension and heating of the material, associated with difficult fibre paths can prevent surface contact of some tows. AFP machines use flexible rollers to apply the material but the short contact times may be ineffective to get sufficient adherence [1, 2]. One of these resulting defects is called bridging, see Figure 9.

Several ways have been investigated to either prevent defects from appearing or to check and repair the corresponding plies [1, 5, 30]. As stated in previous sections, gains in AFP manufacturing process to reduce the occurrence of defects will mostly come from better numerical fibre path planning, higher integration of selected material properties adapted to

robot capabilities, and optimized processing parameters [31]. On the other hand, manufacturers also work on repairing the plies with defects during the manufacturing of panels. Some techniques involve manual visual inspection or the help of lasers able to detect thickness abnormality at the surface of the laminate being made [1, 31]. However, this technique is very time consuming and thus expensive because technicians have to stop the AFP machine every ply, make repairs if required, before the next ply can start. Other techniques to detect defects are using additional tools plugged on the robot head to analyze the plies as they are being laid down. New technologies can even stop the robot at the exact time a defect is produced to cut this section and restart the process. Once defects are detected, both repair or rejection of AFP-made parts are important investment decisions because they are time consuming and labor expensive.

According to our industrial partner, the occurrence of side-to-side half gap / half overlap generated by tow steering makes these defects of major interest in the understanding of the performance of AFP manufactured parts. Other types of defects are not as often encountered as side-to-side half gap / half overlap, as shown by Bell Helicopter in a study in 2015 [25], see Table 1. Side-to-side half gap / half overlap represents more than 57% of all defects that have been counted on a representative helicopter part. It happens when a tow is misaligned[5] – here referred to as half gap / half overlap or tow steering – which is the focus of this thesis. Figure 11 represents different tows labelled from #1 to #9. Tow #6 is not aligned correctly along the other tows. Tow #6 partially overlaps tow #7. Figure 12 shows a laminate structure with one gap and one overlap side-to-side corresponding to the half gap / half overlap defect configuration, in different orientations. Dimensions of coupons and defects in Figure 12 are representative to the manufactured § 3. Test plan.

[5] End to end gaps and/or overlaps are not discussed in this thesis.

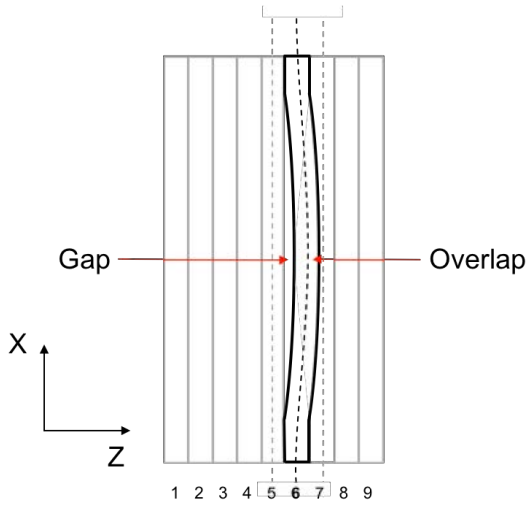

Figure 11 Tow misalignment creating half gap / half overlap defect

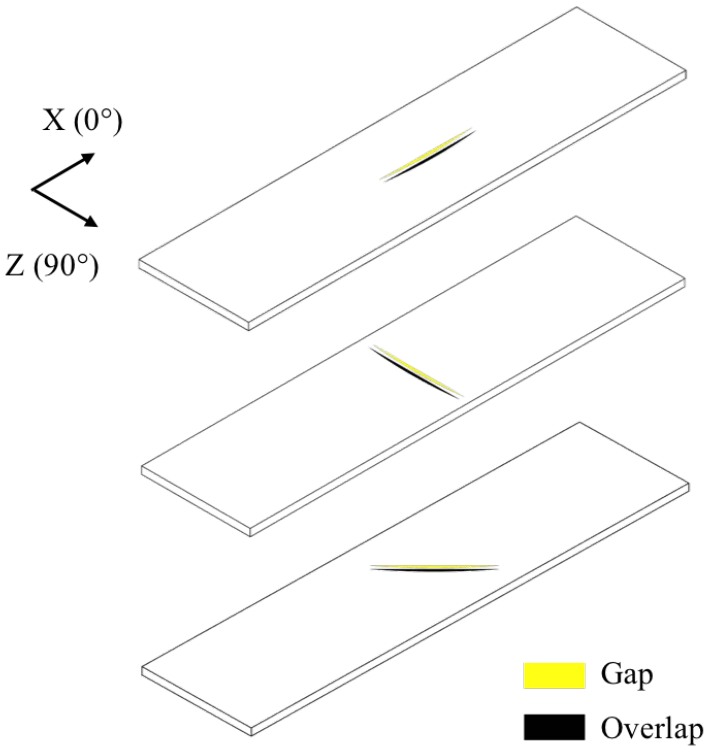

Figure 12 One half gag / half overlap defect in different orientations

A gap is a low stiffness region while an overlap is on the contrary a high stiffness region. This brings local asymmetry in the laminate and it also creates out-of-plane waviness visible through the thickness. Waviness can be partially controlled by the use of caul plates for compaction during the cure cycle. This means the laminate will have same thickness everywhere and that plies inside the panel will have varying thickness due to the presence of

flaws. Defects may affect mechanical performance detrimentally. The impact of this specific half gap / half overlap defect on the mechanical performance of laminates has not been extensively studied but relevant research on the effects of single gaps and single overlaps are shown in the literature review.

Table 1 Defect occurrence - Bell Helicopter [25]

Defect type	***Average percentage of total defects (%)***
Material & processing	9.6
Half gap / half overlap	57.1
Wrinkling	12.9
Bridging	12.5
Other design related defects	7.9

1.5. Motivations and objectives

The aerospace industry has to comply with strict norms and regulations. They enforce the use of high margins of safety to make sure the composite structures, with their so far inevitable flaws, will resist the loads as they have initially been designed for. This is a major drawback to the use of composite materials because they have been chosen for their light weight but manufacturers have to make thicker panels than necessary because the effect of defects is still not well known. Composite materials are expensive and the AFP manufacturing process is still slow because of regular repairs of spotted defects during AFP process inspections. In order to reduce the down-time and interaction with robots, it now seems more suitable to consider the effects of defects early in the design of composite structures in order to more accurately size the panel according to real structure performance. By addressing this topic and considering the mechanical behavior of composite panels with embedded defects, manufacturers will get competitive advantages: certification of composite structures with flaws, time savings in part inspection, increased manufacturing yields and more efficient structures using less material.

The objectives of this work are first to understand the mechanical response of composite structures with embedded side-to-side half gap / half overlap defects by varying some specific parameters on experimental coupons, and secondly to develop predictive numerical methods using finite element modelling. This study is interested in tension, compression and fatigue loading. This research aims to develop guidelines to better design composite structures made by AFP techniques.

2. Literature Review

Gaps and overlaps can cause a reduction in mechanical performance by changing the behavior of a composite structure under loading. Therefore, the effects of defects made by the AFP manufacturing process have widely been studied in the literature. It is important to understand how the size and distribution of such gaps and overlaps influence the strength and failure development. However, most of the studies are interested in specific geometries or configurations which are not side-to-side half gap / half overlap defects. Most studies are interested in single gap or single overlap while it appears the addition of gaps and overlaps side-to-side has significantly more mechanical effects [4, 7, 32]. New emerging approaches tend to develop numerical tools using Finite Element (FE) modelling methods to analyze fracture mechanics at the coupon level [13, 33].

2.1. AFP manufacturing parameters

Half gap / half overlap defects can appear when the computer-controlled head is tape-laying down a complex-shaped area of a fuselage, especially when the curvature is important. The steering capabilities of the AFP process are dependent on both the AFP machine and the fibre parameters, see Table 2. Also, the tolerance in the fibre placement head movement, steered fibres, and tow width variation contribute to the introduction of gaps and overlaps [1].

Table 2 Manufacturing parameter & consequences

Parameter	***Consequences***
Creel temperature	Ease feeding of tow in AFP head
Fibre tension	Affect part & tow placement quality
Compression	Cohesion between plies
Heating	Part quality & stiffness
Laydown speed	Fibre impregnation by resin
Fibre tackiness	Part quality & cohesion between plies

Due to the presence of curved surfaces, fibres need to be steered to keep their orientation on the mold. The appearance of half gap / half overlap defect due to steering happens at the intertow area of a tape, before compaction, and at the interband area – adjoining tapes – due to the lack of accuracy in the lay down process of the AFP machine. These defects create both reduction of strength and a change of stiffness compared to pristine – without defect – conditions.

Manufacturers want to increase the productivity of their lines thus increasing the speed of laying down by AFP process. Software improvements come by fibre path planning found in Debout et al. [34] where layup savings can reach up to 33% reduction as published by Lukaszewicz et al. [1, 35]. Optimization of manufacturing parameters on a simple flat component or cylindrical fuselage part is interesting to be more productive and reduce the occurrence of defects. However, it appears more factors especially related to downtime of machine inspection and repair need to be better addressed. In fact, from an estimated productivity of 41.3 kg/h for AFP [1], the real productivity achieved is suffering a knockdown of 80% [36]. Improvements need to be done on faster material refilling, or more efficient cleaning because an AFP machines does not lay down material during up to half the time [1].

The speed profile followed by the AFP machine is particularly important to avoid defect development during steering. This thesis is interested in tow misalignment also referred to as a half gap / half overlap defect. During steering, inner tows are subject to compression and outer tows suffer from increased tension. If the forces at stake are too high, bridging or buckling can appear but generally tows are losing the original alignment. AFP feasible radii can be as small as 51 cm compared to large 600 cm for ATL technologies [1, 26].

Limitations of steering also have a lot to do with the material properties of the prepreg that is used. In fact, tackiness has a major effect on part final quality. Since the speed of AFP manufacturing is increasing, the material is less compacted and better material tack is required.

However, speeds hit records up to 2m/s so that brand new technologies are required and Bristol [20, 21] researchers are on good tracks to develop Continuous Tow Shearing (CTS) machines where the head is no longer rotating but translates along the diagonal. This technology brings new steering challenges but it also offers potential extremely short steering radius.

2.2. Static tension and compression

Most configurations that have been studied in recent years are interested in gaps and overlaps running through the entire specimen. These investigations were primarily of interest to understand what tolerance AFP heads should follow between each tape being laid down. Even there, conclusions differ. In fact, a quick look at results from this literature review shows that investigation in tension loading shows gaps have less effects than overlaps because a gap is missing fibres, while compression loading gives the opposite effect due to waviness and buckling considerations.

2.2.1. Experiments

In 2010, Croft from McGill University [7] used CYCOM 5276-1 to manufacture quasi-isotropic laminates $[45/0/-45/90]_{2S}$ and all defects were oriented in the 0° direction, along the length of the coupons. No caul plates were used during the cure cycle. Figure 13 shows some schematics of the cross section through some defects.

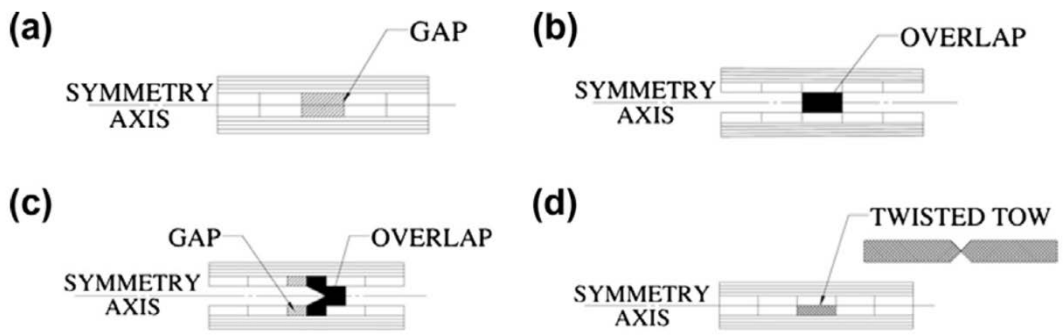

Figure 13 Cross sections of embedded defects [7]

The defect width for the half gap/overlap configurations was 0.616in (15.64mm) wide, from the beginning of the gap to the end of the overlap. With an average 4% knockdown in tensile strength, half gap / half overlap defects appear more critical than single gaps or single overlaps. On the right of Figure 14 are shown the results in tension where single overlaps slightly increase the strength and single gaps reduce it. On the left of Figure 14 are shown the results in compression where it appears single overlaps increase the strength by 7% compared to pristine conditions and half gap / half overlap defects do not have an effect at all.

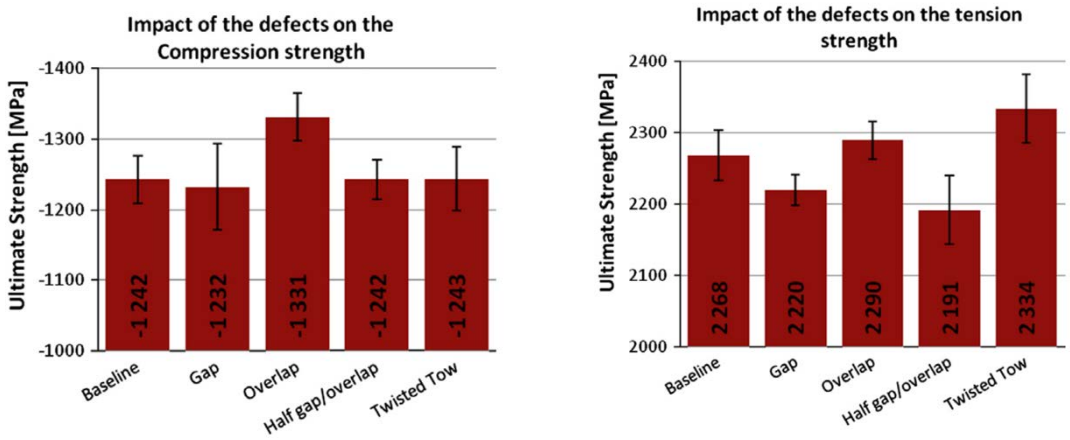

Figure 14 Compression and tension results of different defected configurations [7]

Moreover, Croft [7] made some microscopic observations which show not too excessive waviness through the thickness of the coupons with single overlaps and single gaps, compared with higher waviness of half gap / half overlap coupons. The coupons were made with soft tooling so the plies do not change thickness but the overall laminate changes thickness in the region of the defect. Gaps are clearly filled with resin and gaps are very well defined with only a slight fibre flow from high fibre volume content to lower ones. This means the overlaps carry more load without changing the laminate much which explains the slight increase in tension and compression strength. Gaps are softer regions where defects appear due to stress

concentration around the pockets of resin as observed by Croft [7] in his failure mechanism analysis section.

Side-to-side gaps and overlaps oriented in the 90° direction have been studied by Sawicki and Minguet [37] under compression in notched and unnotched coupons. Size and location of defects were reported and it appears that coupons with defects of at least 0.03in (0.762 mm) width had a strength knockdown of up to 27%. Wider defects did not have larger knockdown factors. Notched and unnotched specimens achieved similar performance. They failed because of significant out-of-plane waviness according to the authors' observations because waviness leads to buckling instability. Since half gap / half overlap defects show strong waviness, the prediction of mechanical performance is more difficult to assess [37, 38]. Side-to-side gap/overlap defect fabrication is shown in Figure 15.

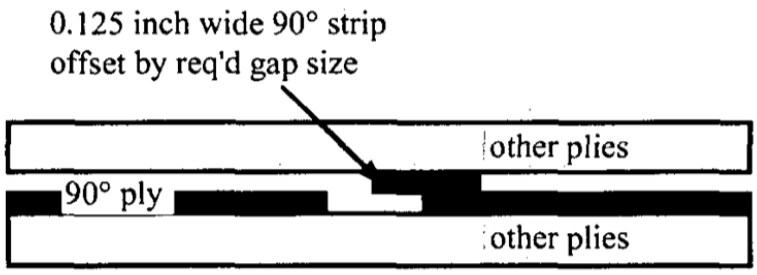

Figure 15 Fabrication of gap/overlap defect [37]

Hsiao and Daniel [39] were also interested in the effects of fibre waviness on compressive strength of carbon epoxy laminates. They emphasized the previous observations made by Sawicki and Minguet [37] that out-of-plane waviness causes failure due to increased shear stress. Wang et al. [40, 41] went further by studying the effect of waviness on early delamination of fibre glass composite. They concluded waviness causes degradation of resistance against buckling behavior.

Zhao [40] studied the effects of in-plane fibre waviness on mechanical properties of composite laminates under tension. Composite specimens were manufactured using AFP

techniques and defects of different magnitude of tow steering were embedded in the laminates. The magnitude of in plane waviness was controlled using axial compression strain measures. The larger the axial compressive strain is, the greater the formation of fibre in-plane waviness would be formed. Zhao showed good correlation between 2D laminate theory and maximum stress failure criterion. The 1.2% compressive strain configuration had a significant degradation of both tensile modulus and strength down to 25% and 57% respectively.

Lan et al. from University of South Brittany in Lorient, France [6, 42, 43] used different symmetric layups - $[(90/\ 0)_2/90]$ and $[0/90_5/0]$ for tension tests, $[(45\ /+45\ )_3/\ 45]$ for shear tests and $[90_4/0_3/90_4]$ for compression tests - fabricated with an AFP machine to study the effects of single gaps and single overlaps running through the entire width of specimens tested under different loading. They were also interested in the effect of caul plates used during the cure cycle of some specimens. Caul plates tend to homogenize the laminate structure by encouraging a resin flow from pristine defect free regions to gap for example. Using caul plates, the thickness of laminates is constant while composite panels manufactured without caul plates show great thickness variation at the location of defects – increased thickness at overlaps and decreased thickness at gaps, see Figure 16. Using the author's own observations, the use of caul plates plays a major role in the structure of composite because it heals the defect regions.

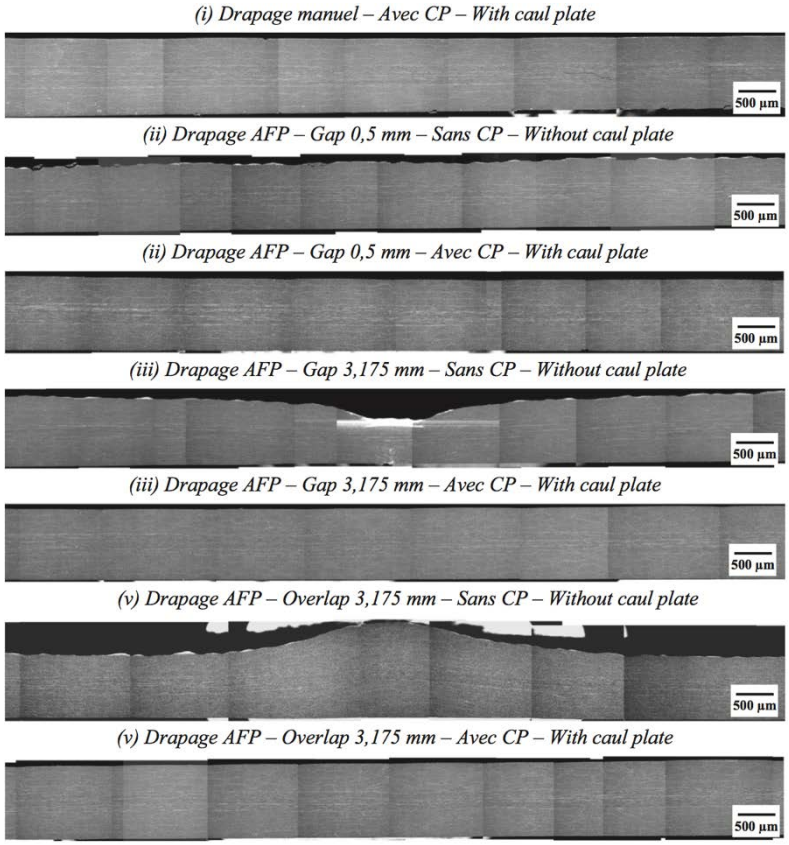

Figure 16 Thickness profiles of different configurations with or without caul plates [43]

The effect of embedded defects on mechanical performance were quantified using tension, shear and compression tests. Max strength under tension varied very little compared to defect free specimens, either with gaps or overlaps, with caul plates, and any defect size. Without caul plates, wider defects have more effects on tensile strength. In shear and without caul plates, max strength decreases when gaps are wider up to a 12% knockdown for 0.25in (6.35mm) wide gaps. The use of caul plates reduces the knockdown in shear with large gaps down to 9%. With caul plates, the modulus is not changed in compression or tension when gaps are embedded but it slightly increases with overlaps because of the buckling of specimens. Caul plates or type of defects do not have any effect on shear modulus. Under compression, the max strength is similar for both gaps and overlaps configurations with 12% knockdown when a caul plate is used, and 20% knockdown without caul plates. Under tension, the variation of thickness without the use of caul plates does not affect the ability of 0° plies to transfer the load. The

failure would randomly occur when caul plates are used while the plates break near the singularity without caul plates.

In 2018, Woigk [32] from Bristol University manufactured specimens following the stacking sequence $[+45_2/90_2/-45_2/0_2]_{3S}$ by hand layup with embedded defects, see Figure 17. Even if the specimens were not made by AFP, they assumed the final quality and properties of the laminates would be the same. The defects that have been studied are single gaps, single overlaps and a mix of single overlaps and single gaps in the same structure. It was shown that single gaps have more effects than single overlaps. Single overlaps can also increase the performance in strength of some specimens: +9.5% in compression, +3% in tension. A mix of gaps and overlaps reveal the largest strength knockdown factors: -14% in compression, -7.4% in tension. Defects have more effect under compression than under tension. Defects were 2mm large and ran through the entire width of the specimens. It is also stated that these configurations would most likely not appear in a typical AFP manufactured structure as these specimens represent worst case scenarios.

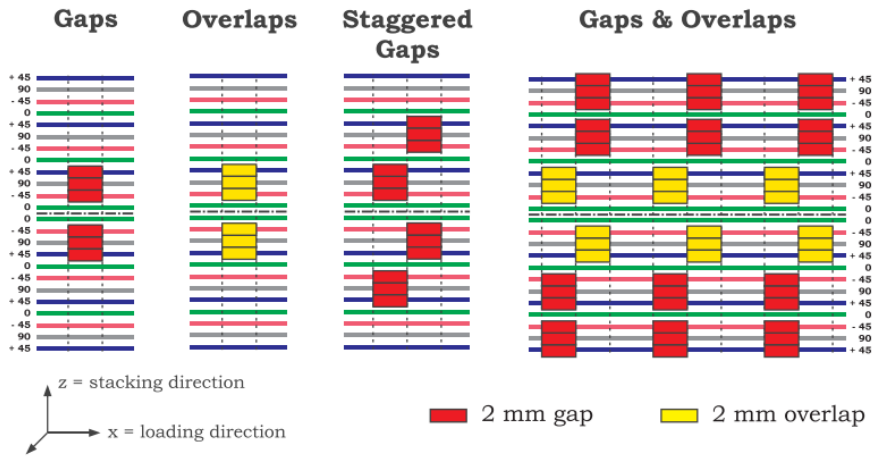

Figure 17 Configurations of gaps and overlaps tested in tension and compression [32]

Marouene and al. [44] from Polytechnique Montreal investigated the influence of single gaps and single overlaps on open hole composite specimens made by AFP manufacturing techniques. Since gaps and overlaps can occur anywhere on a composite structure made by

Automated Fibre Placement, it can happen that fasteners are placed near those defects. Both numerical and experimental approaches were studied to understand the mechanical performance and failure initiation in open hole specimens. 0° and 90° oriented gaps and overlaps were embedded at different locations near the open hole: centered or shifted. Depending on their locations, defects can have a positive or negative impact on the compression strength. It has been shown that it is very important to represent the microscopic observations in the model to accurately predict experimental results. Both numerical and experimental results agree with a high correlation using progressive damage evolution techniques in the model. 0° gaps have positive effects when they are centered and negative effects when they are shifted while overlaps have positive effects when they are shifted and no effect when the are centered.

2.2.2. Healing: caul plates and defect staggering

Cartié and al. [42] from the University of South Brittany studied the effect of caul plates and showed to what extent it can heal the defects made by AFP manufacturing techniques in composite laminates. Defects embedded in a laminate composed of plies of the same orientation disappeared during the cure cycle due to the use of caul plates and compaction. This effect if called healing. The resin flows with fibres from pristine defect-free regions to singularity areas. The homogenization of the microscopic structure during compaction with caul plates gives the laminates defect-free like properties. For layups composed of different orientations of plies, the role of the caul plate is less important than it is for unidirectional laminates but it still encourages resin and fibre flow, constant laminate thickness. With the use of caul plates, final properties tend to approach the reference defect-free baseline.

Marouene [44] shows the rearrangement of the plies during the consolidation process which prevents the formation of singularities in the laminates. A progressive damage modelling of gaps and overlaps confirms the importance of considering microscopic observations. In fact,

the defect geometry can change during consolidation and final performance is different with this consideration. The effects of embedded defects depend on their dimensions, the orientations of the plies with embedded defects and on the location of the defects relative to the open hole.

Blom et al. [45] from Delft University of Technology studied the stiffness and strength of tow-steered laminates. They observed 7% knockdown when defects were staggered and 15% when there was no staggering. Blom showed that staggering smooths out defects and singularities out. Laminate variations disappear when several defects are close to each other through the thickness.

Falco [26, 27] was interested in the effects of defects on tensile loading of variable stiffness laminates cured without caul plates, notched and unnotched, see Figure 18. Those embedded defects correspond to fibre angle discontinuities due to curved fibre paths in Variable Stiffness Panels where two orientations of prepreg meet on a specific layer. The presence of gaps or overlaps has an important effect on the laminate thickness at the location of defects: it increases by 15% with overlaps and decreases by 20% with gaps. However, specimens with staggered gaps have only a 5% local thickness reduction.

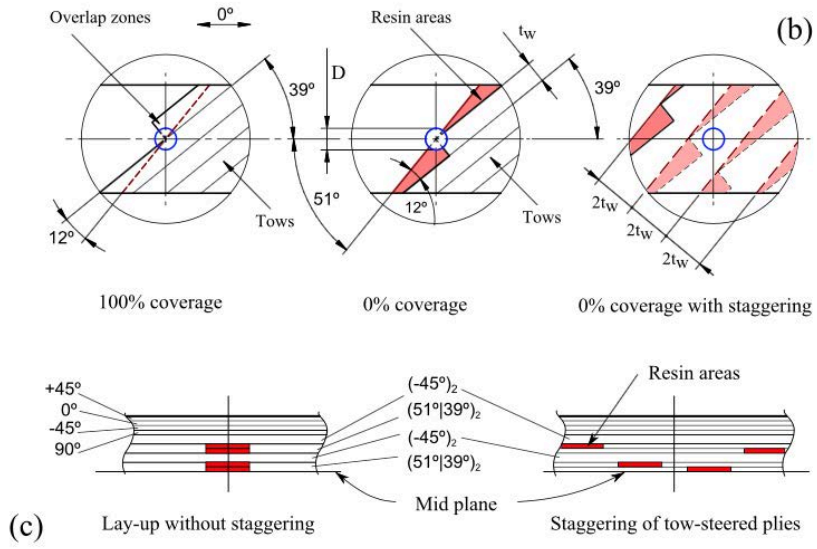

Figure 18 Configurations of interest top view (b) and through the thickness (c) [26]

Falco [26, 27] showed that the largest strength knockdown factor on unnotched laminates was obtained with gaps at 20%, not overlaps – 10%. Staggering gaps reduces the resin rich pockets and encourages effective load transfer. It is shown that staggering is an effective way to reduce the effects of defects on a composite structure. Gap staggering reduces the tensile strength with a 8.6% knockdown. The defect geometry was analyzed with micrographs and Digital Image Correlation (DIC) techniques were used to monitor strain field during tensile tests. The DIC analysis shows that the large delamination starts at the location of defects probably due to the increased interlaminar shear stresses, followed by matrix cracking and fibre failure.

2.2.3. Modelling

Blom et al. [45] developed numerical models to explore mechanical performance of AFP made composite structures with defects. The study is interested in tow drop areas where gaps are created due to fibre curvilinear path planning. In fact, an AFP robot can lay down fibres following a full overlap or full gap strategy. This defines the degree to which tow drop off are covered. It can vary from 0% to 100% in which case gaps do not exist, triangle tow-overlaps are made instead, see Figure 19. This type of defect is present all over the structure and its magnitude is defined as the ratio of area of gap or overlap over the surface of the laminate. The model is using the maximum stress criterion that has been adapted to consider non-linear shear behavior and progressive energy-based damage of fibres. The Authors showed important tensile strength knockdown up to 20% corresponding to regions with maximum 10% tow drop per area.

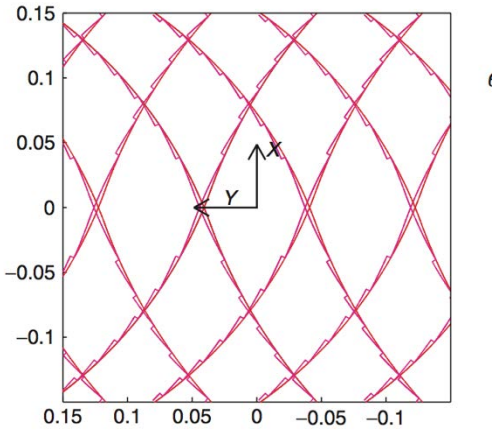

Figure 19 Full plate model with triangle overlap

Heinecke et al. from the Institute of Composite Structures and Adaptive Systems in Germany [46] was interested in the structural behavior of AFP made composite panels with three type of defects: narrow gaps, wide gaps and wide overlaps that are present between each tape laid down by the AFP head. Therefore, defects are regularly present in the laminate. They used three approaches: analytical based on the rules of mixture, virtual test – finite element modelling with delamination fracture mechanics- and multiscale analysis – finite element modelling with simplifications. Inputs in their models are elastic properties of unidirectional prepreg, material strength and shear non-linear behavior. The stiffness matrix of prepreg is degraded once the failure criterion is reached which leads to a progressive damage propagation. The authors show that depending on the model and considered failure criterion, results vary slightly and the fracture initiation changes. Gaps reduce stiffness and strength by 10 to 20% while for the overlap configuration, the observed knockdown was 22% compared to baseline defect-free laminate. No experiments were held to confirm these models. Waviness was not considered. Out-of-plane effects may have led to different results if they were considered in their model according the authors.

Fayazbakhsh et al. from McGill University [8, 28, 29] studied the effects of single gaps and single overlaps with finite element modelling using a new method called the “defect layer

method". Defects are defined with different material properties and ply thickness variation. For instance, a gap is defined as a rich resin region and the corresponding region in the ply has resin properties. For overlaps, the layer had the same properties everywhere but the local thickness was increased. Two laminates have been obtained from optimization algorithms based on different buckling and in-plane stiffness objectives. First design offers maximum achievable buckling load and the second maximum in plane stiffness and buckling load. Then an algorithm written by the author determines the fibre path an AFP robot should follow, using a full gap strategy or on a full overlap strategy. Many defects are introduced in the model. Only elastic properties are input as the model does not study maximum strength or progressive damage. Gaps reduce buckling capability by an average of 12% on both designs and overlaps increase it by an average of 30% on both designs. Gaps reduce in plane stiffness on both design by an average of 14% while overlaps increase it by an average of 10% on both designs. These numerical results have not been compared to experiments.

Marrouze and Abdi from the university of South Carolina Columbia [3, 47] defined the multi-scale progressive failure analysis (MS-PFA) approach to study the effects of gaps on the mechanical performance of composite structures. This approach is based on the numerical mechanical characterization of a small region of interest containing a defect at the mesoscale level, see Figure 20.

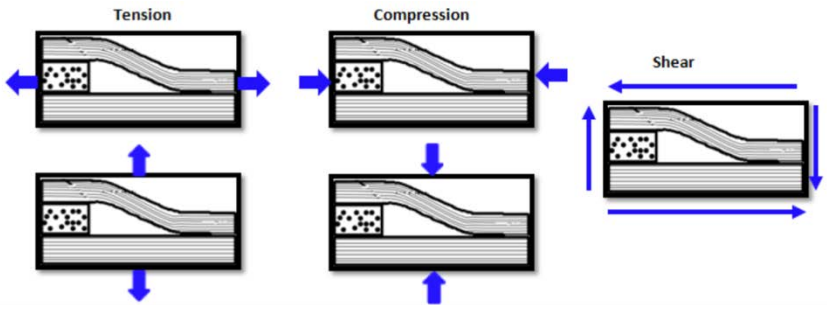

Figure 20 Unit cell cross section representative of defect [3]

Once tensile, compressive and shear properties of the element with defect are characterized, this unit cell is integrated into a larger macroscale structure in a Finite-Element model following a specific gap distribution, see Figure 21.

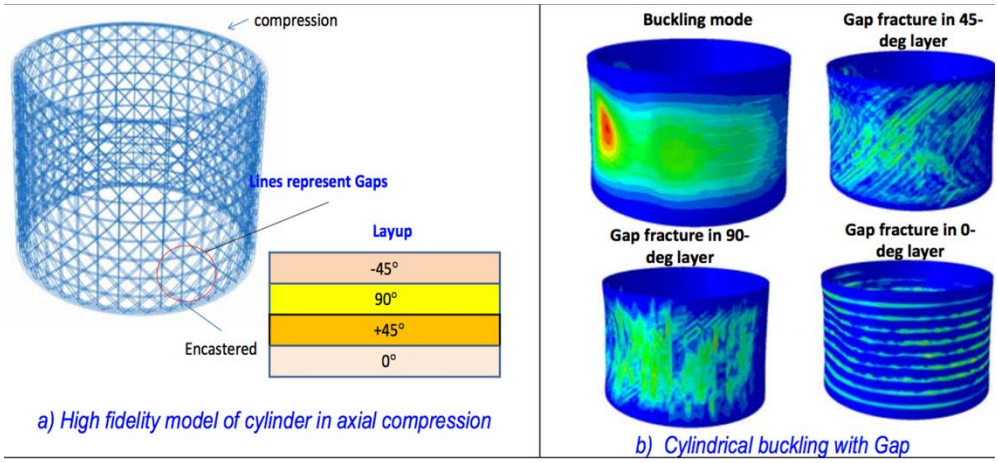

Figure 21 Cylindric buckling of macroscale fuselage with embedded gap unit cells [3]

This way, degraded material properties are locally implemented into a structure to model the flaws made by AFP manufacturing process. MS-PFA approach considers damage initiation and damage energy-based evolution of a crack based on strain and strength formulation. Plies are modeled with delamination capabilities since cohesive interactions are defined. Their research concluded that the degradation of material properties is due to fibre waviness. It is possible to change the magnitude of waviness by changing the tow thickness. However, playing with the gap length does not cause any larger knockdown. This method can be used to predict damage caused by manufacturing under different service loading – tension, compression, shear.

In 2013, Li Xianqian at the University of Bristol [33] developed a finite element model considering a Weibull survival probability. Experiments showed that the size of composite specimens is a very important parameter which influences the final strength of the laminate [3, 48]. The strength of a laminate decreases when the size of the tested specimen increases. This "size effect" can be approached by statistical analyses of defect occurrence in material volumes and microstructures, manufacturing induced defects and boundary conditions during testing.

The Weibull approach evaluates the probability of a laminate to initiate a crack and then to search for the element that experiences the maximum tensile stress. While previous models [49] have already integrated post-processing Weibull analysis to Finite-Element modelling results, Li Xianqian was interested in the damage propagation of a crack. Criterion in Equation was embedded in a user defined material routine.

$$S_i(\sigma) = exp(-V_i(\sigma_i/\sigma_0)^m) \quad (1)$$

where σ_0 is the characteristic strength, m is the Weibull modulus, $\sigma_i$and V_i are element longitudinal tensile stress and volume respectively. The sum of every element probability for failure by fibre tensile breakage gives the crack initiation criterion at the laminate level. When the criterion is met, the element with maximum tensile stress cracks and it is removed during the analysis. Delamination is represented by cohesive interfaces which also prevents too high stress concentrations when a failing element is removed from the analysis. This model showed great correlation with experimental results in 4-point bending of unidirectional laminates: decreasing strains and stresses when specimen size increases and good prediction of mixed mode damages in both delamination and fibres.

In 2015, Li Xianqian at the University of Bristol [13] used his previous model with Weibull failure criterion and element removal approach of progressive damage mechanism to assess the effects of defects made by the AFP manufacturing process. Single gaps, single overlaps and a mix of both gaps and overlaps have been studied both numerically and experimentally. This model is a ply-by-ply analysis on LS-DYNA software in both tension and compression. The laminate modelling algorithm considers ply waviness and hard or soft tooling, with or without caul plates, during cure cycle, respectively. This means a ply shrinks to become a gap or a ply thickness increases to become an overlap, see Figure 12.

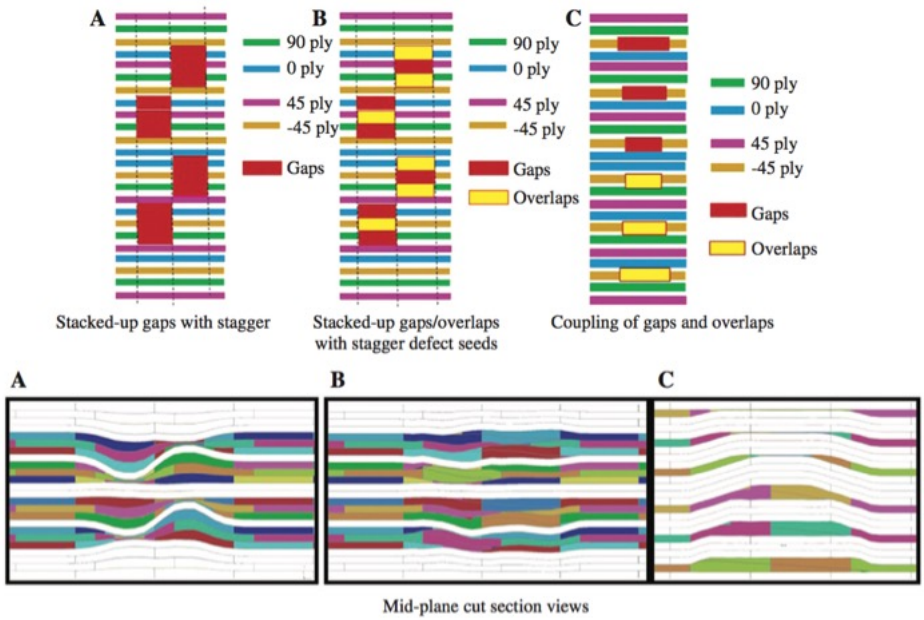

Figure 22 Modelling of gaps and overlaps of different configurations [13]

At this location, the ply with embedded defect has adapted material properties calculated using both the rules of mixture and geometric stiffness consideration based on thickness change, (see Eq 2.), where T stands for thickness and the suffix "_0" denotes the pristine properties.

$$E_{11}(T) = E_{11\_0}\frac{T_0}{T} + E_{resin}\left(1 - \frac{T_0}{T}\right) \quad (2)$$

$$E_{22}(T) = E_{22\_0};\ E_{33}(T) = E_{33\_0};\ G_{12}(T) = G_{12\_0};\ G_{13}(T)$$

$$= G_{13\_0}\ G_{23}(T) = G_{23\_0}$$

Other plies below and above have their thicknesses adjusted locally which creates out-of-plane waviness. The material simulated was IM7/8552 and the layup was $[45/90/\ 45/0]_{3S}$. The Author wanted to study the effect of defects and understand to what extent waviness was playing an important role in the final properties of laminates with embedded defects. Thus, two types of defect staggering were used, see Figure 23.

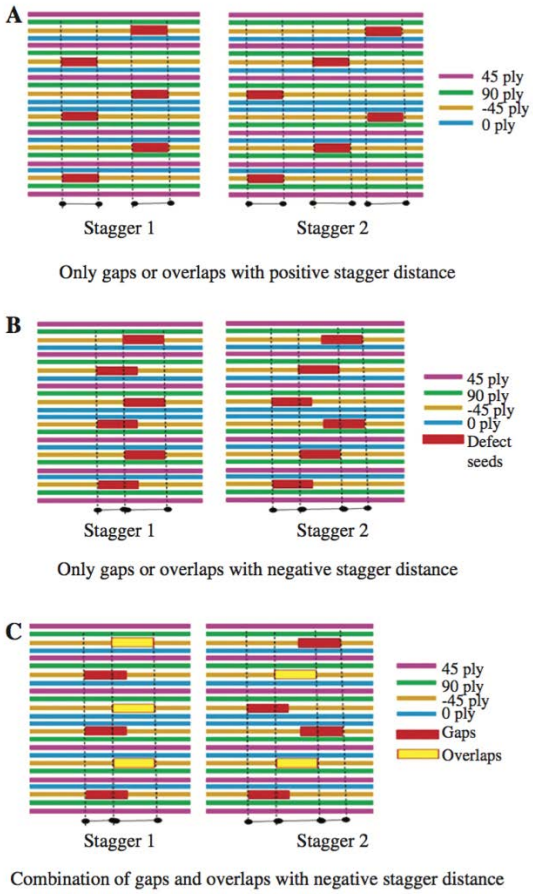

Figure 23 Different gap and overlap configurations [13]

The stagger number #1 has single gaps or single overlaps aligned through the thickness while stagger #2 has an important stagger between defects. Stagger #1 is expected to have more out-of-plane waviness than #2. Modelling results show that single gaps and single overlaps cause larger knockdown in compression – average of 20% – than in tension – average of 10%. Embedded defects in +45° or -45° oriented plies have more effects than in 90° plies. +45° and -45° oriented defects have similar behavior. The strength knockdown caused by gaps is larger than the strength knockdown caused by overlaps. Defects following pattern #1 have more effect than with the pattern #2. The last observation can be an explained by the larger out-of-plane waviness in #1 than in #2. Li Xianqian [13] also studied some configurations of mixed single gaps and single overlaps but never half gap / half overlap defects. The results for this configuration are shown with a varying stagger. The more overlaps and gaps that are aligned

through the thickness, the less significant is the effect on maximum strength. This means the average laminate properties at the cross section of the defect location are close to the pristine defect free baseline. This makes sense because the overlaps fill in the gaps of surrounding plies. Recently in 2018, Woigk [32] manufactured some specimens with the configurations analyzed by Li Xianqian [13] to back up the modelling results. Woigk [32] found good correlation between experimental and modelling results.

The above modelling work shows the importance of an accurate modelling of gaps and overlaps in their geometry: waviness, material properties, rules of mixtures and thickness change. Out-of-plane waviness has an important effect since compaction with caul plates tends to homogenize the material properties, creating a flow of resin and fibres from overlap to gap regions. Since the different plies are not all subject to the same defects, delamination plays an important role in the through-the-thickness load path and stress concentration factor. In order to capture the failure mechanism, the choice of failure criterion is as important as the use of the right values for the energy-based material evolution properties.

2.3. Fatigue

The literature on fatigue for composite materials is voluminous. However, the effects of AFP manufacturing defects on the fatigue response of composite laminates have barely been studied in the literature [50]. Researchers use experimental investigation helps them draw design guidelines for the industry. New developments in non-destructive inspection technologies as thermography imaging techniques led to enhanced analysis of crack initiation and fracture growth [51]. In general, mechanics of failure can be catastrophic or progressive. In fatigue, the crack starts at weak spots like defects in the material where high stresses concentrate. If the material can still carry loads, then the crack will propagate until the structure is too damaged to sustain its integrity. Evidence of damage can be detected in one of the many forms of failure: matrix cracking, fibre-matrix cracking, delamination, void growth and fibre

cracking. For cross-ply laminates, damage is initiated with delamination at the edges then it propagates. Matrix cracks appear before fibre breakage at failure [52, 53]. Cyclic life decreases when the amplitude increases at constant mean stress. Fatigue life also decreases when either temperature or frequency increases [54-56]. The type of reinforcement has an important effect on the fatigue resistance of a laminate. Non-woven fibres perform better than woven fabric, and stiffer fibres perform better than soft fibres in fatigue because matrix/fibre interaction suffers from high fibre deformation [57].

Fatigue resistance of composite also depends on the presence of defects. Colombo et al. were interested in the effect of delamination on glass fibre composites. The static strength of such laminates with embedded delamination does not change while the fatigue life is different than defect-free specimens. The fatigue life was much shorter with high stresses thus the defect is activated in fatigue at high stress levels [58].

In 2016, Y. Elsherbini [50] from Concordia university in Montreal analyzed the effects of gaps end-to-end on the fatigue life of composite structures made by Automated Fibre Placement manufacturing techniques. This specific type of gap appears at the end of a tow when the AFP placement head starts again with an offset. The configuration of interest had only one gap at the middle of the coupons following $[0_9]$ carbon epoxy layup. The specimens were manufactured without caul plates, using an autoclave during the cure cycle, and gap's dimensions are 0.125in (3mm) by 0.25in (6.35mm) which corresponds to a tow width. Degree of cure was checked using DSC techniques and void content was measured very low using an electronic microscope. The Author used infrared thermography imaging techniques to monitor the crack initiation and propagation throughout the life cycles of defected specimens. Tension-tension cyclic loading tests were conducted on unidirectional carbon epoxy laminates using ASTM D3039 standard [59]. Fatigue tests were performed at stress ratio of 0.1 and frequency 5Hz. Elsherbini also developed a damage model (FPDM) to predict fatigue damage

propagation. At any applied stress, the fatigue life of defected specimens is lower than the pristine defect free reference specimen. The higher the applied stress, the higher the knockdown factor on fatigue life. It appears the defects have more effects at higher stresses since the S-N curve of defected specimens is the further away from the S-N curve of pristine specimens, see Figure 24.

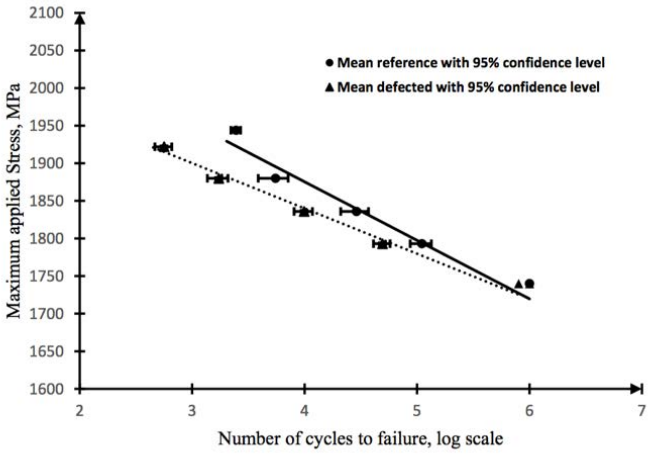

Figure 24 Unidirectional laminate S-N curve [50]

When the applied stress decreases, both S-N curves tend to the same fatigue life. Thus, at lower stresses the effect of gaps on the fatigue life is negligible. Experimental and simulation results showed good agreements. Elsherbini found that IR thermography is an efficient non-destructive technique to monitor the damage propagation. This technique is able to detect the spreading of damage initiated at the location of the defects. In fact, the energy dissipated at the surface of the specimens is non-homogeneous and areas of higher temperatures correspond to damage propagation due to the storage of energy at stress concentration spots.

Elsherbini published another study in 2017 [51, 60] where the author developed a method based on IR thermography imaging to easily find the stress threshold stress under which the fatigue life of a composite panel does not suffer from the embedded gaps. Traditionally, a lot of specimens must be tested at different stress levels to draw S-N curves and to define a threshold stress point under which reference defect-free specimens and defected specimens start

behaving the same way, same fatigue resistance. This widely used technique is the Wohler method. In his previous study Elsherbini [50] used a unidirectional laminate (UD). In this new study, Elsherbini [51] was also interested in cross-ply and quasi-isotropic laminates using the same tension-tension fatigue specifications as described in his previous works [50]. Defected specimens have end-to-end gaps in the 0° orientation at the middle of the coupons, middle ply, using the same dimensions as defined in the previous paragraph. For each stacking sequence, S-N curves for the pristine and specimens with embedded gaps converge at this threshold stress obtained by extrapolation, see Figure 25.

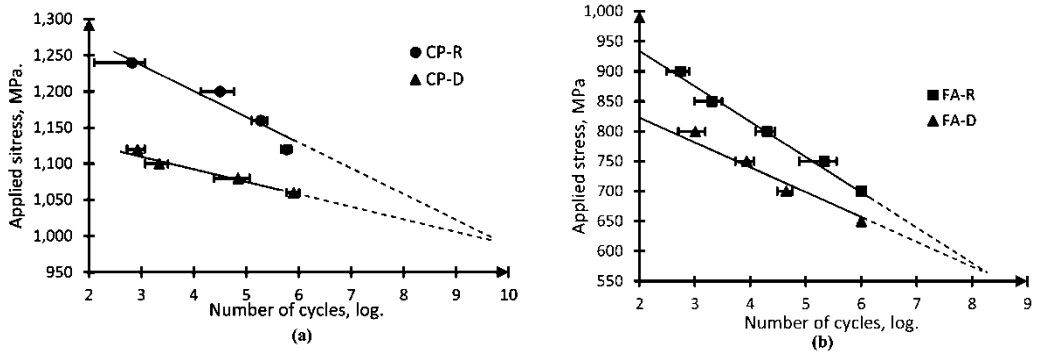

Figure 25 S-N curves of Cross-Ply laminate (a) and Quasi-Isotropic laminate (b) [51]

Therefore, the effects of defects on fatigue life depends on the applied stress. The knockdown factor is increases when the average cyclic stress level increases. The author is also using a method proposed by Risitano [61-63] to find this threshold stress to save cost of material and time, using IR thermography imaging techniques. The same defected specimens are tested up to 1000 cycles at different stress levels. For each configuration, depending on the applied stress, the gaps have different effect and the magnitude of crack growth is different at any specific moment in the fatigue evolution. This difference in damage spreading can be monitored thanks to the energy dissipated, captured by the IR thermography pictures. By plotting the slope

of temperature change at the surface of the specimens, see Figure 26 the author can define a stress threshold corresponding to the activation of crack growth due to embedded gaps.

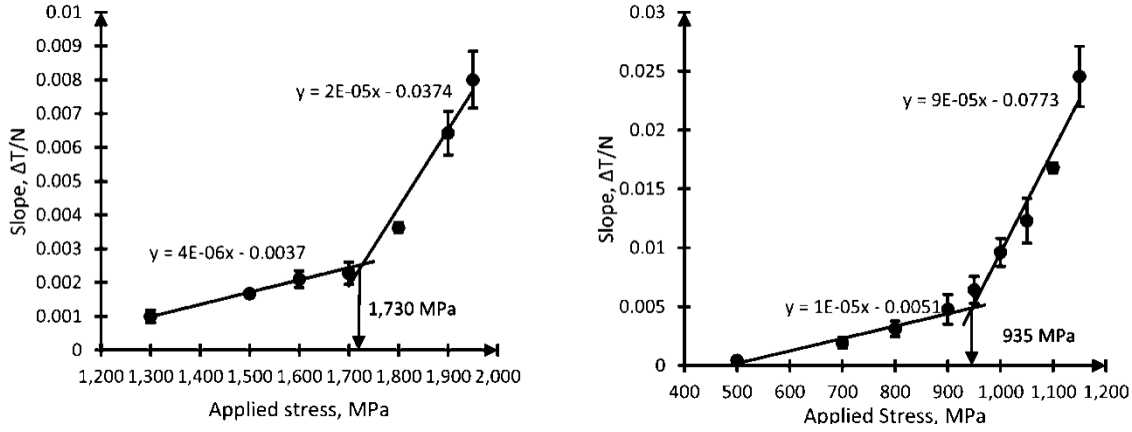

Figure 26 Unidirectional laminate on the left, Cross-Ply laminate on the right [51]

The comparison between Wohler and IR Thermography techniques shows very good agreement and important time saving. The author performed an intensive microscopy campaign on specimens at different stresses levels around the threshold point, at different points during the fatigue evolution. Under this threshold point, the delamination from the gaps stops propagating after a certain time and the temperature at the surface of the specimens is stabilized. The final fracture of defected specimens show the same characteristics as the pristine configurations. Under this threshold point, the gaps do not have more effects than the natural heterogeneity of a composite coupon.

Marine and al. [6, 43] studied the effect of cyclic loading on angle ply laminates using the following stacking sequence $[(-45\ /+45\ )_3/\ -45]$. The tests were performed following the same standard as for quasi-static shear loading, ASTM D3518 [64]. The testing machine used an increasing load, by steps of 0.8kN, until the specimen breaks while a biaxial strain gauge (JYOWA KFG-10-120-D16-11) glued on the surface of each specimen is monitoring the deformation. This setup measures the shear properties of this carbon epoxy Cytec 977-2 material and its damage propagation behavior. Different configurations are studied: pristine

defect-free or specimens with gaps or overlaps, manufactured with or without caul plates, see Figure 27.

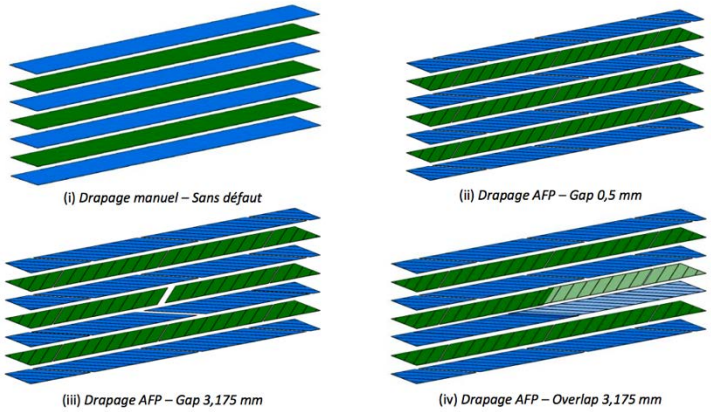

Figure 27 Configurations of specimens tested in cyclic shear loading [43]

The stiffness of the tested specimen changes during the fatigue life. Plastic deformation appears quickly after three cycles at a shear strain of 0.15%, see Figure 28. This threshold of three cycles appears in Figure 29 as the initiation of stiffness degradation. It is the same for all configurations, regardless of the use of caul plates and type of defects. Then, the damage propagates and the same stiffness observations are made without significant change between the response of each configuration.

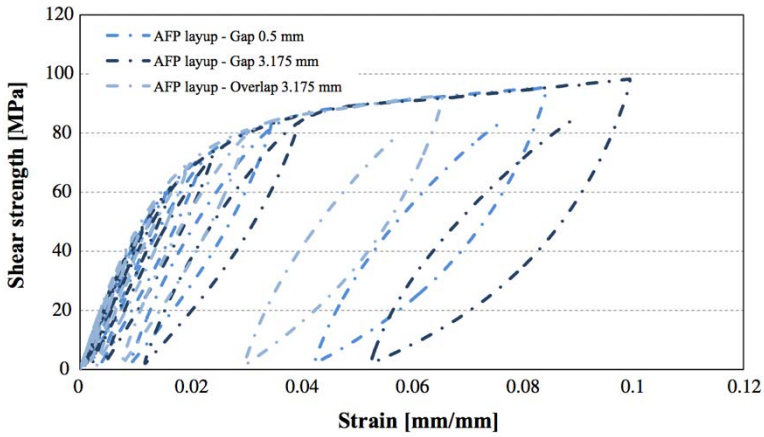

Figure 28 Stress-Strain curve of different configurations under shear cyclic loading [43]

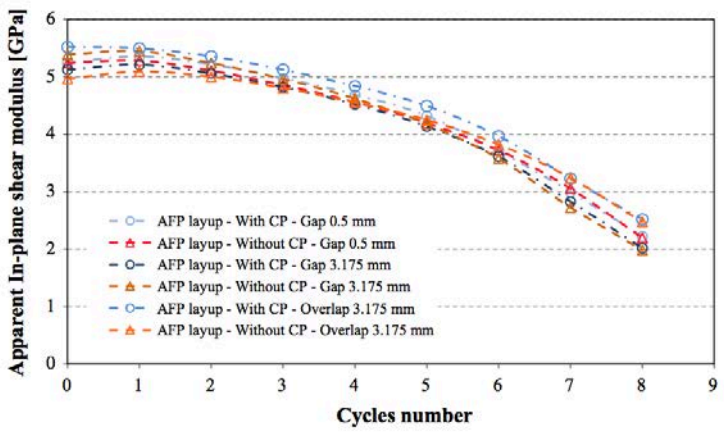

Figure 29 In-plane shear modulus during fatigue life of different configurations [43]

These results show that the embedded defects do not have significant effects on the fatigue response of composite structures under shear loading.

2.4. Conclusion on this literature review

Thus, intensive research was done on the effect of gaps and overlaps and their permutations through experiments and defected specimens but they still represent a small number of all possible configurations [7, 32, 42, 43]. Generally, several defects are required before significant changes happen. The latest developments show the emergence of models that are trying to capture the stiffness and strength performance of tested specimens [13, 33]. Unfortunately, most of these studies do not represent the true geometry of a steered tow creating a half gap / half overlap defect. In past studies, gaps or overlaps were sometimes called "dropped tows" since they spanned the entire dimension of a part. Overlaps tend to have positive effects on both buckling and compression strength while gaps tend to reduce the strength in tension and compression. The effect of both in-plane and out-of-plane fibre waviness has not been thoroughly investigated in the past [3, 13, 40]. The effect of manufacturing parameters, especially the use of caul plates during the consolidation of composite panels, can have an important effect on mechanical performance [26, 27, 42, 44]. The addition of both gaps and overlaps in the same specimens tends to have a more severe effect than single gaps or single

overlaps [7, 13]. This research is putting emphasis on a specific half gap / half overlap defect with a particular geometry, as shown in the schematic Figure 9. This configuration is chosen because it is one the most commonly observed defects in AFP structures. Fatigue resistance of side-to-side gaps and overlaps has never been studied in the literature yet, only single gaps and single overlaps have been studied by Lan [43] and Elsherbini [50, 51, 60].

This thesis develops the empirical investigation of half gap / half overlap defects by establishing a test plan allowing the analysis of orientation, location, and size of defects embedded in tested specimens. Specimens are cured with caul plates to achieve even total thickness throughout the laminate. Each specimen is documented, especially its failure mode under both tension and compression loading. An FEA model aims to predict both structural behavior at the defect level and crack initiation and propagation. This model is a first step to a fully implementable strength prediction tool for composite components made by AFP, which could eventually lead to a virtual optimization tool to be used by engineers. It will allow less experimentation and pave the way for virtual certification techniques of parts made by the AFP manufacturing process. This research gives guidelines on how to design composite structures where defect generation can occur.

3. Test plan

3.1. Layup and defect geometry

The specimens used in this study are carbon fibre-reinforced epoxy composite laminates following a Quasi-Isotropic layup of 16 plies to which one ply of fabric composite is added at the top and bottom, leading to an 18 ply-laminate. Fabric woven plies are added because it is a standard practice developed in the industry, especially at the industrial partner of this thesis. The unidirectional prepreg is T800S/3900-2C and the cross ply woven fabric is T400/3900-2. The layup is $[45\mathrm{F}/(-45\mathrm{T}/0\mathrm{T}/45\mathrm{T}/90\mathrm{T})_2]_s$ where "F" stands for Fabric and "T" stands for Tape. Specimens are manufactured with an Automated Tape Laying (ATL) machine at the National Research Council center in Montreal and cured with caul plates. An ATL machine works on the same principle as an AFP machine, especially for flat panels, as explained in the introduction section of this thesis (see section § 1.3. ATL/AFP Manufacturing Techniques). Defects are manually added to the laminate by stopping the ATL machine at each ply of interest. The manufacturing steps are detailed in the next section of this thesis.

Previous studies were mostly performed on idealized geometries, where overlaps and gaps were rectangular blocks of respectively superimposed and missing tows, spanning the entire width of the specimen [7, 13, 33, 40, 42, 43]. Moreover, processing changes the geometry of those defects of the composite part by squeezing flow and bleeding flow due to debulking during the manufacturing process, the presence of a caul plate, and heating and compaction during the cure [26, 27, 44, 45]. The defect geometry that was chosen in the current set of experiments is commonly seen in industry as the closest representation possible of true half gap / half overlap defect made by an AFP machine [25]. The defects being examined in this thesis occur when one of the tows becomes misaligned, see Figure 11. This misaligned tow momentarily crosses over onto the tow beside it on the same ply. This adds local in-plane

waviness in the specimen. Half gap / half overlap defect ends up having a trapezoidal shape, see Figure 30. It is important to pay attention to the definition of the defect width definition which corresponds to the gap or overlap width used to steer the tow off its pristine path. The gap and the overlap should have the same geometry before the cure cycle. This shape is used in the finite element model, section § 6 Modelling of this thesis, upon modifications made after observations of post-cure micrographs, see section § 5 Microscopy.

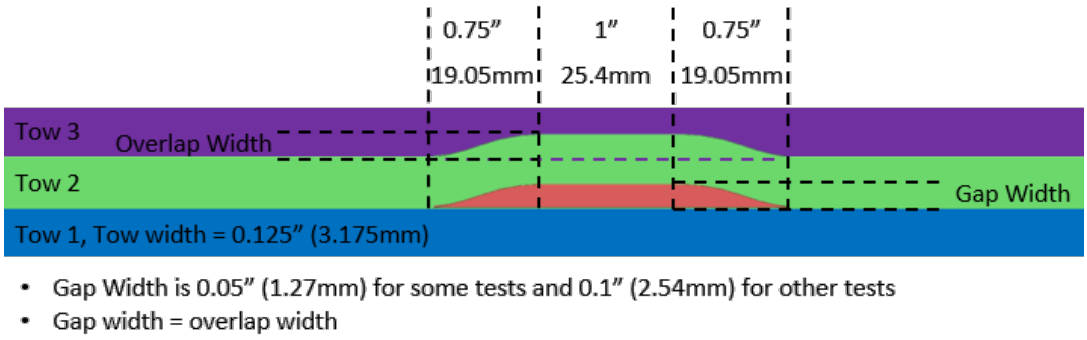

Figure 30 Half gap / half overlap defect geometry [4]

This geometry represents the pre-cured defect geometry before compaction and heat are applied on the panels. It is expected that these dimensions shown in Figure 30 will be different post-cure as it has been observed in the literature [6, 7, 13, 26, 42-44, 65] due to shear flow. This type of half gap / half overlap defect is also expected to have major fibre and resin flow from overlap rich fibre content to gap low fibre content area because the two regions are side by side. Waviness is also expected to be important through the laminate thickness because of the proximity between gap and overlap at each defect location. In fact, an overlap locally adds a ply to the stacking sequence while a gap locally removes one ply. The remaining plies on top and below the defect location will adapt their course to this variation, creating out-of-plane waviness.

3.2. Parameters and configurations of interest

The general shape of the half gap/overlap defect shown in Figure 30 has many parameters such as length, width and curvature of the ends. The length of the defects is fixed in order to fit the largest available test fixture [59]. The total length of the defects is 2.5in (63.5mm). Defect gap width is varied between two values: 0.05in (1.27mm) and 0.1in (2.54mm). Curvature is dependent on length and width.

Three different test plans have been defined for compression, tension and fatigue loading conditions. Specimens were also manufactured to be analyzed with a microscope, see § 5. Microscopy. In tension and compression, 5 specimens of each configuration are manufactured while 9 specimens per configuration are made for fatigue tests. These numbers of specimens per configuration correspond to a minimal statistic population needed to study the variation of the results. Also, for fatigue, specimens are tested at different stress levels to build S-N curves of each configuration. Each test plan is composed of configurations varying:

- the total number of defects
- the width of defects
- the orientation of defects

The defined test plan tries to incorporate worse case scenarios configurations with a superimposed sequence of defects that would probably not happen in a real manufactured part. Experimental results of chosen configurations are then analyzed and compared to modelling results in order to validate the model and its assumptions. To understand the effect of each parameter on the performance of composite structures with defects, several configurations are defined by changing one parameter value at a time, see Figure 31 and Figure 32. 6 configurations are chosen for fatigue, 13 configurations for tension and 13 configurations for compression. An additional pristine defect-free configuration is also added for each loading type to be able to compare experimental results of defected configurations to a baseline.

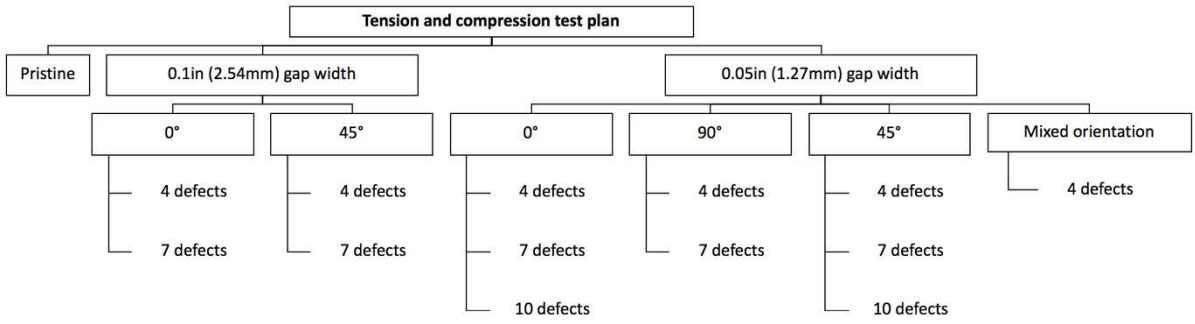

Figure 31 Test plan for static compression and tension

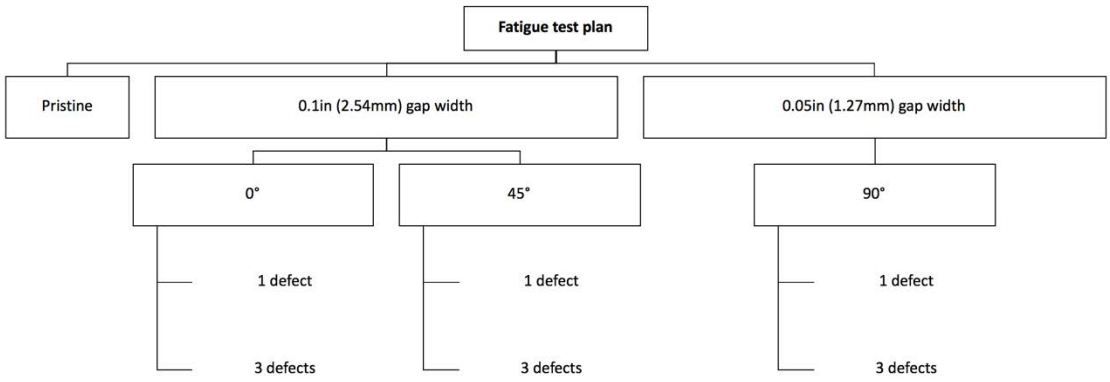

Figure 32 Test plan for cyclic fatigue

Table 3, Table 4 and Table 5 summarize all configurations for tension, compression and fatigue respectively. Chosen configurations have following naming scheme **AGDD.WW** where G stands for "gaps". **DD** refers to the number of defects with gap width of **WW**/10 inch embedded in plies of orientation **A**. Orientation is referred to by a star "*" because it is composed of all four 0°, -45°, 45° and 90° orientations. A similar naming scheme is used for specimens tested under compression and fatigue, though their names start with the letter "C", and finally fatigue uses the letter "F".

A larger test plan would be ideal but it is very expensive in time and money. There was also a lack of available material to make additional configurations, for example in 90° orientation in tension and compression. A manufacturing mistake led to configurations with

0.05in (1.27mm) gap width defects in fatigue while only 0.1in (2.54mm) gap width defects were initially intended. Computational modelling offers the possibility to test more configurations to study a wider range of values for each parameter.

Table 3 Tension test plan

Specimen ID	***No. of defects***	***Orientation of defects (°)***	***Defect width (in)***
pristine	0	N/A	N/A
0G4.05	4	0	0.05
0G4.1	4	0	0.1
0G7.05	7	0	0.05
0G7.1	7	0	0.1
0G10.05	10	0	0.05
90G4.05	4	90	0.05
90G7.05	7	90	0.1
45G4.05	4	45	0.05
45G4.1	4	45	0.1
45G7.05	7	45	0.05
45G7.1	7	45	0.1
45G10.05	10	45	0.05
**G4.05*	4	0, +45, -45 & 90	0.05

Table 4 Compression test plan

Specimen ID	***No. of defects***	***Orientation of defects (°)***	***Defect width (in)***
Cpristine	0	N/A	N/A
C0G4.05	4	0	0.05
C0G4.1	4	0	0.1
C0G7.05	7	0	0.05
C0G7.1	7	0	0.1
C0G10.05	10	0	0.05
C90G4.05	4	90	0.05
C90G7.05	7	90	0.1
C45G4.05	4	45	0.05
C45G4.1	4	45	0.1
C45G7.05	7	45	0.05
C45G7.1	7	45	0.1
C45G10.05	10	45	0.05
*C*G4.05*	4	0, +45, -45 & 90	0.05

Table 5 Fatigue test plan

Specimen ID	***No. of defects***	***Orientation of defects (°)***	***Defect width (in)***
Pristine	0	N/A	N/A
F0G1.1	1	0	0.1
F0G3.1	3	0	0.1
F45G1.1	1	45	0.1
F45G3.1	3	45	0.1
F90G1.1	1	90	0.05
F90G3.1	3	90	0.05

Half gap / half overlap defects are embedded at the middle of the specimens along their length. Locations of defects through the thickness are shown in Figure 33 and Figure 34. The defects follow a stagger through the thickness which keeps a certain balance and symmetry in the defected specimens to avoid unwanted out-of-plane effects.

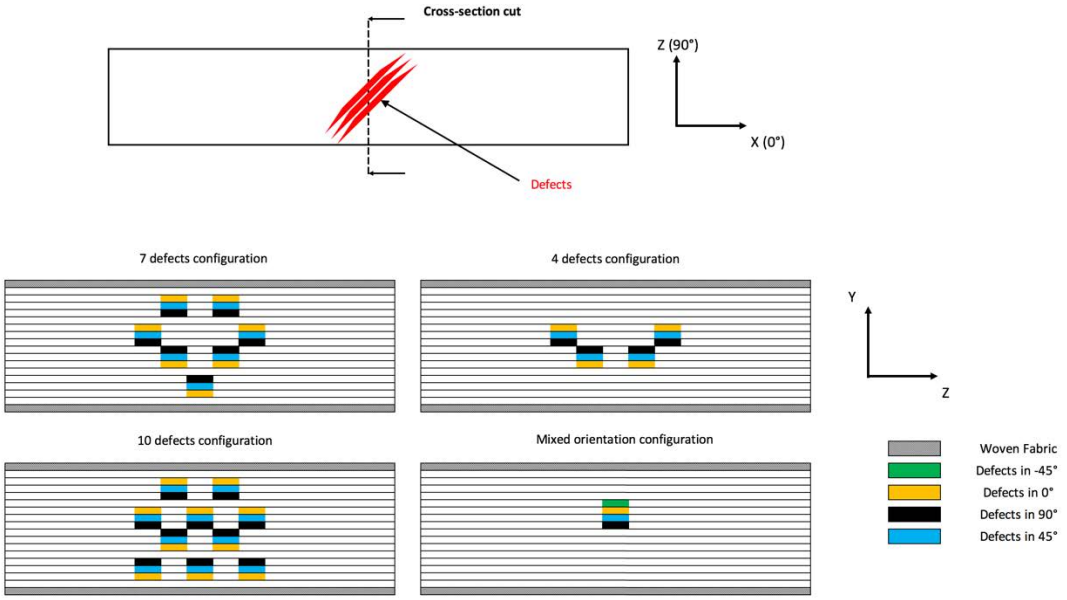

Figure 33 Locations of defects for static tension and compression test plans

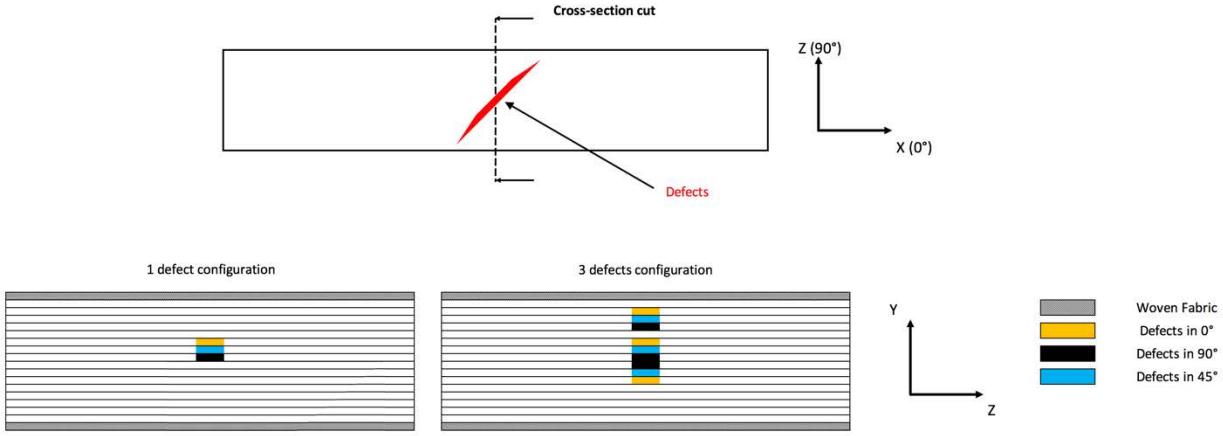

Figure 34 Locations of defects for cyclic fatigue test plan

The mixed orientation and 10-defect configurations are unlikely to happen in the industry on a real part manufactured by AFP process. In the case of the mixed orientations, the motivation is to see if the effect of each defects adds up or on the contrary, whether or not they

neutralize each other. The 10-defects configurations might seem extreme also but this worst-case scenario is pushing the boundaries of the design of experiments plan, which will be used to experimentally validate the Finite-Element model for static tension and compression. These two extreme configurations also increase the number of data points to study the effect of defect density on the strength of manufactured specimens.

3.3. Coupon dimensions

Dimensions of coupons have been chosen by consideration of ASTM D3039 [59] for static tension and ASTM D6484 [66] for static compression and cyclic fatigue. Two sizes of coupons are defined, see Figure 35 and Figure 36. On these two figures, the grip section corresponds to static tension ASTM D3039 [59] loading type while ASTM D6484 [66] has an anti-buckling fixture with a window at the location of defects only as shown in Figure 37. Two ASTM D6484 fixtures of dimensions corresponding to those of coupons shown in Figure 35 and Figure 36 were used for static compression and cyclic fatigue loading. Coupons with configurations that have 0° oriented defects and pristine defect-free specimens have a smaller width than coupons with 90° and 45° oriented defects to reduce the required material quantity for manufacturing. It was believed that the width would not have any impact on the results and on the analysis of the effect of each parameter. Only a minimum edge-to-defect distance was considered to prevent edge-effects during the experiments (see next paragraph).

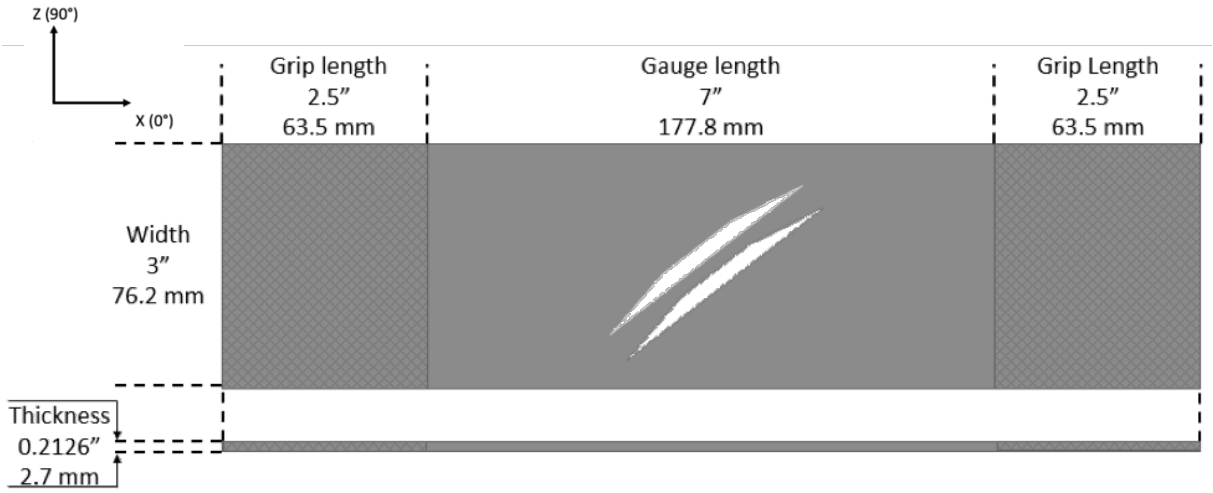

Figure 35 Dimensions for 90° coupons, 45° coupons and mixed orientations coupons [4]

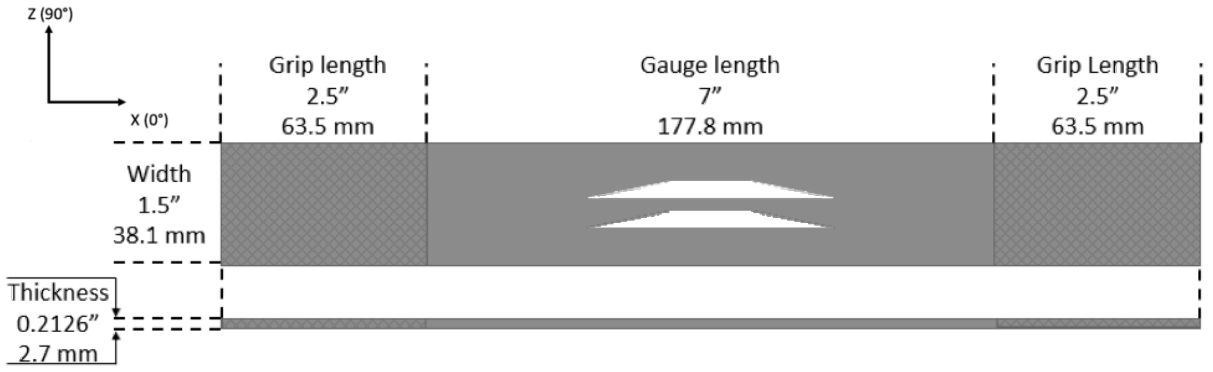

Figure 36 Dimensions for 0° coupons and pristine coupons [4]

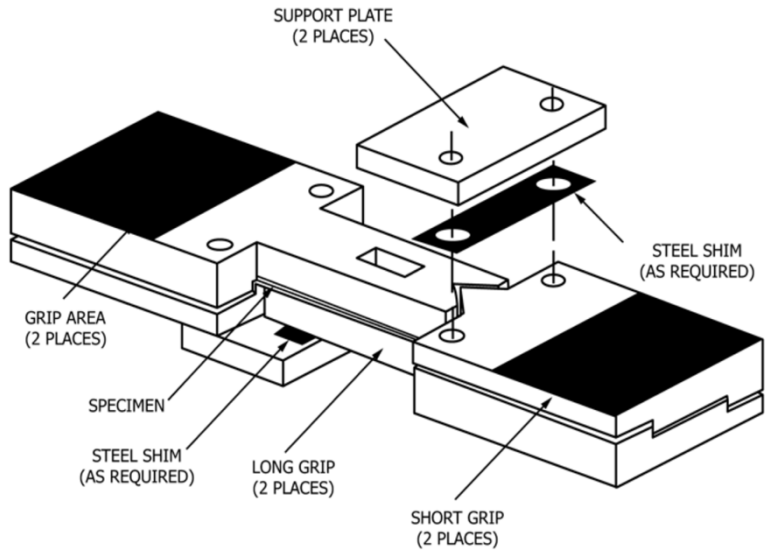

Figure 37 Anti-buckling fixture ASTM D6484 [66] for static compression and fatigue

The edge effects are important to consider during the sizing of experimental coupons because a short defect-to-edge distance can lead to early crack initiation and strength reduction which may not represent the true mechanical behavior of real structures where the defects are generally far from any edges in the structure. In 1995, Lessard et al. [68] built a 3D model to analyze the stress concentration occuring at the edge of composite laminates with varying widths and thicknesses. Their model results are in good agreement with previous work from Becker [69], Lagace and Kassapogolou [70], Pagano and Pipes [71] as shown in Figure 38.

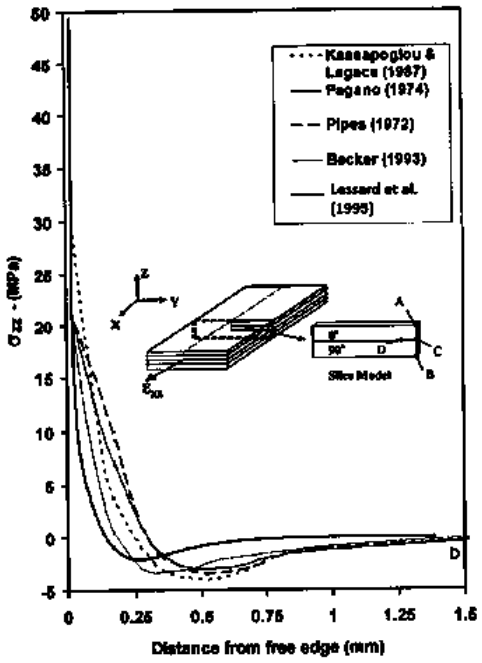

Figure 38 Comparison of edge effects from different studies by Lessard [51]

The model developed by Lessard et al. has a high number of elements near the expected stress singularity, providing more accuracy to the Finite-Element analysis. Results show that the stresses at the free edge are independent of the width (Figure 39) but dependent on the thickness of the laminate Figure 40.

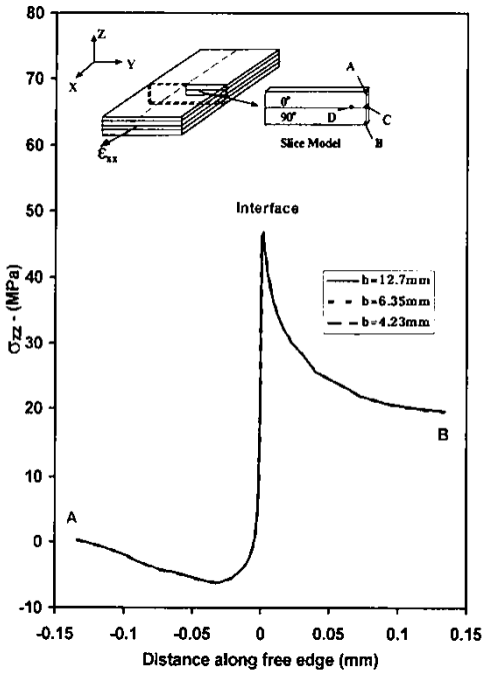

Figure 39 Interlaminar normal stress along AB varying width with constant thickness [51]

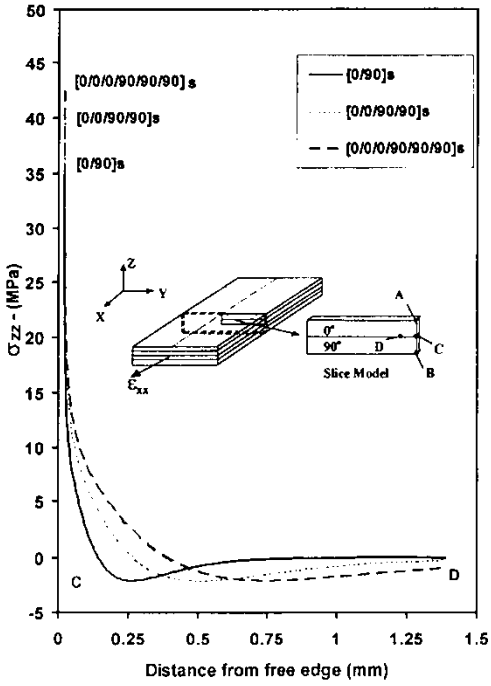

Figure 40 Interlaminar normal stress along CD varying thickness with constant width [51]

The magnitude of stress increases with the laminate thickness. From Figure 40 it is shown that the interlaminar normal stress reaches a plateau at a distance roughly close to 0.9 times the laminate thickness. In other words, at a distance from the edge of 0.9 times the thickness, the laminate no longer sees the edge effect singularity. In order to be safe in the sizing

of the coupons, the dimensions were such that the embedded defects were always further than 1.5 times the thickness away to the coupon edges. Since the layup of interest is composed of 18 plies, this safe distance is estimated to be 0.16in (4mm).

4. Manufacturing and quality control

4.1. Manufacturing

A total of 194 specimens were cut from 6 large panels of 15in (381cm) by 26in (660cm) for tension, compression and fatigue testing. Manufacturing was performed at the National Research Council (NRC) facility in Montreal, while the curing took place at STELIA Aerospace in Mirabel and the cutting was done both at Bell Helicopter in Mirabel and at McGill University.

4.1.1. Layup process and defect generation

At the National Research Council, a 4-axis gantry type ATL machine built by Automated Dynamics was used to lay down composite prepreg on a flat polished stainless-steel metal table bolted to the ground. The prepreg was laid down on a vacuum bag that was set up at the surface of a stainless-steel metal table. The first and last plies (fabric woven prepreg layers) were manually laid down. The robot head can be seen in Figure 41. It can move along X Y and Z axis and also rotate along Z to position the tape in every direction required in the layup: 0°, -45°, 45° and 90°. The tape comes from storage units located at the top of the machine down to the head placement section and it is kept at constant cool temperature of maximum 65°F (18°C). This temperature is referred to as the “creel” temperature. Manufacturing parameters are summarized in Table 6. The nozzle temperature corresponds to the air temperature blown from the hot torch towards the tape at the moment it is laid down. Each panel was manufactured in two to three days. From one day to another the panel was kept under vacuum in a freezer. Panels were carefully thawed to not jeopardize the final panel quality.

Table 6 Manufacturing Parameters

Speed (mm/s)	Pressure (kg)	Nozzle (°C)	Creel (°C)	Room (°C)	Humidity (%)
140	25	100	14	23	34-42

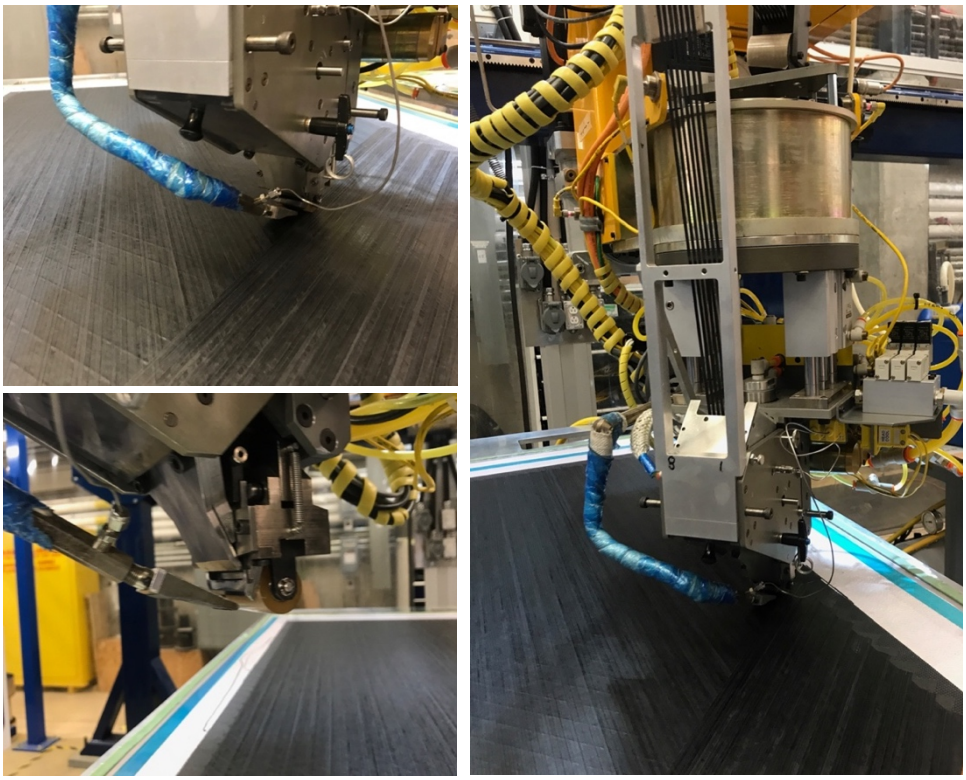

Figure 41 ATL machine head during tape placement at NRC, Montréal

Half gap / half overlap defects are manually embedded in the panels at specific locations. A precise Excel datasheet gathered all locations and corresponding plies at which defects should be placed. After each ply of interest, the ATL machine was stopped and the position of the tow to be steered off its pristine path was marked. Templates made of Mylar sheets were used to find the position of defects, see Figure 42. At this point, each selected tow was carefully segmented, peeled off and placed back to manually create the defect geometry. The segmentation was made in a way that the cuts are not located in any specimen so that no coupon

contained cut tows. A Mylar template of the exact geometry of the half gap / half overlap defect was used to place the segmented tow.

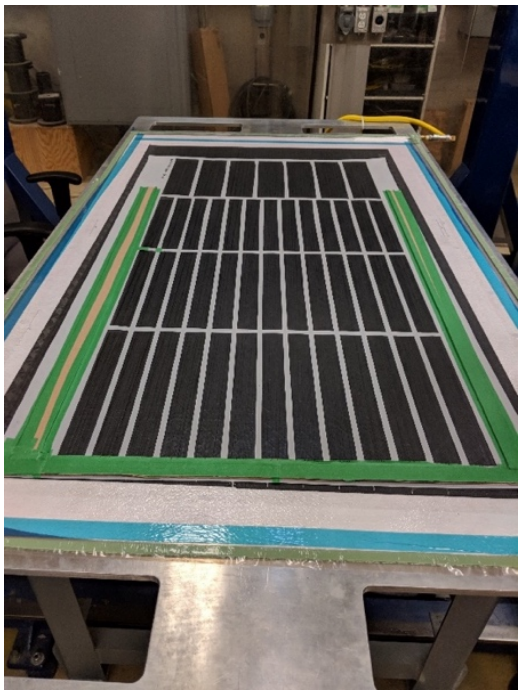

Figure 42 Mylar pattern to mark locations of defects to be embedded [4]

4.1.2. Cure cycle

The cure cycle shown in Figure 43 was given by the resin manufacturer Toray [72]. The finished panels were moved from the table where they were manufactured and placed onto polished caul plates, see Figure 44. The bagging process is shown in Figure 45. Quality of the bag was checked prior to curing as the leak rate should be less than 2.0" Hg (6.77 kPa) over 5 minutes. Panels were cured with caul plates in an autoclave at controlled temperatures profiles monitored with thermocouples placed in the layup. A pressure of 85 psi and a temperature ramp of 3°F (1.7°C) to 350°F (177°C) were applied for 130 minutes. The panel curing was performed at STELIA Aerospace under Bell Helicopter supervision. Hard tooling with caul plates were used. Due to the presence of hard tooling, there is an increased compaction pressure at overlap areas and a reduced pressure at gap areas. This tooling minimizes the waviness on the outer plies especially in the defect regions.

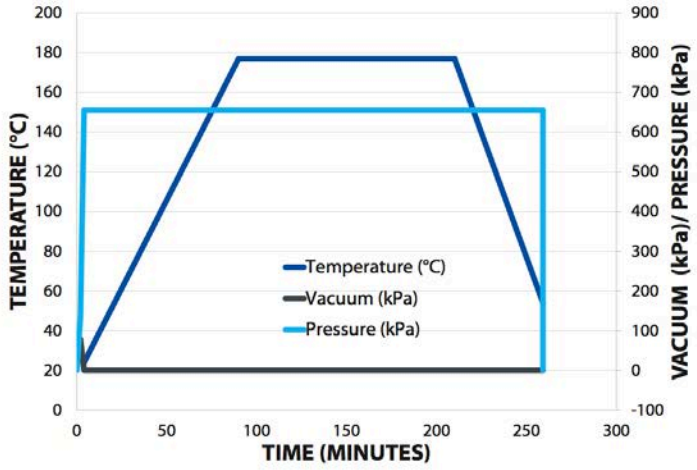

Figure 43 Cure cycle temperature and pressure [72]

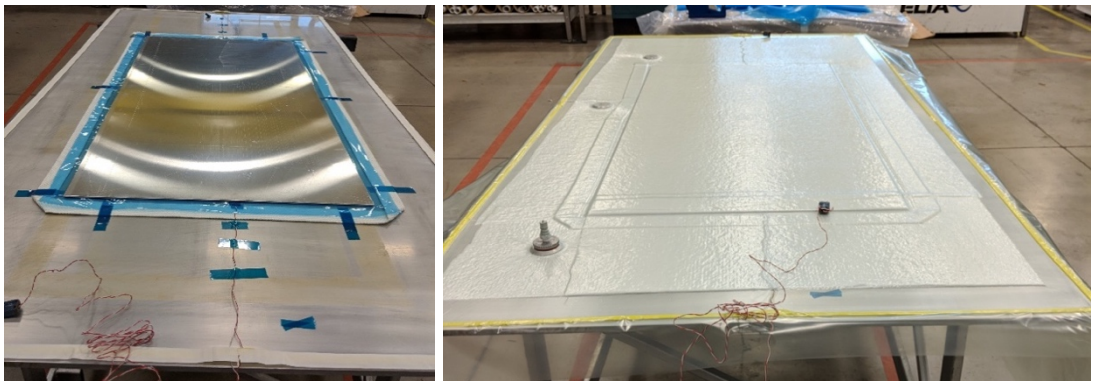

Figure 44 Composite panels with vacuum bag and caul plate ready to be cured [4]

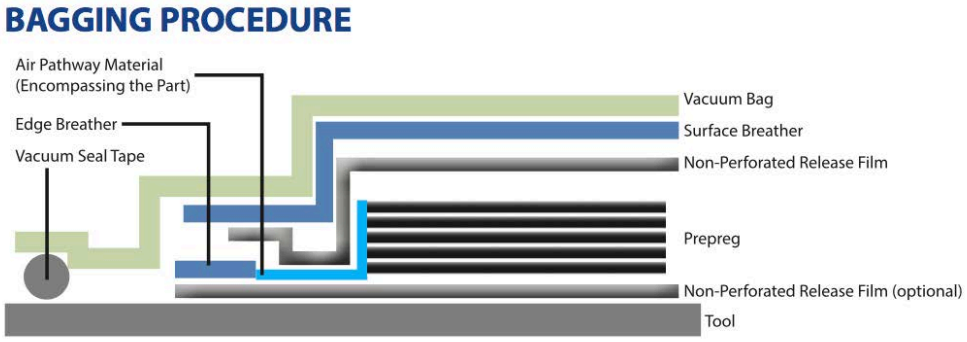

Figure 45 Bagging process [72]

4.1.3. Cutting

After curing, the panels were marked with lines to cut each coupon separately, see Figure 46. Panels were first cut into three pieces at Bell Helicopter's facility in Mirabel and then each specimen was cut from the panels at McGill University using a 2.5 mm thick diamond blade on a wet table saw designed for composite structures.

Figure 46 The Author drawing lines to mark each individual specimen prior cutting

4.2. Quality control

4.2.1. Panel visual inspection

Even though the ATL machine was used on a flat surface, some features and defects happened during the lay down process. A lot of attention was necessary at any moment of the laying down process to check the quality of the panel. Each ply was inspected and every spotted defect was manually corrected without damaging nearby plies. Among the defects naturally generated by the ATL machine were fuzz and bumps as shown in Figure 47, also unwanted half gap / half overlap features, see Figure 48. A fuzz is a small bump of a tow that appears because of a debris located right underneath the prepreg. It can be dust or rich resin pockets.

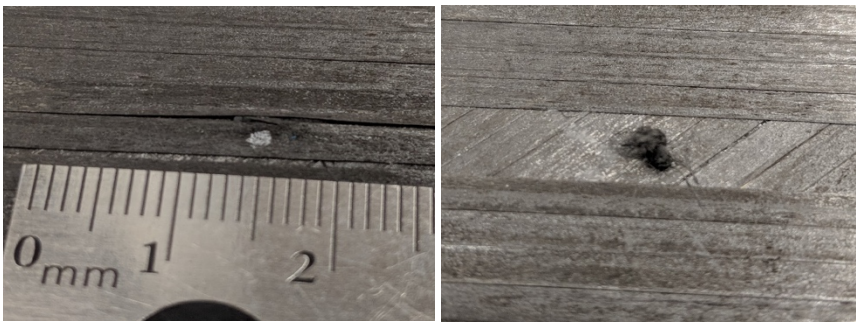

Figure 47 Unwanted fuzz defect on the left and the dust that created it on the right [4]

Figure 48 Half gap / half overlap unwanted defect

During the manufacturing, defects were manually embedded using a Mylar sheet cut to the exact wanted dimensions. However, the execution is not perfect since the Mylar pattern could fold when the segmented tow was steered down. Pictures were taken to evaluate the accuracy of the lay down process and compare with the drawing in Figure 30. This analysis shows an average 4%-dimension variation along the width of the defect and 8% variation for the length of the defect. Below, Figure 49 is a picture of an actual half gap / half overlap defect during tests for using the Mylar sheet pattern (this Mylar sheet is not represented in Figure 49). The dimensions of the defect in Figure 49 should be compared to Figure 30.

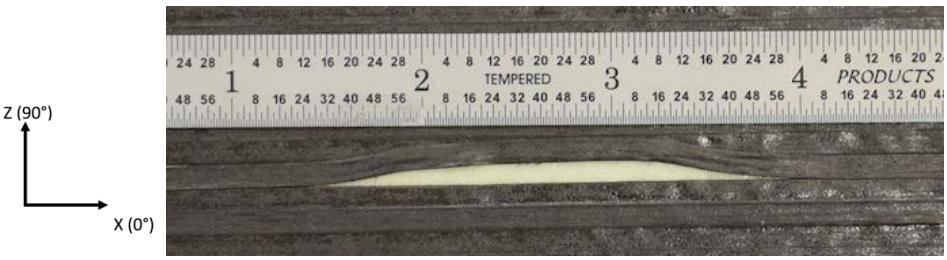

Figure 49 Defect manually created with Mylar sheet

The specimens were checked to verify their dimensions, edges quality after the cutting process and the absence of delamination. In section § 7 Results and discussion the Author explains the test methods for tension [59], compression [66] and fatigue [66]. Width and thickness of each specimen have been measured with a caliper at both ends and middle. Data gathered on all 194 tested coupons enables an analysis of the accuracy of the cutting post cure cycle. Cutting was very precise since from 2.1% to 4.5% average error to objective dimensions was measured on the width of all specimens. The average thickness is consistent at the three locations of measurement and close to the expected thickness. Another important analysis is the variation of width along each specimen, from one end to the other. The width of the specimens varies in each coupon by an average of 0.3% for large coupons and by an average of 0.7% for small coupons. The small variation of width along each coupon should not have significant effects on the mechanical behavior of coupons. Results of this analysis are summarized in Table 7.

Table 7 Analysis of specimen dimensions

	Coupons with 90°, 45°, mixed orientations defects		Coupons with 0° defects and pristine configuration	
	Width	Thickness	Width	Thickness
Objective (mm)	76.2	2.718	38.1	2.718
Average measured (mm)	75.4	2.7	36.4	2.7
Error to objective (%)	2.1	0.7	4.5	0.7
Maximum variation (%)	10	1	5.5	1
COV (%)	2	0	1	0
Average COV along each specimen (%)	0.3	0.5	0.7	0.5

4.2.2. Non-destructive inspections

In order to ensure that no unwanted defects appeared during the cure cycle, different non-destructive methods were applied [50, 73]. Thanks to the help of the Research National Council in Ottawa, 5 randomly chosen specimens of different configurations were analyzed using X-Ray, thermography and ultrasonic scanning methods. X-Ray is expected to show the presence of unwanted non-composite particles in the laminates [73].

Ultrasonic scanning measures time difference between the emission of acoustic signals and their reception by reflection on material surfaces. A singularity in the reception of the signal means that the acoustic wave went through non-even material of different properties. This means for example that gaps and overlaps will appear differently because their constitution is different to the rest of the laminates [73].

Thermography is a non-contact method that detects difference of temperatures on a specific surface. Since gaps are rich resin regions and overlaps have high fibre volume fraction it is expected that the energy stored in each region is different from each other. IR Thermography was used to detect defects [73] in fibre glass panels [74], carbon/carbon composites [75] and carbon/epoxy [58]. The detectability of defects decreases linearly by increasing the depth, and also increases with larger damage area. Since the depth of defects is an important parameter to detect them by thermography, it is expected that some patterns (Figure 31 and Figure 32) of embedded defects would not be clearly visible. Also 0.05in (1.27mm) wide defects might not be as visible as those 0.1in (2.54mm) wide.

From this non-destructive analysis, it was expected to see embedded defects and to be able to check their locations and to determine the eventual presence of unwanted defects like single gaps and/or single overlaps. Figure 50 shows the pictures from the IR camera and some embedded half gap / half overlap defects that were spotted, using red circles to highlight. Only 45G7.1 and 90G7.05 specimens have their defects clearly visible in their corresponding

orientation. It is not possible to count the number of defects, but they are present at the location they are expected to be. Specimen F90G1.05 has an apparent fuzz remaining highlighted with a blue circle in Figure 50 even though visual inspection during manufacturing was supposed to remove all of these types of defects. X-Ray images in Figure 56 do not show any defect in any of the analyzed specimens. The fuzz that was observed on IR images is not visible through X-Ray inspection. Ultrasonic inspection technique gives images of the different embedded half gap / half overlap defects especially in configurations with 0.1in (2.54mm) wide defects in Figure 51 and Figure 53. Thinner defects of 0.05in (1.27mm) width are less visible in Figure 52 and Figure 54 than wider defects. Also, in the case of configuration F90G1.05 there is only one defect embedded so its image on the picture is not as pronounced as for configurations with more defects. The mixed orientation configuration in Figure 55 is not clear either because defects are both thinner and in different directions so their visualization is more diffused.

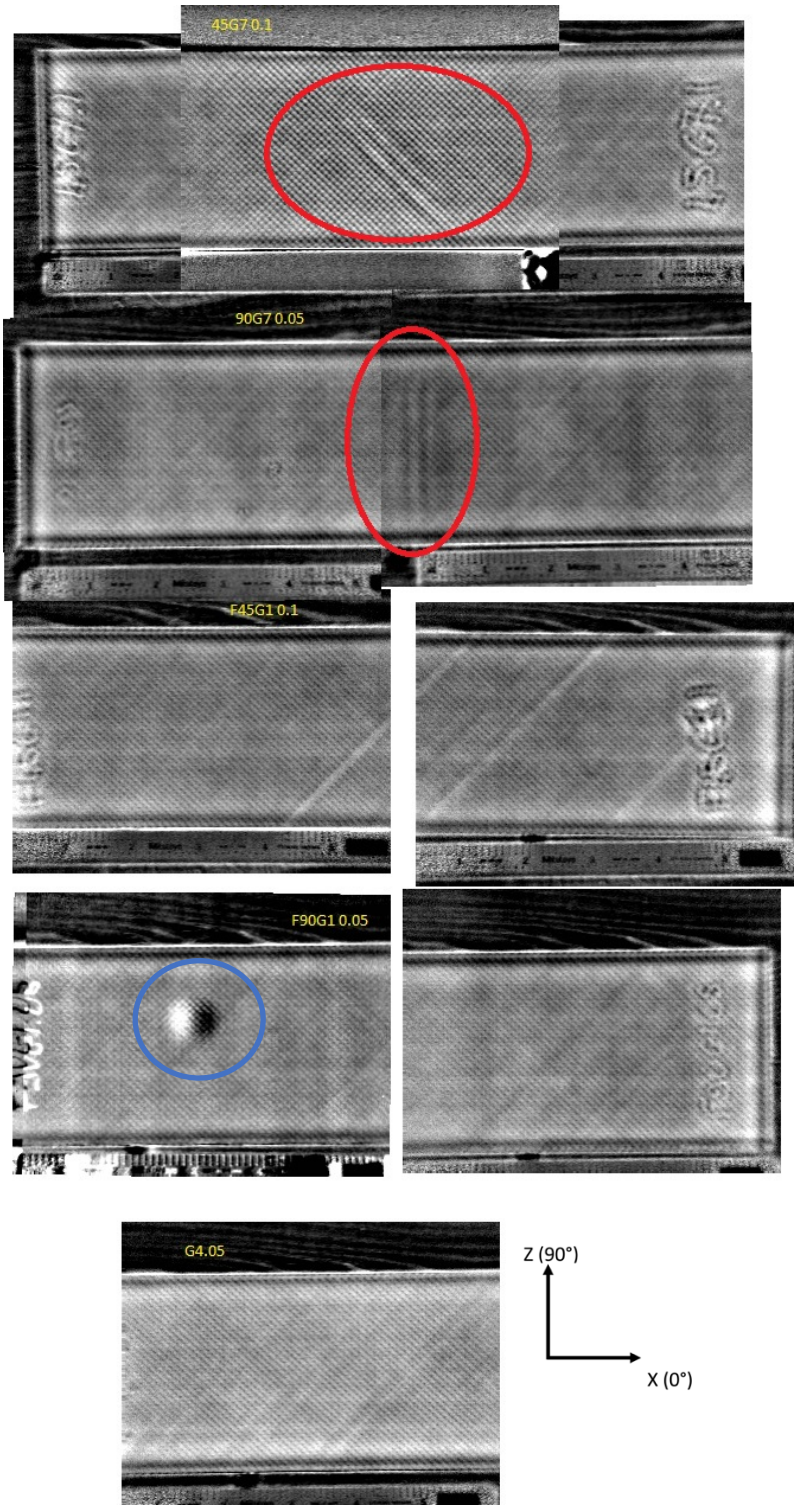

Figure 50 IR Thermography inspection

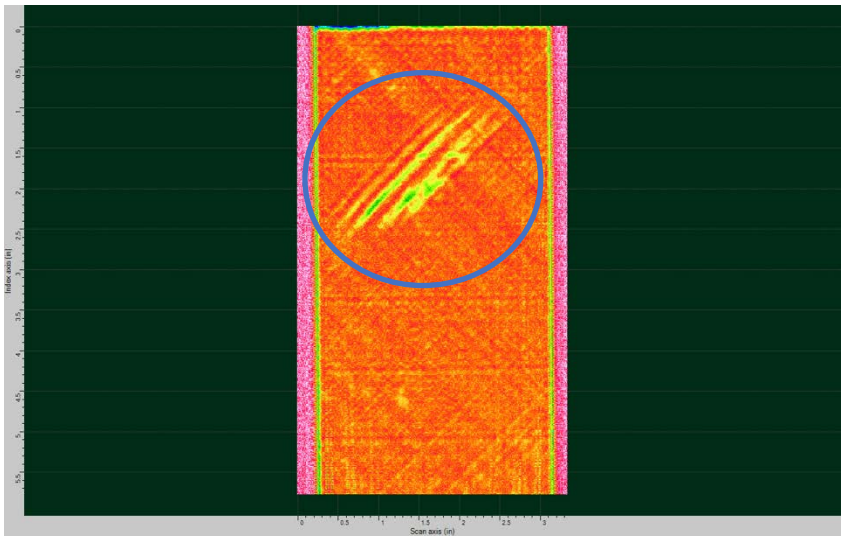

Figure 51 Ultrasonic technique: 45G7.1

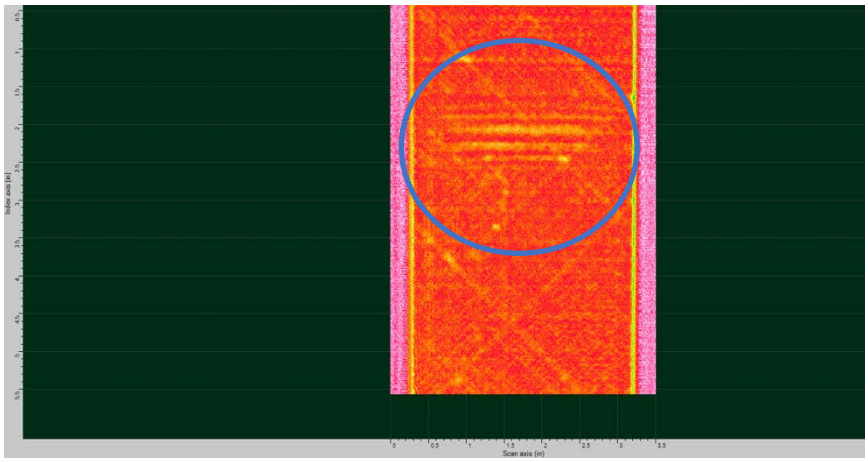

Figure 52 Ultrasonic technique: 90G7.05

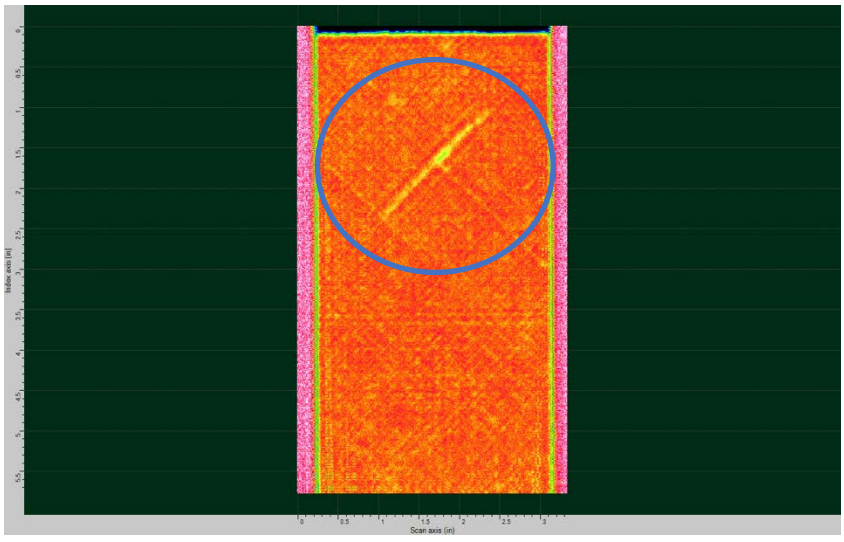

Figure 53 Ultrasonic technique: F45G1.1

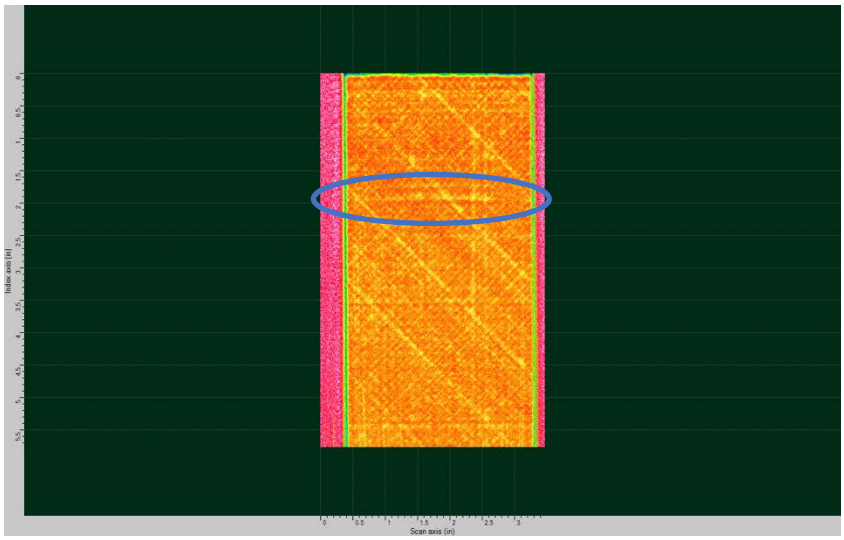

Figure 54 Ultrasonic technique: F90G1.05

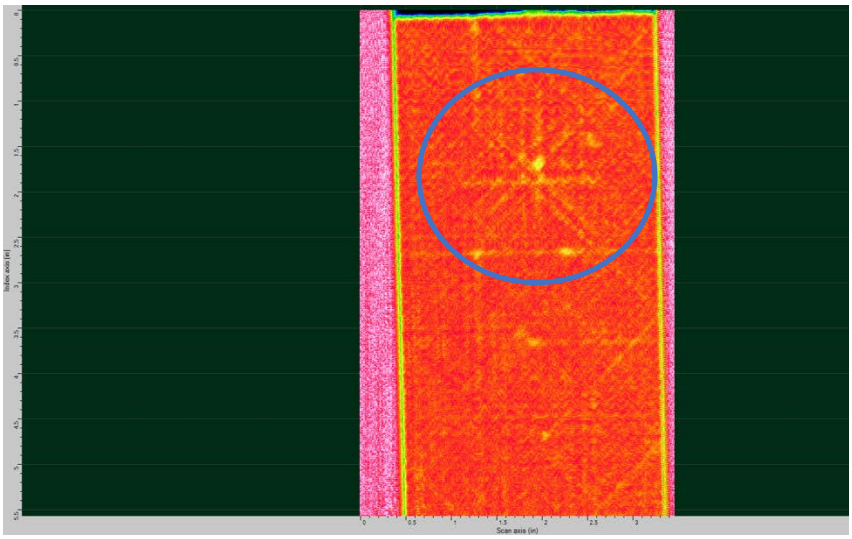

Figure 55 Ultrasonic technique: mixedG4.05

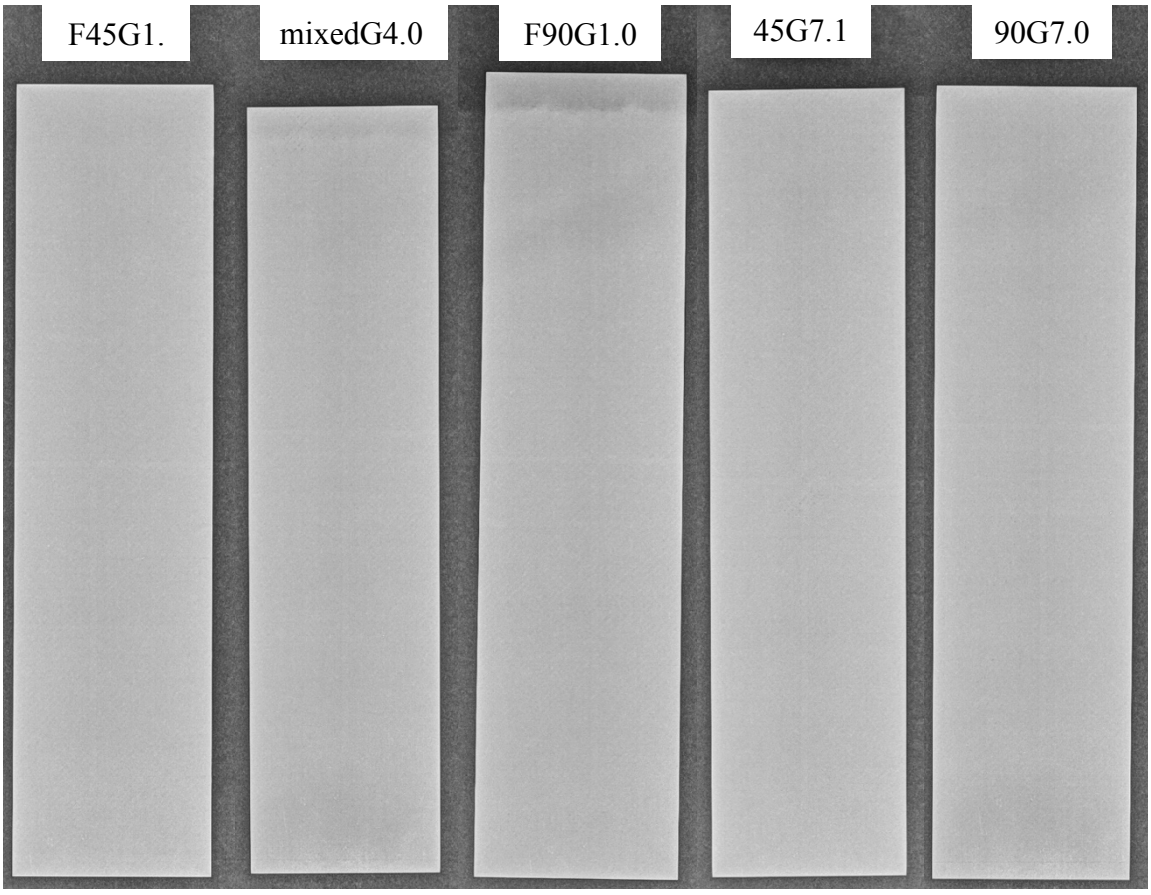

Figure 56 X-Ray inspection

The above in-situ analysis using non-destructive inspection techniques showed that embedded half gap / half overlap defects are present at the right location with the right orientation in the inspected specimens. The size of embedded defects could not be precisely measured because their imprint on the different pictures is not clear enough.

Laminate quality goes beyond just the verification of defect locations. A thorough microscopic analysis is required to check layup sequence, correct through the thickness staggering pattern of defects and overall mesostructure characteristics, see next section § 5 Microscopy.

5. Microscopy

The use of caul plates for compaction during the cure cycle of manufactured panels is expected to have an important effect on the geometry of the half gap / half overlap embedded defects. A lot of work on AFP manufactured defects emphasized the importance of using caul plates to control the overall laminate thickness [6, 13, 42, 43]. A few researchers highlighted the through-the-thickness out-of-plane waviness due to the presence of defects [7, 13, 42, 45]. However, no reference in the literature could be found on the comparison between pre-cure versus post-cure defect geometry. The effects of the number of defects and their staggering patterns on the in-situ out-of-plane ply waviness is also of interest and to be investigated.

In this section is presented the microscopic methodology that was followed to study both real helicopter composite structures given by Bell Helicopter [25] and manufactured specimens. Computer analysis of polished specimen's cross-sections observed with a microscope was performed. Representative helicopter structure and manufactured specimens are compared to each other regarding the following parameters: interlaminar spacing between plies, verification of stacking sequence, fibre volume fraction, and overall mesostructure characteristics. The results of this study are used in the modelling work to accurately represent tested specimens in the Finite-Element simulations.

5.1. Microscopic methods

Sample preparation, casting, polishing and image optical analysis of various composite cross-sections obtained from diamond saw cutting are derived from the recommendations found in specific work related to this material [76, 77]. The followed microscopic methodology is mainly taken from Krumenacker [78] who studied the mesostructure quality of composite corners: waviness and void content. Image analysis methods are described in the Mil-Handbook-17 [79].

5.1.1. Cast preparation

The structure of interest is first dissected using an automated lab-scale wet 15cm diameter diamond blade saw running at 3000rpm and moving at a feed rate of 0.07mm/sec. Cutting lines had previously been marked around the location being investigated. Specimens are carefully cleaned and labelled. The dissected material should fit in a box of 25 × 50 ×20mm, which correspond to the dimensions of the casting limits. Cut sections are positioned in the casting boxes with the face of interest oriented upward. Then, the casting boxes are filled with two-part epoxy resin, degassed during 30 minutes at room temperature, and pressurized for one day at room temperature. This whole process guarantees the quality of the final resin casting by removing all air bubbles and maximizing transparency.

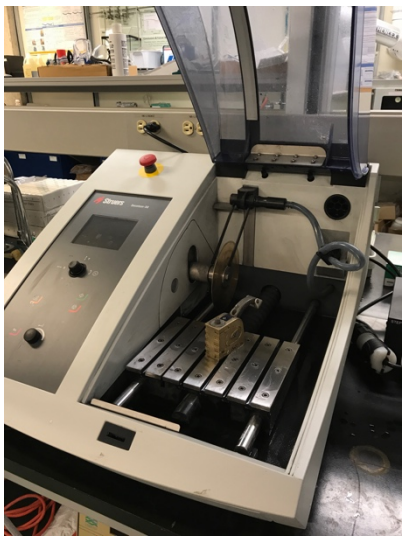

Figure 57 Automated electric saw

5.1.2. Polishing

To prepare the cured epoxy casts for microscopic observation, the surface of interest is polished following a several step process from plane rough grinding to fine polishing. These steps have been thoroughly tested in the literature for carbon composite polymer matrices [79].

Two motorized polishers are used. The first polisher is composed of a turning table with grinding paper at 200-P grit and tap water lubrification. It is used to manually remove evident bulks at the surface of interest. “-P” stands for the European convention of grit sizing. This first polisher is also used to cut the casts’ edges which could damage the second polisher. The second polisher is then used for refined surface treatment. It is an automated labscale polisher with MetLab Forcimat head applying 50N of force on the mounted epoxy casts in contact with a platen of grinding paper. The head and the platen both turn at 150rpm in counter direction and are reversed between steps so that the cast is evenly polished.

Figure 58 Manuel polisher 200-P grit on the left and automated polisher on the right

6 steps of maximum 5 minutes are applied from large grinding to refined polishing: 220-P (68µm), 600-P (26µm) , 1200-P (15µm), 12.5µm, 5µm and finally 0.3µm. Each step aims at removing the scratches made by the preceding one. The goal is to have smaller scratches than the minimal element size of interest visualized using the microscope. The carbon fibre diameter of the specimens is approximately 5µm explaining the use of smaller polishing grits. The last step of polishing can be run for 5 minutes or more, until the surface finish is close to a mirror and that each fibre orientation in the laminate shows a different light reflection. In fact, due to

the heterogeneous structure of composite materials, fibres oriented in the plane of the micrograph reflect much more light than other oriented fibres. The casts are very carefully cleaned in an ultrasonic bath Branson 2510 then dried with compressed air. The polisher automated head is also carefully cleaned between each step using lint-free cheese cloth.

5.1.3. Image capture on a microscope

The polished surfaces are observed using Nikon Eclipse L150 microscope with automated stage and bright light illumination. Two different objectives are used: ×10 and ×20 zoom. The picture resolution with ×10 zoom is 0.581µm/px and pictures have 1920 × 1200px definition with arbitrary chosen exposure, gain and gamma correction values. The software used to control the microscope can take pictures and build mosaics out of several of related pictures in order to get large dimension observations.

The mosaics produced are analyzed using ImageJ software following the image analysis technique found in Mil-Handbook-17 [79]. Thresholds are applied to turn pictures into grey scaled images: resin, voids, foreign bodies and fibres are visualized with different grey tones. The software counts the number of pixels of each color to give for example the fibre volume content and void content. According to Mil-Handbook-17 [79], at least 20 pictures with more than 100 visible fibres have to be analyzed per specimen to get a statistically correct fibre volume content evaluation.

5.1.4. Sources of error

Each embedded defect is located in a tiny zone of each mosaic. This microscopic analysis aims to separately study gap and overlap in each half gap / half overlap embedded defect. As mentioned in section § 5 Layup and defect geometry, a gap in each defect has a maximum width of 0.1in (2.54mm). Thus, it is impossible to gather 20 pictures of each zone of interest and it is unlikely to find 100 fibres in one of them [78].

Other sources of error include poor sample mounting having an effect on the apparent fibre orientation, polishing artifacts, poor automatic threshold quality and insufficient resolution or lighting. Mil-Handbook-17 [79] discusses methods for the majority of the previous errors.

Other methods like chemical matrix digestion techniques can be used to determine the fibre volume content of pristine defect free specimens. However, the dimensions of defect regions are very small. It is not possible to be precise enough with digestion techniques to evaluate the evolution of fibre volume content along the length and width of each defect. Also, imaging techniques can be used to evaluate fibre waviness. CT-Scan techniques could be used to have a 3D representation of a defect to very precisely measure both fibre volume content and orientation along each defect. CT-Scan techniques were not performed for the specimens in this thesis but are suggested as future work.

5.2. Microscopy of a representative helicopter part

The sponsor of this thesis, Bell Helicopter, provided a with few samples from a representative helicopter part made using the AFP manufacturing process. During manufacturing of the helicopter part, an operator examined the quality of the layup at each ply and corrected any defect that was bigger than the acceptable standard used at Bell Helicopter. Maximum width of gaps acceptable is similar to what is studied in this thesis. These samples were analyzed at Bell Helicopter using non-destructive inspection techniques (ultrasonic methods). As described in the section § 4.2.2 Non-destructive inspection, any observed attenuation of signal during the inspection means there is heterogeneity in the composite structure. This feature can be a gap or an overlap or any other type of defect, as shown in Figure 9. As shown in Figure 59, the locations of largest attenuation -6 dB in blue correspond to curved sections which makes sense according to the literature review because the AFP head steering

capabilities are limited. From this observation, 5 samples were cut off for microscopic study, represented in red in Figure 59.

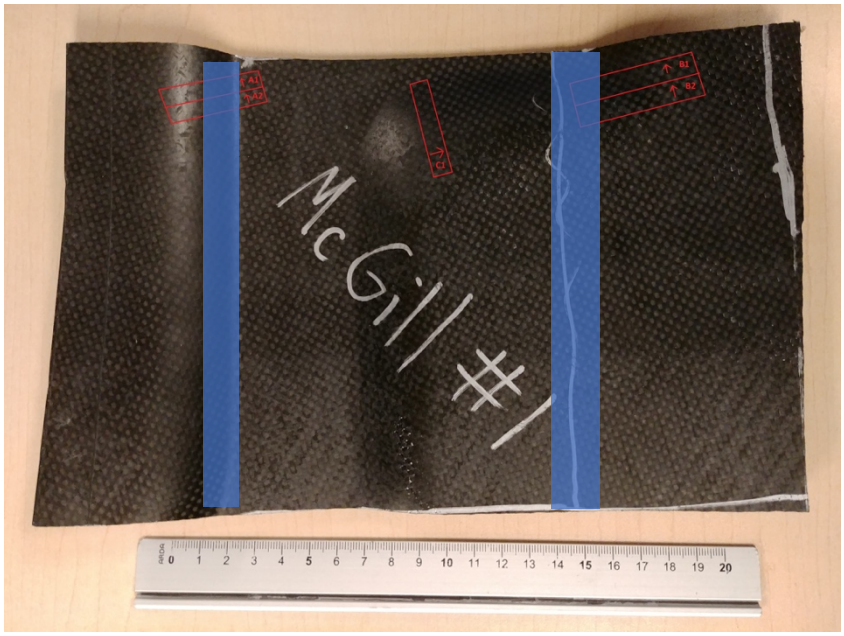

Figure 59 Helicopter representative part given by Bell Helicopter for microscopic study

As explained earlier, no defect was purposely embedded in this part. Any defect would have appeared naturally. A few gaps and overlaps were spotted during observation under the microscope. Figure 60 shows micrographs of cross section with spotted gaps circled in red and green. Gaps in red are filled with resin while green indicates gaps that are mostly filled with fibres due to both waviness and shear flow. The average size of observed natural gaps is 0.04in (1mm).

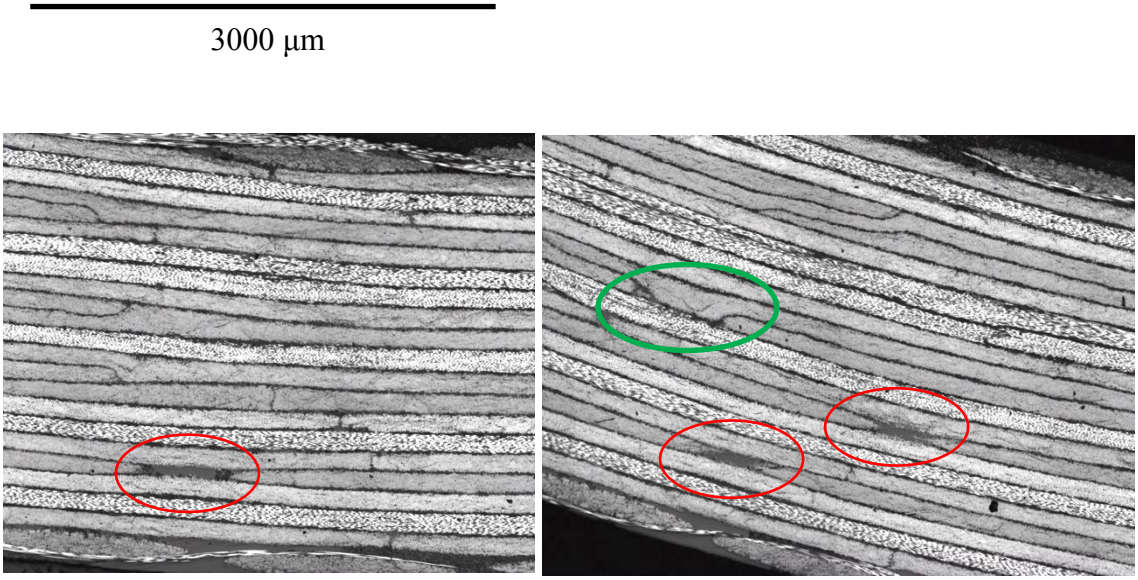

Figure 60 Helicopter representative part cross section with located gaps

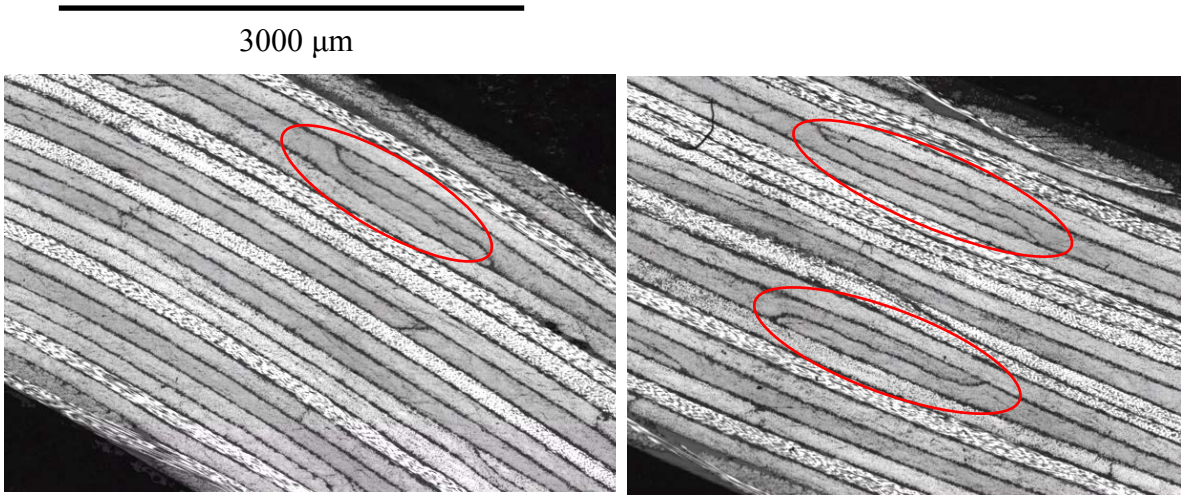

Figure 61 Helicopter representative part cross section with located overlaps

Figure 61 shows other regions of the same micrographs with located overlaps circled in red. The average size of located overlaps is 0.06in (1.5mm). Sometimes, it can be difficult to make the difference between splices and overlaps. However, the defects marked with red circles are overlaps because of the fibre orientation and their size.

Among all other characteristics, the average interply thickness is measured and the stacking sequence of Bell's part is composed of 18 unidirectional plies instead of the 16 used to manufacture experimental specimens. One Fabric woven ply is placed at the top and bottom

of the laminate in both manufactured specimens and Bell's parts. The type of defects observed in the representative helicopter parts, the inter layer thickness and different ply thicknesses are compared to the analysis of manufactured specimens in the following section.

5.3. Microscopy of specimens with embedded defects

The main objective of the following microscopy study on manufactured specimens is to gather information on the real after cure geometry of defects. A quantitative analysis of the change of shape of defects is performed in different configurations. The post-cure average defect geometry will be used in the model presented in the section § 6. Modelling. The effect of defect staggering with different patterns on the out-of-plane waviness is qualitatively assessed by visual observation.

5.3.1. Cross sections of interest

Four different specimens corresponding to four different configurations were selected to perform the study. The four coupons of interest are chosen based on different orientations, number of defects and sizes:

- 45G7.1
- F45G3.1
- 90G4.05
- *G4.05

Each specimen was cut at three different locations transverse to the embedded defects, as shown in Figure 62. Two cross sections are at the sides of the defects and one cross section is at the middle where the defect is the widest. The cross sections on the sides of the defect are located approximately one-third of the defect length away from its middle position relative to a perfectly manufactured defect). Thus, the analysis of these side cross sections will give qualitative information on the healing of the defect and its final length. If no defect is observed

on the sides but it is observed at the middle cross section, this means the defect partly healed on the sides to finally disappear during the cure cycle.

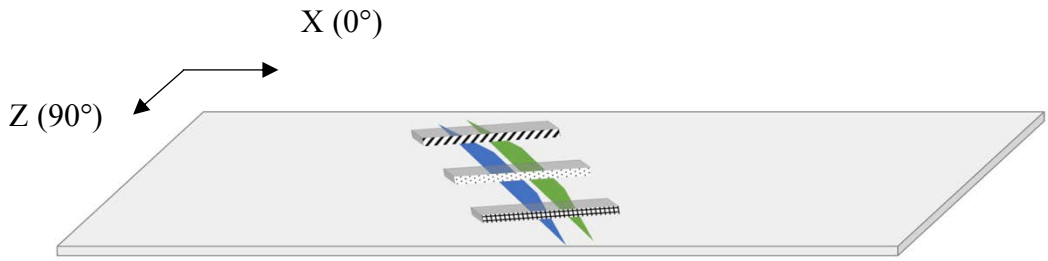

Figure 62 One embedded defect: gap in blue, overlap in green, microscopy sections

Once the three microscopic samples are cut off from their specimen, they are mounted together in the same casting. Each sample is about 1in (25.4mm) long by 0.2in (5mm) wide. *Figure 63* shows the arrangement of the three samples in one casting. The cross-section surfaces of interest which will be observed using a microscope are represented with different drawing patterns corresponding to Figure 62. The two brown rectangles correspond to wood sticks used to keep the three microscopy samples aligned in the casting when the epoxy is poured inside the mould.

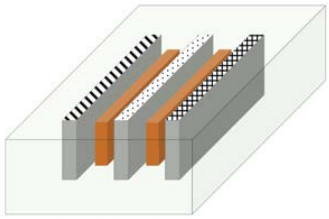

Figure 63 Three-sample casting arrangement

5.3.2. Mesostructure characteristics and comparison to Bell part

Measurements and qualitative observations of micrographs, reveals the real ply size, interply thickness and out-of-plane waviness which all are essential for a better understanding

of the mechanical response to these type of manufacturing defects. These measured parameters will be inputted into the finite-element model.

In Figure 64, highlighted by green circles are the interfaces between tows laid down by the ATL machine which, all together, create a tape and eventually a ply.

Pristine defect-free region of the specimens correspond to parallel plies with constant thickness as show in Figure 64. The 16 unidirectional plies and the top and bottom fabric plies are clearly visible. A zoom-in allows to see the orientation of fibres ply-by-ply and to recognize the layup stacking sequence. Figure 62 which shows that cross sections are transverse to the defect so in the case of 45° defect orientation, fibres of 45° plies will appear circular to the microscope while fibres of -45° plies will be in parallel lines. Fibres of other plies appear elliptic.

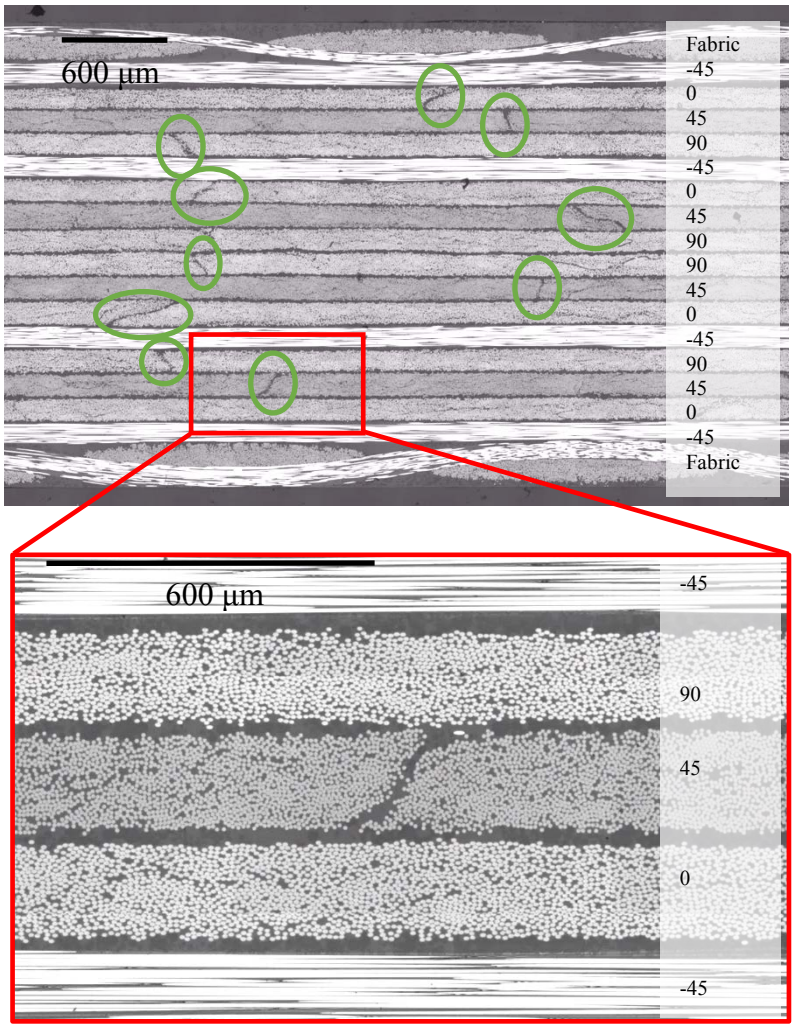

Figure 64 Pristine defect free region micrograph

Another aspect of the mesostructure studied on the micrographs is the presence of a large number of observed grey bubbles between plies. Those bubbles are not voids otherwise the laminate would likely fall apart. The grey color is close to the color nuance of the resin. According to the manufacturer Toray, the epoxy used in the prepreg is toughened with added particulates [72]. These particulates are not located inside a single ply but always at the inerface between two layers. The size of the particulate corresponds to the interlaminar thickness. Two plies cannot get closer because the toughener particulate size is too large to migrate between fibres within the layers themseleves. In Figure 65, few interlaminar layers are highlighted by red rectangles and the toughener is represented using a black threshold. There appear to be more

particulates of toughener than resin itself in the interlaminar layer regions. Manufactured specimens and Bell's parts have the same resin and toughener particulates.

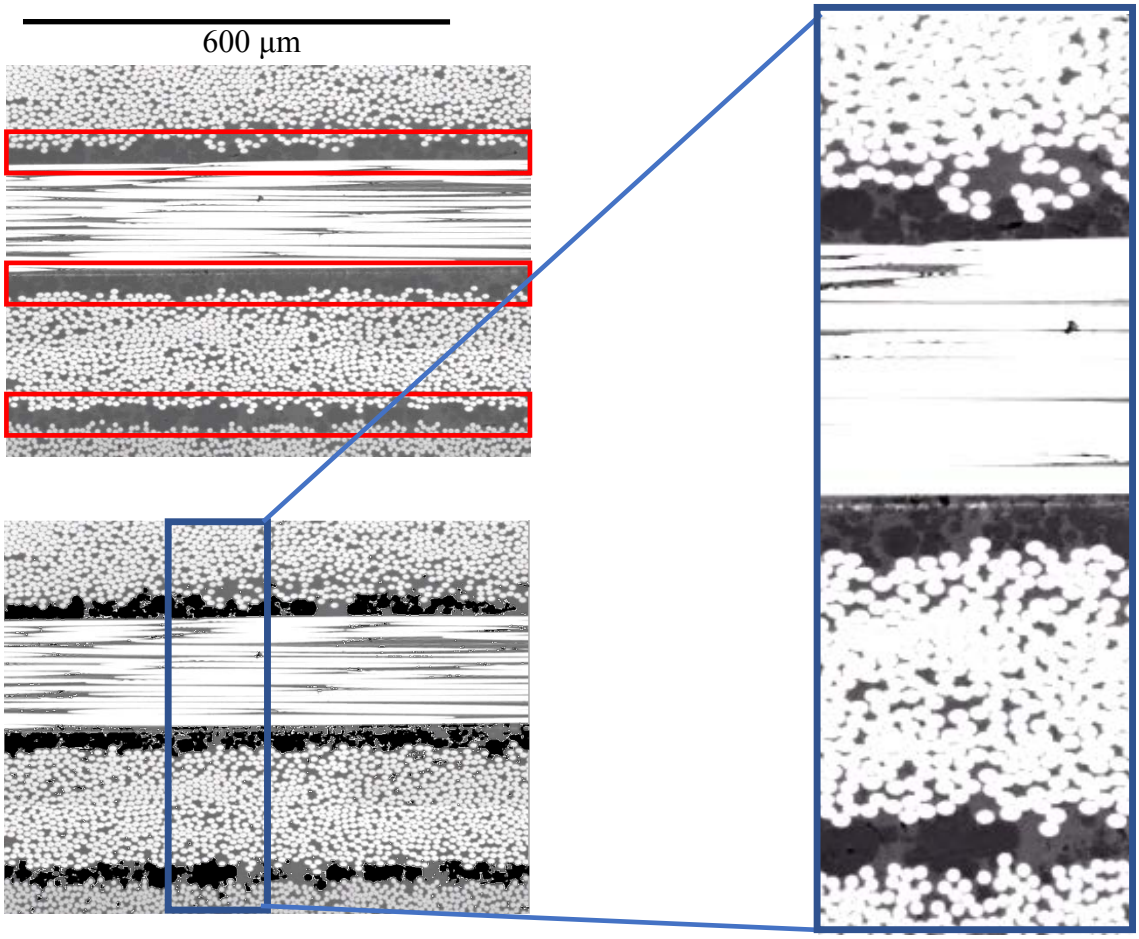

Figure 65 Pristine region - interply layers with toughened particulates

The interlayer thickness was measured at different locations in pristine defect free regions of the micrograph. The average interlayer thickness is close to the value observed in Bell part. Unidirectional plies are found to be a bit thinner by 10% than the corresponding value found on the manufacturer datasheet while fabric are found thicker by 20%.

5.3.3. Defect post-cure geometry

From the four specimens studied with the microscope, only two showed visible defects in the cross sections analyzed: 45G3.1 and 45G7.1. The mixed orientation *G4.05 configuration is difficult to analyze because, as shown in Figure 62, the cross sections are transverse to the defect. However, 4 different orientations are present in *G4.05. The cross sections were made at -45° to see +45° defect. No defect was visible on any of the three cross sections of *G4.05. The micrographs revealed an organized mesostructure without waviness, with only a few small overlaps – probably splices – at the middle cross section. For the 90G4.05 specimen, the cross sections were made at 0° along the length of the specimen but none of the three micrographs showed any defects. No clear overlaps or gaps were visible. The defects were probably located a bit off so that the cross sections did not go through them or the defects healed very well. More micrographs of other configurations should be analyzed in the future to understand the extent of the healing phenomenon of embedded defects during the cure cycle.

Configurations 45G3.1 and 45G7.1 both show all half gap / half defects that were embedded during the manufacturing of specimens. While the middle cross sections – Figure 67 and Figure 69 – show the right number of defects at their expected location, not all the defects appear on the side cross sections. Only one side cross section shown in Figure 70 of the configuration 45G7.1 shows 2 half gap / half overlap defects out of 7 while none are visible for 45G3.1 (micrographs not shown because the laminate mesostructure is pristine). Since defects are visible primarily in the middle cross sections but not always on the side cross sections, it seems that defects have healed due to shear flow of fibres and resin during the cure cycle. It appears that defects smaller than 0.06in (1.5mm) wide at least partially healed during the cure cycle. More configurations of defects 0.05in (1.27mm) wide will be studied in the future to verify this theory on other micrographs.

Figure 66 and Figure 68 highlight the plies in which defects have been embedded during manufacturing process. A half gap / half overlap defect corresponds to a misaligned tow. Since the gap size is smaller than a tow width, the misaligned tow is not entirely overlapping the tow beside it. Before the cure, gap and overlap have the same width. However, on the following micrographs, the size of the gaps is not the same as the size of the overlaps. Figure 71 shows the proposed partitions of a half gap / half overlap defect. An "Overlap" is defined as the actual overlap of two tows. The "Flow" region is a triangle section, formerly of resin, with fibre filling in the gap.

In case of the configuration 45G3.1, the three overlaps are on top of each other, and the three gaps are also on top of each other. The laminate is composed of 18 plies. The overlap overall laminate section is composed of three additional plies (21 plies) and the gap section is logically locally missing three plies (15 plies) but the laminate thickness remains constant everywhere because of the use of caul plates during the cure cycle. While waviness is apparently less important in 45G3.1 than in 45G7.1, the change of geometry is significantly more important in 45G3.1, as reported in Table 8 Amount of geometry change of the average half gap / half overlap defect. The average overlap in 45G3.1 is 31% wider than the pre-cure geometry while the average overlap in 45G7.1 is 24% wider than the pre-cure geometry. Gaps are 23% smaller in 45G7.1 but 40% smaller in 45G3.1 than the pre-cure geometry. This change of geometry is explained by the different ply thickness at the overlap section. The average overlap is 260 µm thick for 45G7.1 while it is 205 µm thick for 45G3.1, thus a difference of 30%. Also, the fibre volume fraction is just 1% different in the overlap sections of the two configurations. However, approximately the same quantity of material is present, only its distribution is different between 45G7.1 and 45G3.1.

Another aspect observed is the shrinkage of interlayers at the overlap section where they almost disappear while resin toughener should prevent the plies to get closer as explained in

the precedent section § 4 Mesostructure characteristics and comparison to Bell part. This suggests that a resin flow carrying the toughener particulates occurs from the overlap section toward the gaps.

Gaps are mostly filled by fibre waviness from above and below plies in 45G7.1 because gaps and overlaps are staggered on top of each other so additional tows in overlaps tend to fill in gaps through-the-thickness. Gaps in 45G3.1 configuration show more resin content than fibre content. Also, the two gaps present in the micrograph of 45G7.1 side section are much smaller and filled with resin. It appears that the plies above and below the gaps do not have enough space to curve as observed in middle cross sections where gaps are much wider, as shown on Figure 70.

Table 8 Amount of geometry change of the average half gap / half overlap defect

Middle cross-sections compared to post-cure geometry	Overlap	Gap
45G7.1	24%	-23%
45G3.1	31%	-40%

Two new regions are introduced as “Flow” from overlap to gap and from pristine ply to gap. The Flow regions correspond to resin and fibre filling in the gaps. These two regions correspond to a gradient from high fibre content in overlaps to low fibre content in gaps. Their fibre volume content is measured from observations with ImageJ software. Flow regions have 6% less fibre volume content than pristine plies.

Figure 72 shows the change of half gap / half overlap defect geometry, pre-cure versus post-cure, obtained from micrograph observations. The pre-cure defect was composed of gap and overlap side-by-side of the exact same size. Since side cross-sections do not always show

the defects observed in middle cross sections, the total length of defect was reduced by 20%. Post-cure gap and overlap have different widths too. Two new regions are defined as “Flow” which refers to a change in fibre volume fraction, gradient from the overlap rich in fibres to the gap, rich in resin. Gaps are not only filled with resin but also fibres coming from ply waviness. Waviness is not always the same from one configuration to another. It depends mostly on the location of the plies with defects through-the-thickness and also on the defect pattern. Finally, this new average geometry and corresponding material properties are used for the modelling part of this thesis.

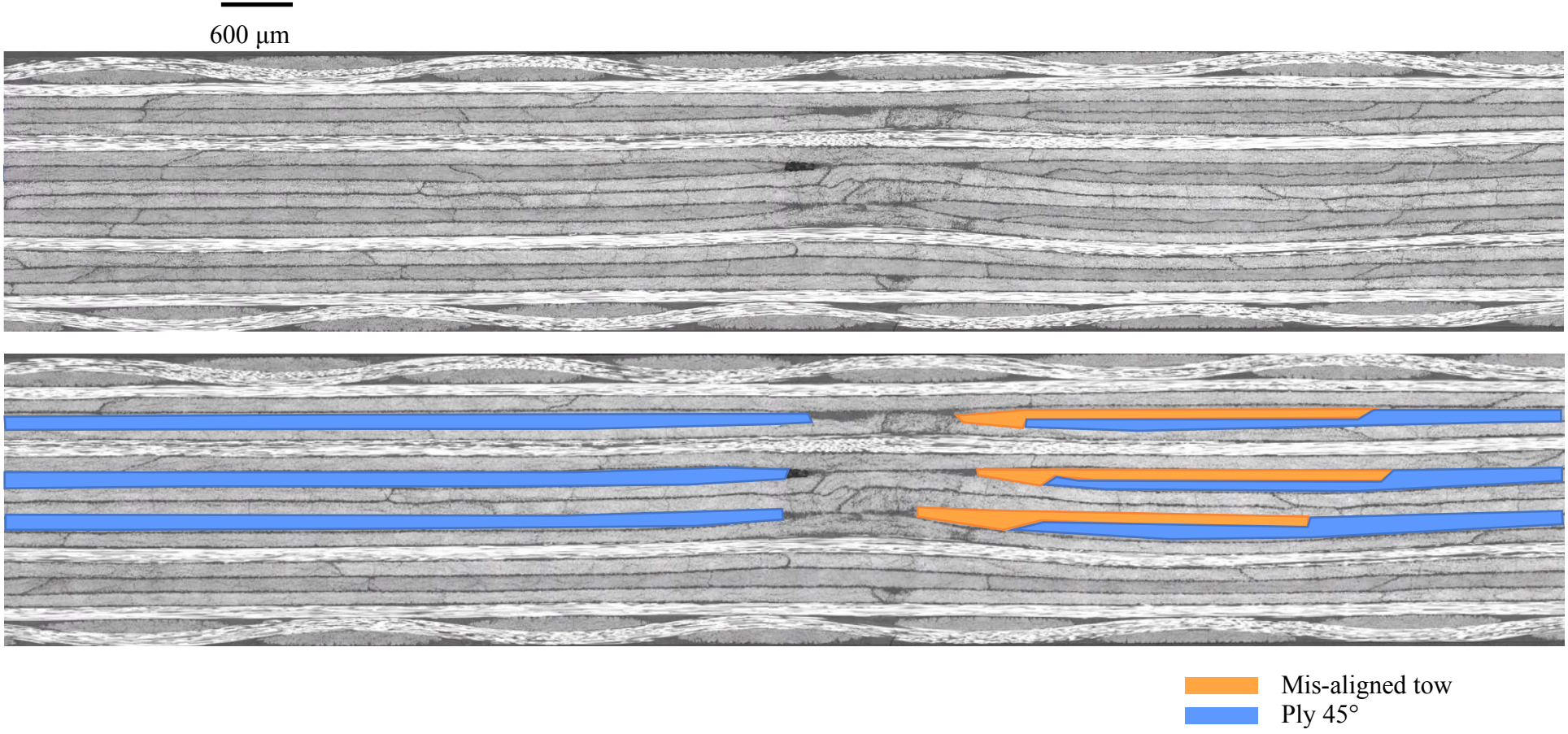

Figure 66 Middle cross section – 45G3.1 highlighted defects

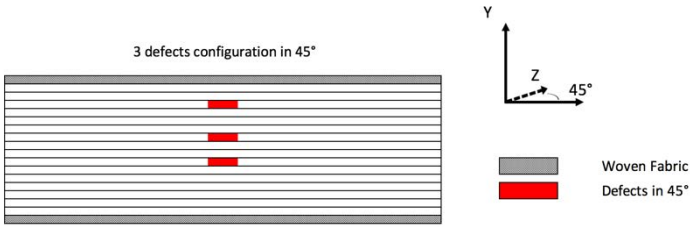

Figure 67 Configuration 3 defects in 45° manufacturing plan

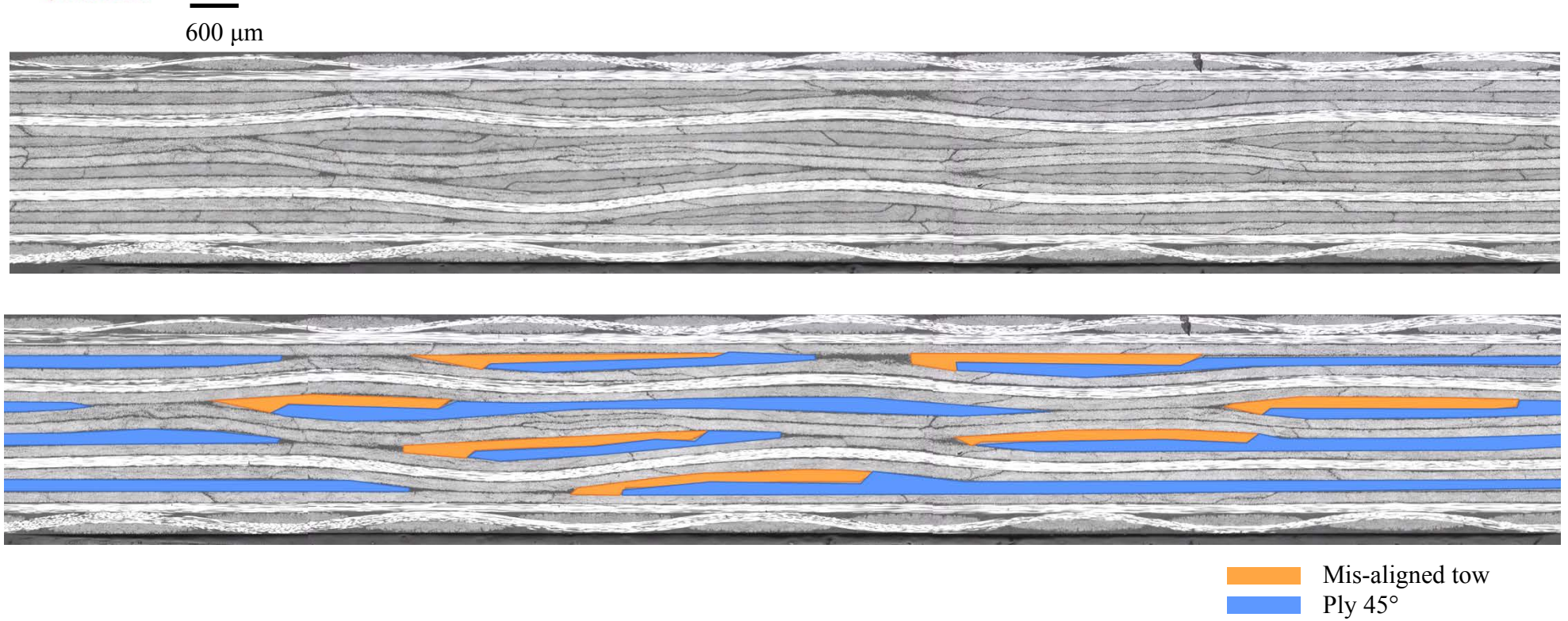

Figure 68 Middle cross section – 45G7.1 highlighted defects

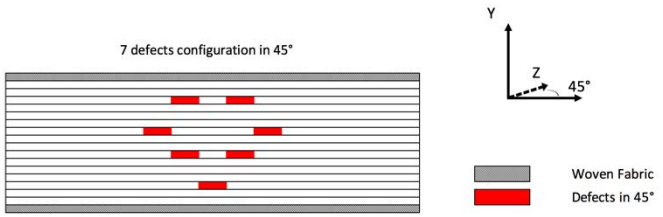

Figure 69 Configuration 7 defects in 45° manufacturing plan

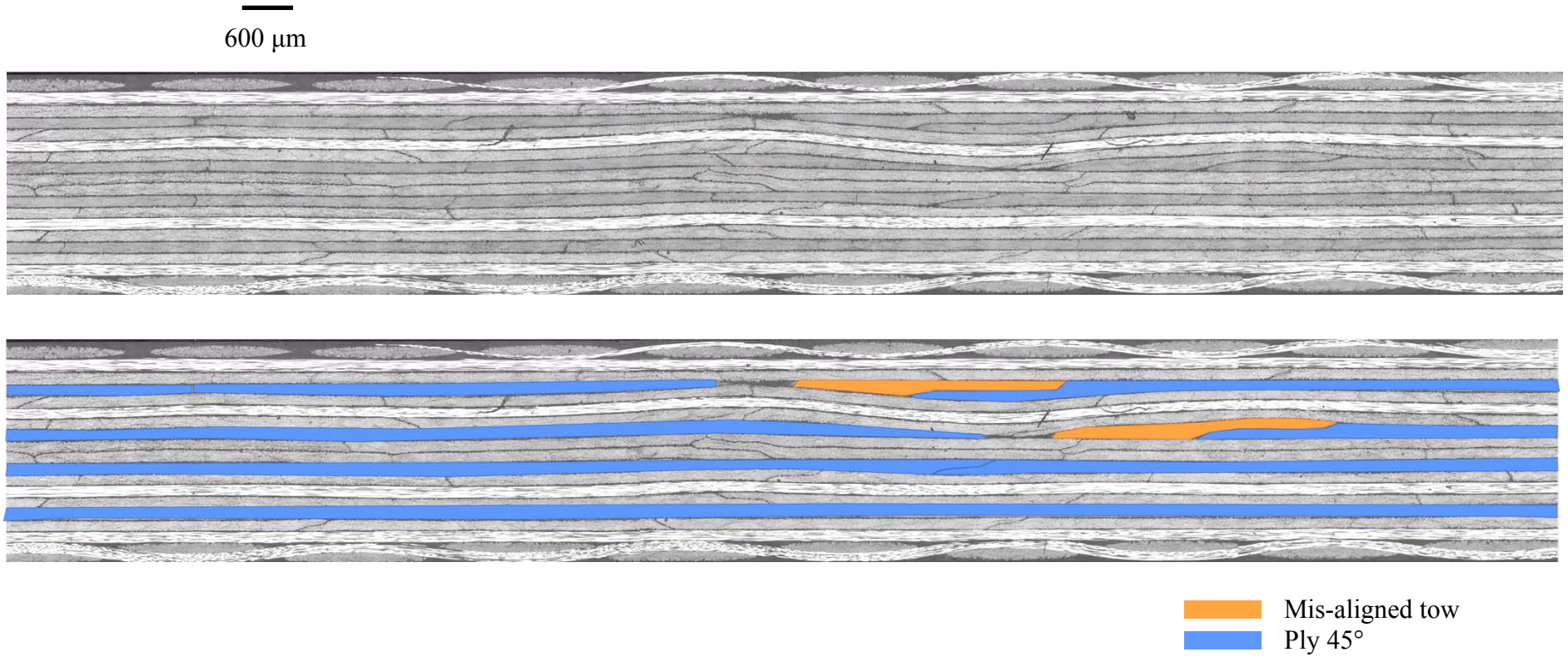

Figure 70 Side cross section - 45G7.1

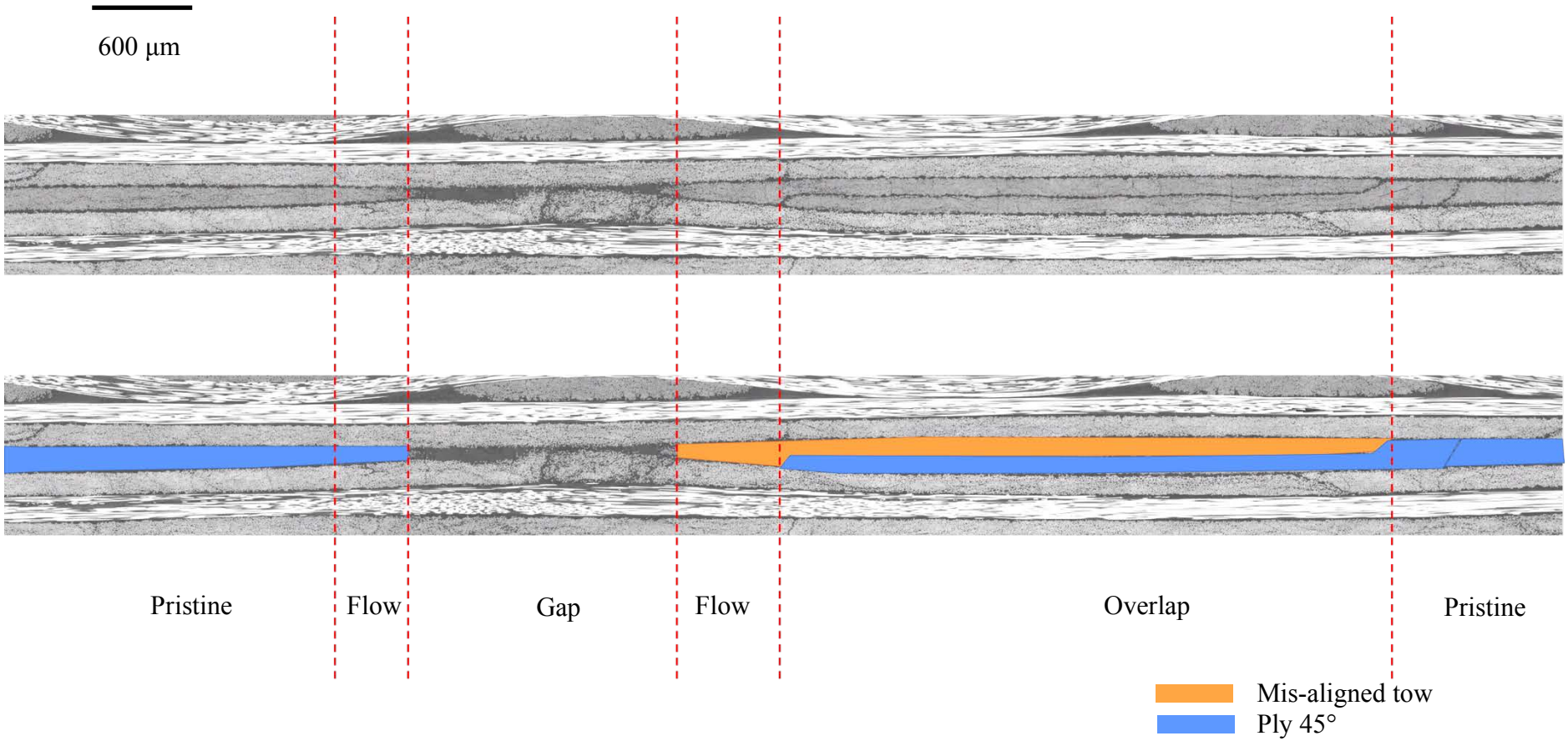

Figure 71 Analysis of one half gap / half overlap defect

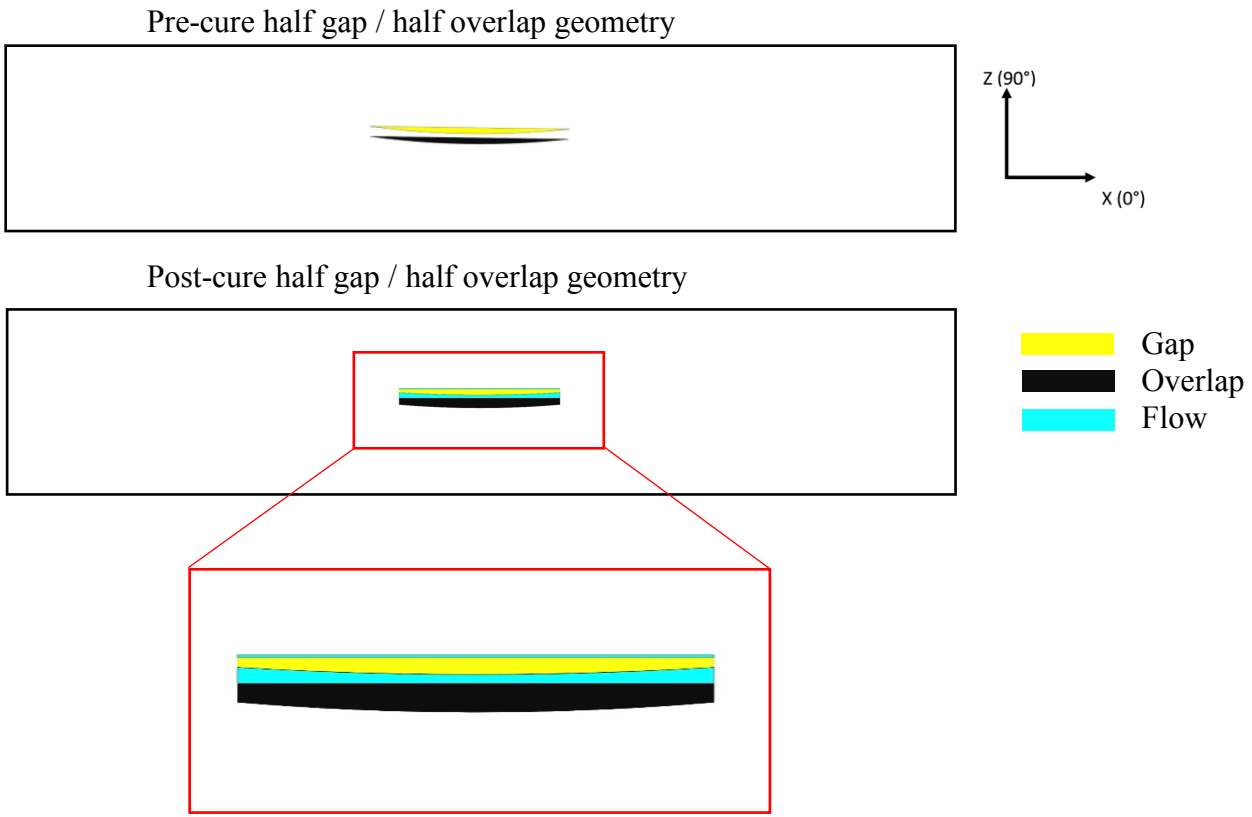

Figure 72 Change of geometry pre-cure versus post-cure

6. Modelling

The experimental test matrix cannot cover all possible configurations of defects and stacking sequences. For this reason, a Finite-Element (FE) model is used to simulate laminates with embedded defects in static tension and static compression with the goal to study any configurations in the future. This model follows a novel approach to represent the real post-cure defect geometry presented in the previous section § 5.3.3 Defect post-cure geometry. The model is validated with a standard quasi-isotropic pristine defect free configuration. The experimental data gathered from the different testing campaigns is compared to the model results in the next section § 7 Results and discussion.

6.1. 3D Assembly

The model developed in this thesis follows a ply-by-ply approach. Each ply is modelled separately. Two consecutives plies are connected to each other by a cohesive layer to allow for debonding and delamination. This 3D model strategy allows to capture out of plane stresses which are very important when defects are introduced in the laminate. Since the manufactured laminates have an 18-ply stacking sequence – see section § 3 Layup and defect geometry – the model is composed of 18 composite plies and 17 cohesive layers. The main assumption of this model is that defects only have an effect on the mechanical properties of the plies in which they have been embedded. Therefore, defects are only represented in the plies they were intended to be placed in. Out-of-plane waviness is not represented; thus plies are modeled in the plane.

To represent a pristine defect-free specimen, the assembly is composed of only one 3D body. This body is longitudinally partitioned into 18 plies and 17 cohesive layers. The material mechanical properties and fibre orientation are applied one-by-one to each 3D ply layer. Two composite plies are separated by a cohesive layer which represents for the layers of resin and particulate toughener observed in the microscopy study, see Figure 65. The thickness of

cohesive layers is taken from microscopy measurement. However, both the thicknesses and material properties of both fabric and unidirectional plies are taken from the manufacturer datasheet [72] because the material properties are normalized on a certain ply thickness and fibre volume fraction. The Author considered it was important to stay consistent when using the given datasheet. Thus, the model assembly is slightly thicker than the manufactured laminates because of the extra cohesive layers. In fact, the ply thickness given by the manufacturer already includes the cohesive layers. However, this increased laminate total thickness does not change the overall stiffness or strength because cohesive layers do not carry in-plane load by definition of the cohesive elements and mechanical behavior [80].

When a defect is embedded, the corresponding ply is modeled in a separate body of a single unidirectional ply thickness. The overall model assembly is then composed of several 3D bodies. For example, if only one ply only has defects, the assembly is composed of three bodies as shown in Figure 73: a group of pristine defect free plies corresponding to the top laminate layers (in green in the figure), the defected ply (in blue in the figure), and a group of pristine defect-free plies corresponding to the bottom laminate layers (in red in the figure).

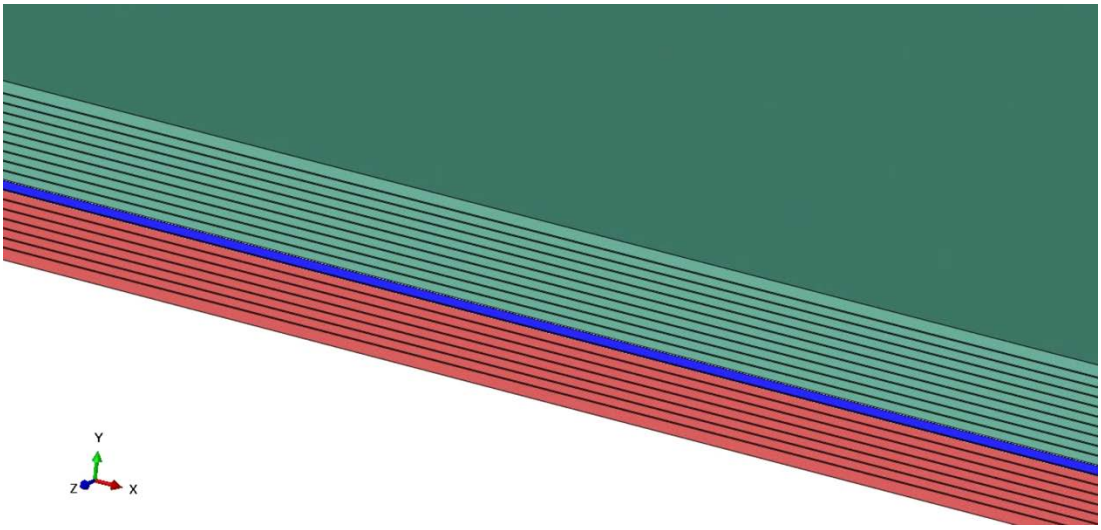

Figure 73 Side view of a model of a laminate with one embedded defect

Thus, the stacking sequence is always the same. Two consecutive bodies touch each other but they do not share the same nodes. An interface interaction is used to tie the nodes in contact of two bodies to prevent unwanted displacement.

6.2. Material behavior and cohesive law

The model uses a ply-by-ply lamina approach with in-plane damage mechanics and out-of-plane delamination is considered using traction separation law. Each fracture mechanism is stress based failure criteria using different interactions between stress components to accurately predict failure due to stress concentrations.

The proposed model is based on continuum mechanics of thin plate theory (each layer has a small thickness compared to the planar dimensions). The composite behavior relies on the classical laminate theory and Hashin's criteria to predict failure, with additional fracture damage parameters based on energy considerations.

$$(\sigma_f \geq 0): \left(\frac{\sigma_f}{\sigma_L^T}\right)^2 + \left(\frac{\tau}{\sigma_S^L}\right)^2 = 1 \tag{3}$$

$$(\sigma_f \leq 0): \left(\frac{\sigma_f}{\sigma_L^C}\right)^2 = 1 \tag{4}$$

$$(\sigma_m \geq 0): \left(\frac{\sigma_m}{\sigma_T^T}\right)^2 + \left(\frac{\tau}{\sigma_S^L}\right)^2 = 1 \tag{5}$$

$$(\sigma_m \leq 0): \left(\frac{\sigma_m}{2\sigma_S^T}\right)^2 + \left[\left(\frac{\sigma_T^C}{2\sigma_S^T}\right)^2 - 1\right]\frac{\sigma_m}{\sigma_T^C} + \left(\frac{\tau}{\sigma_S^L}\right)^2 = 1 \tag{6}$$

In the above equations, σ_f, σ_m and τ are the components of the effective stress tensor for fibre direction, matrix direction and shear respectively; σ_L^T and σ_T^T denote longitudinal and

transverse tensile strength respectively; σ_L^C and σ_T^C denote longitudinal and transverse compressive strength respectively; σ_S^T and σ_S^C denote shear strength.

Once any of the composite elements reach one of the Hashin's failure criteria (i.e. fail), their individual properties are degraded at a rate which is defined by the fracture energy dissipation formulation. The rate at which stiffness properties are degraded depends on the failure criterion that was reached. Damage propagation is modelled by linearly softening the material (i.e. ply) based on fracture energy dissipation.

Mechanical properties of carbon/epoxy are available from the manufacturer. The mechanical properties required in the model are summarized in the next tables.

Table 9 Elastic lamina required input

E1 MPa	E2 MPa	Nu12 /	G12 MPa	G13 MPa	G23 MPa

Table 10 Hashin's criteria required input

Longitudinal Tensile Strength MPa	Longitudinal Compressive Strength MPa	Transverse Tensile Strength MPa	Transverse Compressive Strength MPa	Longitudinal Shear Strength MPa	Transverse Shear Strength MPa

Table 11 Damage evolution required input

Longitudinal Tensile Fracture Energy N-mm	Longitudinal Compressive Fracture Energy N-mm	Transverse Tensile Fracture Energy N-mm	Transverse Compressive Fracture Energy N-mm

Delamination in a composite corresponds to interply failure. It can have an effect on the near plies and the delamination model depends on the cohesive elements. They transfer the load through-the-thickness but they cannot carry in-plane load so cohesive elements do not influence the in-plane laminate stiffness. Stiffness of cohesive elements is estimated from the matrix only elastic properties given by the manufacturer as explained in [80].

Modelling of cohesive behavior requires the input of maximum stresses for the quadratic nominal stress failure criterion and fracture toughness GIc, GIIc, GIIIc for damage evolution in the three delamination modes. The failure criterion is represented by Equation where the stress tensor consists of three components: two in-plane transverse $t_t$and shear components t_s and one out-of-plane along the normal direction t_n. The damage evolution is based on energy and the mixed mode interaction model which is represented with the Benzeggagh-Kenane (BK) form [80]. Cohesive fracture properties, such as fracture toughness values have to be determined experimentally by Double Cantilever Beam (DCB) testing. Values for cohesive damage initiation and evolution behavior of carbon epoxy composite are found in research work which showed successful analyses [13, 33].

$$\left(\frac{t_n}{t_n^0}\right)^2 + \left(\frac{t_s}{t_s^0}\right)^2 + \left(\frac{t_t}{t_t^0}\right)^2 = 1 \qquad (7)$$

Loading was applied with a constant ramp but when elements started to fail and degrade, the step size was decreased to achieve convergence. A sensibility study performed on the step size showed that below a certain value, mechanical performance and the maximum strength are not changing anymore. It was also found that the overall model stabilization parameter in the step definition toolbox has an effect on the minimum step size reached during degradation. The smaller the stabilization, the smaller the step size. Simulations with different stabilization values were run to find the threshold value under which computational time did not bring further accuracy in the results.

6.3. Half gap / half overlap defect definition

The defect geometry has been studied in § 5.3.3 Defect post-cure geometry. A half gap / half overlap defect has been decomposed in three characteristic regions: gap, flow and overlap

as shown in Figure 74. The flow region is narrowing toward the gap and it is considered trapezoidal. Gaps are not only filled with resin but also with fibres from nearby plies. The gap is considered to be a thin rectangular region in which fibres and resin are mixed. The overlap region is represented as a wide rectangle composed of the two superposed tows.

Each region is characterized by different mechanical properties which are estimated by the measure of the volume fibre fraction and the use the rules of mixtures. The rules of mixtures formulas can be applied to evaluate the new material properties based on fibre and matrix only elastic and strength properties. Those formulas are the following equations for tension, the same formulas are used to define compression properties:

$$E_{11} = (1 - V_f)E_m + E_f \cdot V_f \tag{8}$$

$$X_t = (1 - V_f)X_m + X_f \cdot V_f \tag{9}$$

$$\frac{1}{E_{22}} = \frac{(1 - V_f)}{E_m} + \frac{V_f}{E_f} \tag{10}$$

$$\frac{1}{Y_t} = \frac{(1 - V_f)}{Y_m} + \frac{V_f}{Y_f} \tag{11}$$

Where:

E_{11} = composite longitudinal modulus
V_f = fibre volume fraction
E_m = neat matrix modulus
E_f = neat fibre modulus
X_t = composite longitudinal tensile strength
X_m = neat matrix tensile strength
X_f= neat fibre tensile strength
E_{22} = composite transverse modulus
Y_m = neat matrix tensile strength
Y_f = neat fibre tensile strength
Y_t = composite transverse tensile strength

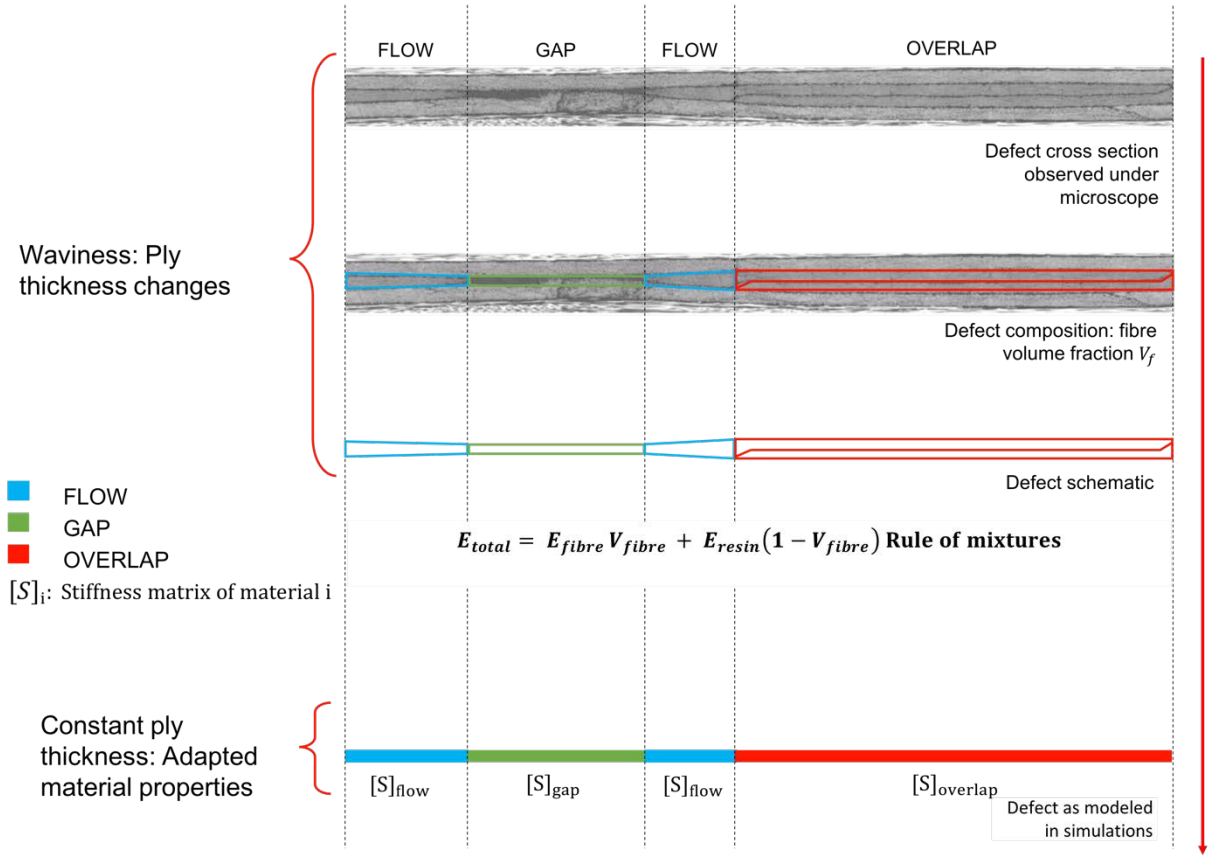

Figure 74 From microscopic observation to defect modelling

6.4. Mesh

Due to the presence of defects in the model, it is difficult to obtain a uniform mesh throughout the laminate. Also, since the plies with defects are modeled separately from the rest of the laminate, two meshes coexist in the model. The plies with defects have a complex mesh with a refined region. The thinnest mesh size equals the dimension of the end of the defect geometry as shown in Figure 75. The post cure defect geometry does not have sharp triangle end as shown in Figure 72 which would otherwise create stress singularities. The mesh size at the defect region is four times smaller than the mesh size of pristine defect-free regions. Triangular elements are used to make a clean transition between the two mesh sizes. The coarse mesh size of the defected plies is the same that is used on pristine plies.

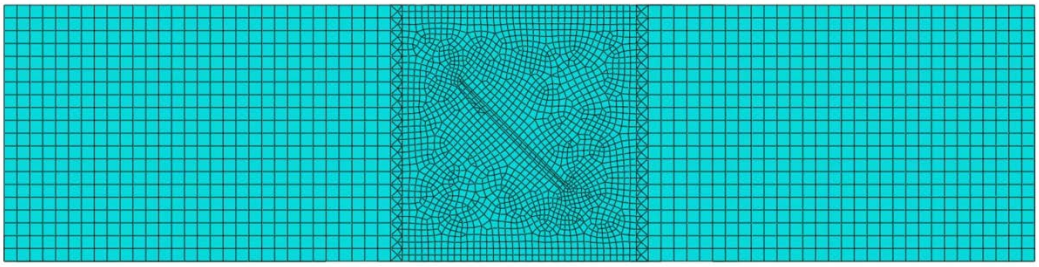

Figure 75 Mesh of a 45° ply with defect at the middle

Continuum shell elements SC8R and SC6R with reduced integration, enhanced hourglass control and second order accuracy are used to model composite plies while COH3D8 and COH3D6 are used to model cohesive layers. Other settings like solver options were left at their default values.

Shear stresses are induced by the high stiffness gradient between the gap and the overlap regions. To accurately analyze the through thickness shear stresses and propagate the effects of defects on nearby plies, each layer is composed of three elements in the normal direction which corresponds to 7 integration points.

6.5. Boundary Conditions: tension and compression

The boundary conditions were chosen to simulate laminates with close conditions to experimental set up for both compression and tension. One end of the laminate is constrained in x-translation while the other one is prescribed with a constant displacement rate. To avoid rigid body motion, two nodes are constrained in y-translation and one node is constrained in z-translation, as shown in Figure 76, on each side of the laminate. All rotations are allowed. The chosen constraints allow Poisson ratio effects, avoiding artificial stress concentrations at boundary conditions.

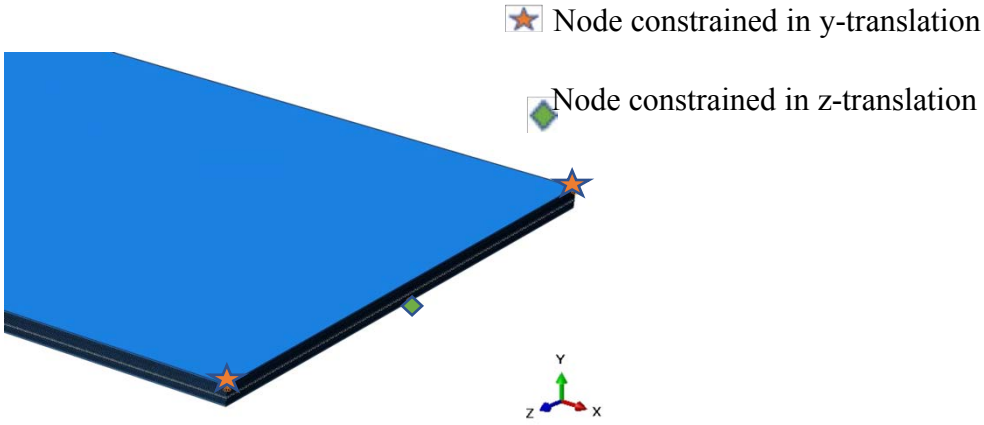

Figure 76 Displacement constraints against full body motion

For compression analysis, nodes at the top and bottom surfaces of the laminate show but a small rectangle corresponding to the fixture D6484 window are constrained in the normal direction y-translation, see picture Figure 37 and Figure 77. This boundary condition represents the anti-buckling fixture.

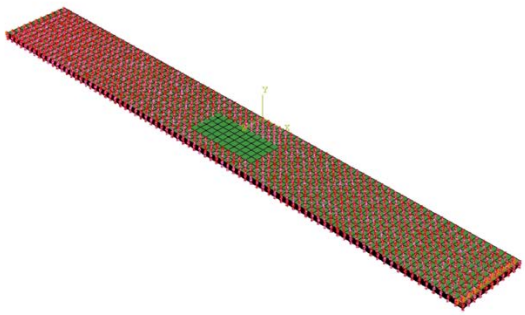

Figure 77 Compression top and bottom surfaces: nodes in red y-translation constrained

6.6. Validation: Quasi-Isotropic laminate

Before analyzing laminates with defects, the pristine defect free quasi-isotropic laminate was simulated and compared to the laminate theory results. The validation of the basic functions of the model without the difficult defect generation will permit to see if the model behaves adequately.

In the FE model, it was observed that in tension the pristine laminate breaks due to stress concentrations near the right and left edges. The stress is not homogenously propagated at the

surface of each ply and elements fail earlier near the constrained nodes. A partition of a few elements large was defined along both the right and left edges where Hashin's failure criteria and damage were removed from the material definition in those two bands. Thus, the model induced stress concentrations still existed but the elements no longer failed earlier. The stress – strain distribution in each ply then corresponds to the analytical analysis of the laminate theory.

In both tension and compression, the model predicts a stiffness less than 3% difference to the laminate theory results while the maximum strength prediction is different by maximum 4%. The pristine simulation results are considered satisfying. The pristine simulation results will be used to normalize the simulated stress strain curves of laminates with defects.

7. Results and discussion

Disclaimer: the numbers in graphs have been normalized in order to protect proprietary company data. This applies to data shown in Figures 80, 81, 85-89, 95, 101-105, 113-116.

7.1. Tensile Tests

7.1.1. Experiments

Tensile tests were performed at Ecole Polytechnique de Montréal following ASTM D3039 [59]. Coupons were set up for loading in an MTS machine of 250kN maximum load capacity. Reusable tabs in aluminium were used under the grips because the coupons were to thin to be clamped when the grips alone were used in their most closed position. Each tab was 0.12in (3.18mm) thick and their dimensions correspond to the grip section in Figure 35 and Figure 36. One end of the coupon was kept fixed, the other was loaded using displacement control at rate of 2mm/sec. The load and displacement were recorded during the experiment which automatically stopped when the load dropped due to catastrophic failure. The MTS machine can be seen in Figure 78. For each coupon, the thickness and width were measured at both ends and in the middle in order to calculate the cross-section area and then the engineering stress.

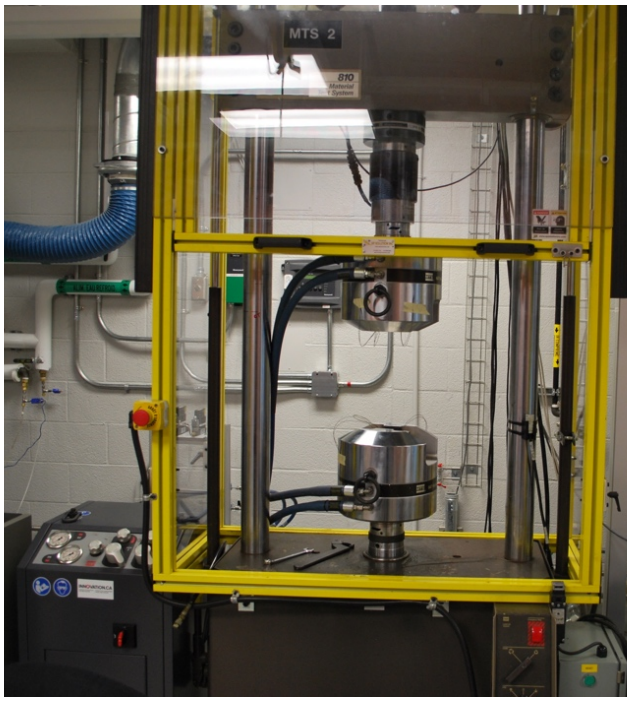

Figure 78 MTS machine at Polytechnique Montréal

All coupons failed by breaking at several locations, sometimes even with pieces flying towards the protecting glass panel, as shown in Figure 79. The fracture path was observed in 45° or 90° independently to the configurations of specimens. 5 coupons were tested per configuration but no pattern would emerge as to the fracture mechanism because most of the specimens were completely destroyed by the tensile tests. Also, 50% of all specimens broke under the grips away from the location of defects. The cause is not clear: grip pressure or bonded tabs may have prevented this phenomenon.

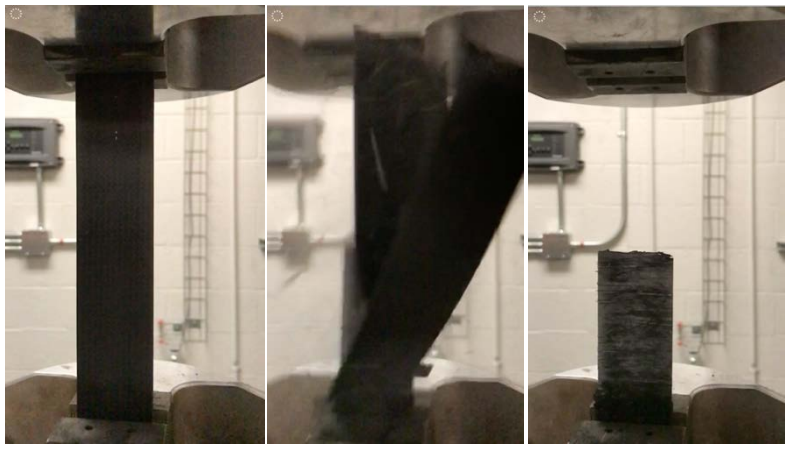

Figure 79 Tensile test failure in slow-motion

The head displacement of the MTS grip cannot be used as a trustworthy measurement of the specimen deformation because the grip may slip while maintaining the specimen. As mean of comparison, few specimens were tested with extensometer and others with Digital Image Correlation (DIC) techniques, especially 90G7.05 configuration.

An extensometer measures the deformation between two fixed points on a specimen. In this research, the extensometer is set up directly at the surface, over the location of the embedded defects. An example of results for the specimen number #4 of configuration 45G10.05 is presented in Figure 82. As shown on the stress strain curve of configuration 90G7.05 in Figure 80, the head displacement shows a non-linearity in the elastic region while the extensometer, located at the defect region, does not show this behavior. This observation was made on all tested coupons. The extensometer can be seen in Figure 82. The extensometer has to be removed before the coupon fails otherwise it could be damaged during coupon failure. The extensometer was removed at half the predicted failure load to increase the safety of this operation. This manipulation is visible on the stress strain curve in Figure 82 at the end of the orange line where a slight drop in the load was measured.

Specimens were also tested by Digital Imaging Correlation (DIC) techniques using a VIC-3D 8 System solution [81]. DIC was used to observe the influence of embedded defects on the strain field during the loading until the final failure. Two high definition stereo-mounted digital cameras are tracking black dots of approximately 0.026in diameter that had been sprayed on the defect region, creating a random pattern required for the quality of the analysis. Cameras and specimen are set up 30in (75cm) away from each other. During the test, the distance between black dots changes. Deformation is recorded and analyzed by an algorithm provided with the digital cameras [81]. The strain is plotted in Figure 80 for 90G7.05. The DIC stress strain curve correlates well with the extensometer measurement and no non-linearity is observed in the elastic region. The DIC is observable to the final fracture of the specimen. The

deformation is still linear while the head displacement shows large non-linearity at large strains thus the need of other ways of measurement for deformation.

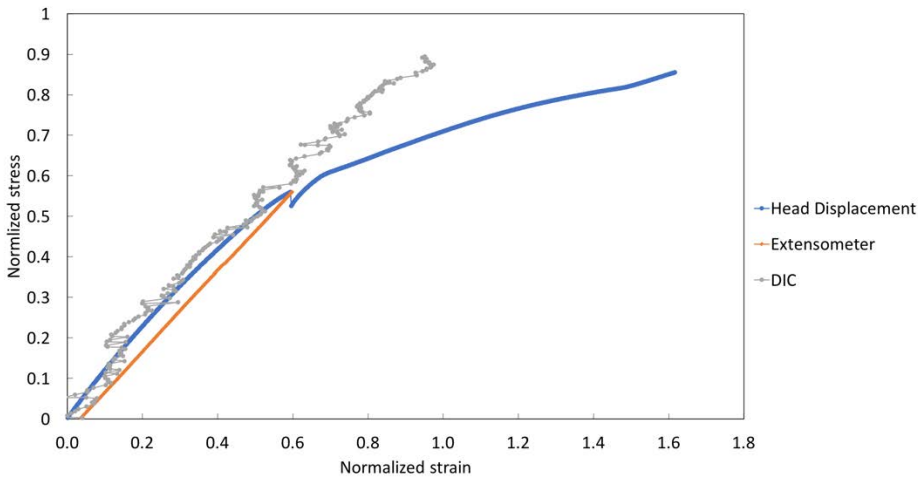

Figure 80 Configuration 90G7.05: stress strain curves normalized on pristine performance

It is suspected that the non-linearity of the head displacement is due to the aluminium tabs used to ensure that the MTS grips were properly gripping the specimens that deformed during the loading. The load of the grips on the tabs progressively curved the tabs. Thus, the load was non-uniformly shared at the surface of the tested specimens causing slippage. This effect was not discovered directly but new aluminium tabs were manufactured for other specimens, solving temporally the problem. Chronologically, the 90G7.05 specimens were tested after 0G7.05. Aluminium tabs were still in good shape for 0G7.05 but were altered during the time that the experiments were running.

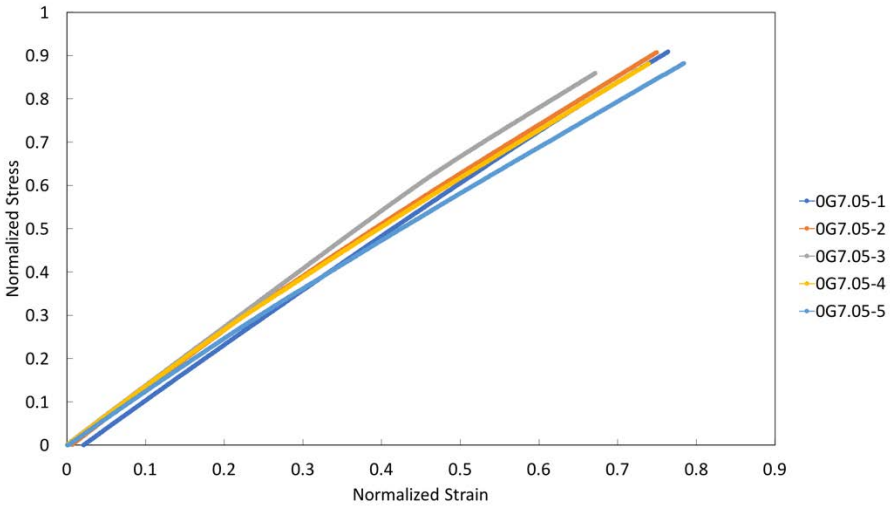

Figure 81 0G7.05: Stress strain curves from head displacement normalized on pristine

The average laminate modulus measured with the extensometer on the elastic region of different specimens is 6% smaller than the expected modulus calculated with classical laminate theory while the average modulus measured with DIC techniques is 10% smaller. The DIC modulus measurement was done with data all the way from elastic to the fracture of specimens so the modulus from DIC measurement is expected to be lower. The average modulus in the elastic region measured with the head displacement is 8% larger than the theoretical modulus with 5% coefficient of variation. In general, the experimental modulus, whichever method is considered, is close by less than 10% to the theoretical modulus.

Figure 82 Extensometer used during tensile test

The main parameter of interest in the tensile tests is the max strength of specimens given by the load cell of the MTS machine. Compared to laminate theory, pristine defect free

specimens failed at a maximum stress 9% lower than the expected theoretical value in tension. Before the fracture, all coupons, even pristine configuration, experienced in tension wide delamination between the 9th and 10th plies which are oriented in 90°, as shown in Figure 83. Each specimen literally opened from the middle toward the grips in such way it was possible to see through the specimens. Grips of the MTS machine prevent further delamination. This damaged structure was able to carry more load with the support of the MTS grips. However, the tests were kept running till failure. It is unsure whether the delamination started on the edge or through the thickness.

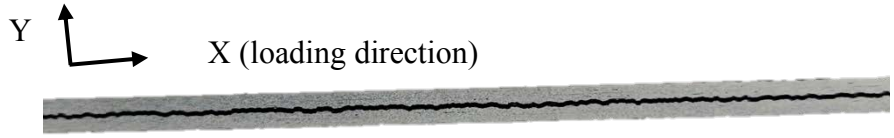

Figure 83 Side view failed coupon with delamination between plies 9th and 10th [4]

DIC was used on one specimen each from three different selected configurations: 0G7.1, 45G7.1 and 90G7.05. The objective was to study the effect of the orientation of defects on the strain field measured by DIC. Ideally the same defect width should have been used but 90G7.1, but was not manufactured. The performed tensile tests were quasi-static and DIC results showed a homogeneous strain distribution during the loading. However, DIC results quickly revealed delamination caused by high strain regions at the edges, for all coupons. Figure 84 shows the results just before failure at more than 95% of the maximum load for each configuration tested with DIC. At the instant before the failure, red spots emerge at the middle of the outer surface. The high strain regions at the edges tend to join those at the middle which is the probable cause of failure. Note that DIC only shows the deformation on the outer surface so it is impossible to see how much delamination there is through-the-thickness using this technique. No correlation between the orientation of defects and high strain regions can be made. It appears the fracture mechanism for the different configurations is highly influenced by a progressive delamination at the vicinity of defects without any certainty that defects played a specific role.

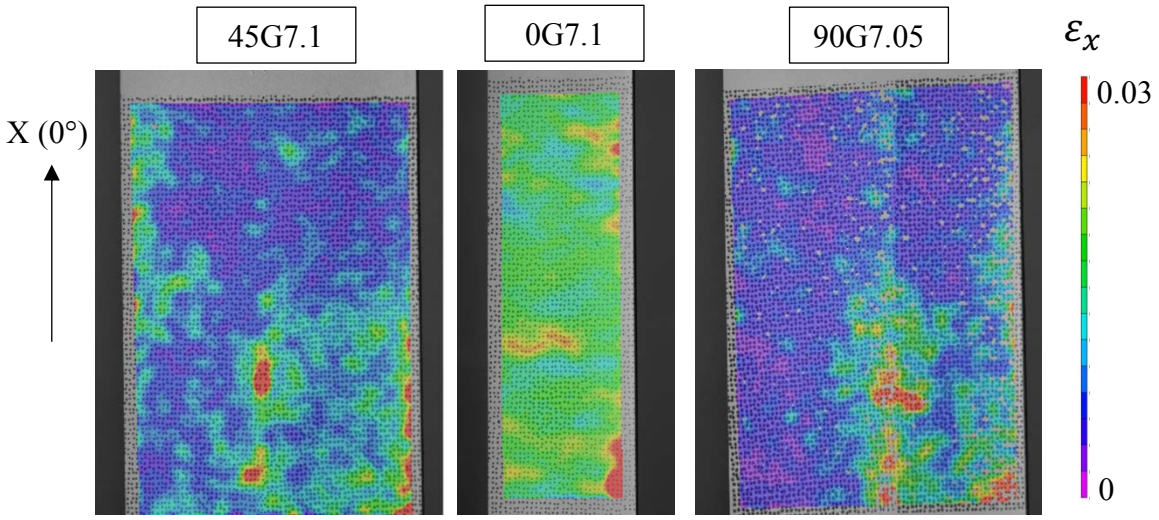

Figure 84 DIC image of 3 different configurations right before failure

The results for the various configurations of defects are plotted in Figure 85 for 0.1in (2.54mm) wide defects configurations and in Figure 86 for 0.05in (1.27mm) wide defect configurations. Their corresponding coefficient of variation is calculated. Each data point is the average normalized max stress of 5 coupons of the same configuration.

$$COV = \frac{\sqrt{\frac{\sum_{i=1}^{N}(x_i - x_{avg})^2}{N-1}}}{x_{avg}} \tag{12}$$

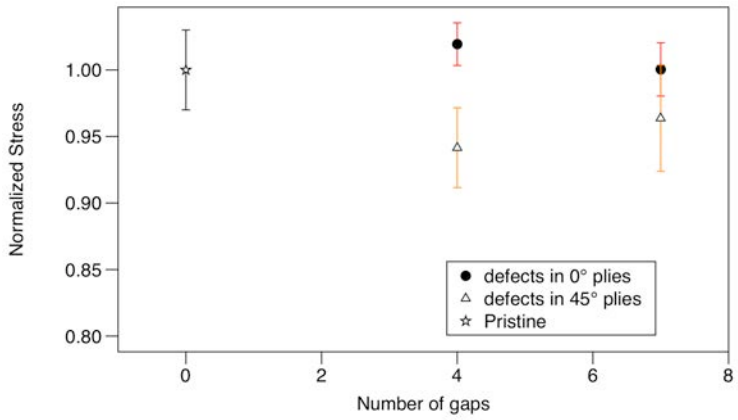

Figure 85 Tensile results - Normalized stress - 0.1in wide defects

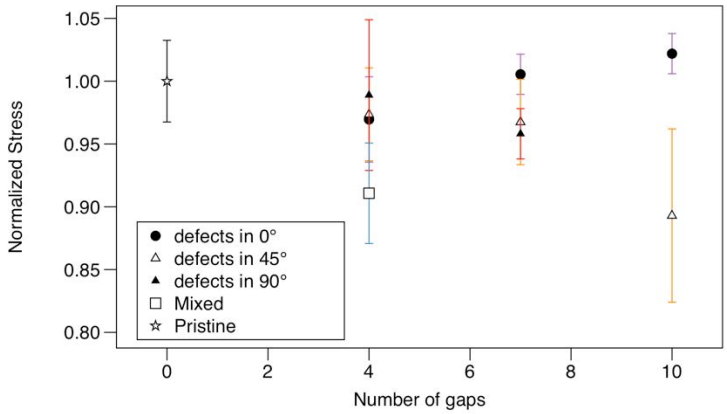

Figure 86 Tensile results - Normalized stress - 0.05in wide defects

Most of the configurations have a coefficient of variation smaller than 5%. Only 90G4.05 and 45G10.05 configurations have higher coefficient of variation, 6.2% and 6.8% respectively. The mixed defect orientation configuration *G4.05 show the largest knockdown factor (9%) for 4 defects. It was expected to be the worst scenario. Considering 0.05in (1.27mm) wide defects, 90° and 45° oriented defects configurations show similar trends: the more defects, the largest the knockdown up to 11% by 45G10.05 which also has the largest scatter. However, 45G7.1 was found to be slightly stronger than 45G4.1 in tension, 4% and 6% knockdown respectively but their scatters close to 4% are overlapping. 45G4.05 and 45G7.05 have close knockdown factors than their wider equivalents, so the effect of size is not clear. Results for 0° oriented defects show almost no effect on the maximum stress of coupons with an average knockdown of 1% for both sizes. It appears that the defect size between 0.1in (2.54mm) and 0.05in (1.27mm) does not have much influence.

7.1.2. Modelling of tensile tests

Modelling results do not correlate well with the experimental data. The model is not conservative for 45° and 90° oriented defects as shown in Figure 88 and Figure 89 while the simulations of 0° oriented defects configurations are too conservative as shown in Figure 87. The model considers the updated post-cure geometry using only a limited number of

observations as explained in the section § 5.3 Microscopy of specimens with embedded defects. None of the 0° oriented defects configurations have been studied using microscopy. The model also does not consider ply waviness and assumes that only the plies in which the defects have been embedded can be damaged. According to the modelling results in Figure 87, the effects of embedded defects in 0° are emphasized by the previous assumptions while the observed experimental results do not show much effect of 0° oriented defects – knockdown of 1%. Conversely, the model does not see any effect of damaged 90° and 45° plies, which is the contrary to the experimentally observed effects. Due to the fact that 0° plies are responsible for most of the load carrying capability of the laminate, the modelling is sensitive to changes related to these 0° plies.

When defects are embedded in 45° and 90° plies, in reality, waviness is thought to play an important role but the model does not represent it: 0° plies are also affected.

When defects are embedded in 0° plies, waviness in 90° and 45° might not play such an important role because these plies do not carry much load. The reason why knockdown factors are so small has probably something to do with the healing process of defects due to shear flow during cure cycle and compaction. The defect post-cure geometry still has to be analyzed with the observation of more configurations especially 0° oriented embedded defects.

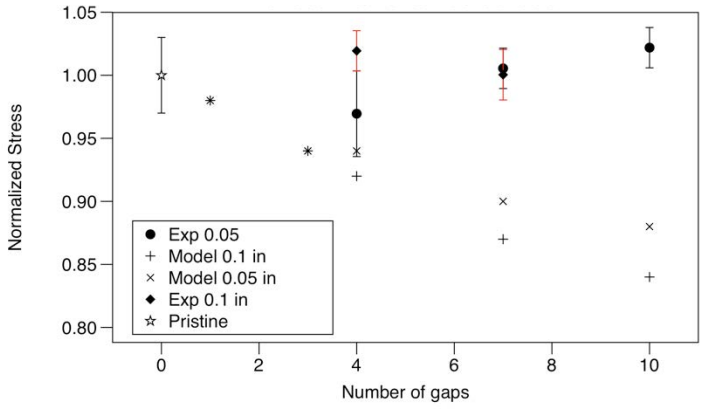

Figure 87 Model tension results - 0° oriented defects

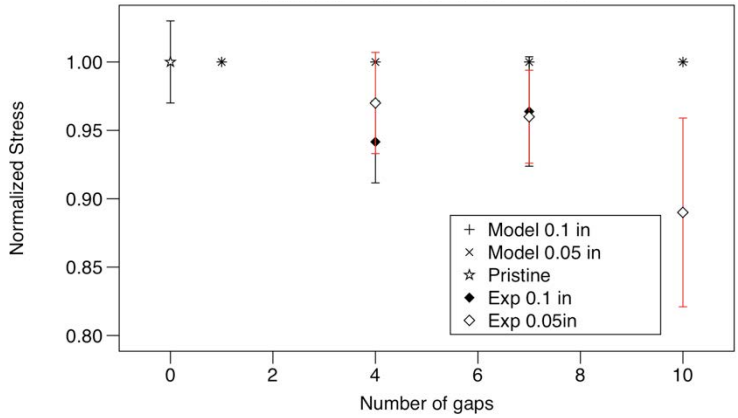

Figure 88 Model tension results - 45° oriented defects

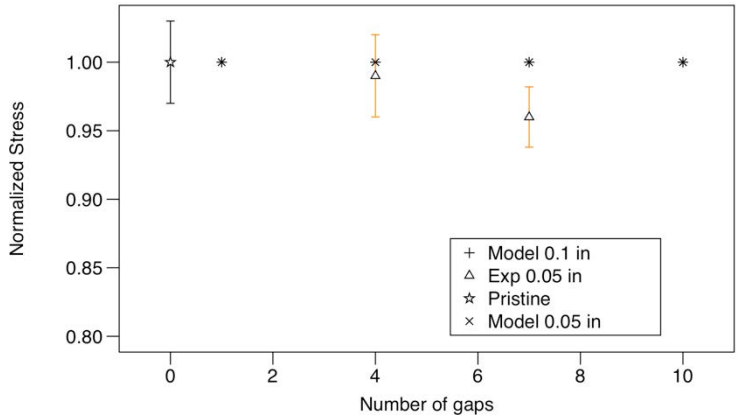

Figure 89 Model tension results - 90° oriented defects

Even if the model does not predict the correct maximum strength, it is still used to study the predicted crack initiation and damage propagation. The overlap is a stiff region so it attracts more load and fails first, whatever the defect orientation. A failure occurs at the middle of the defects and grows along the defect length. A small zone of large strain on the outer ply of each laminate shows the effect of embedded defects, much larger for 0G4.1 (Figure 91) than for 45G4.1 (Figure 92). This means transverse shear is correctly propagated through the thickness in the vicinity of defects and that defects in 0° have more effects according to the model. The defects are not as clearly visible in the DIC results.

Once defects start to fail, delamination around them can also progress. As revealed by the DIC results, delamination initiates very early in the simulation, starting at the edges before

the defects ever indicate any failure. The two regions of delamination grow toward each other as shown in Figure 90.

By the time both delamination regions join each other, 90° plies have completely failed in the matrix direction, at 77% of the maximum total load that is expected by classical laminate theory, even if these defects are embedded inside 90° plies. Thus, defects do not change the behavior of 90° plies in the model. Both 0° and 45° plies fail at the same time:

- In case of 0° oriented defects configurations, the model final failure occurs earlier than for pristine defect-free configurations: 0° plies see fibre crack propagation from the embedded defects to the edges as shown in Figure 94 and 45° plies fail in matrix and shear at the location of defects embedded in 0° plies as shown in Figure 93.
- In 45° and 90° oriented defects configuration models, all plies fail like in the pristine configuration, without any specific stress concentration region. Transverse shear propagates with some stress through the thickness of the laminate but it is not enough to change the final mechanical strength of the laminate.

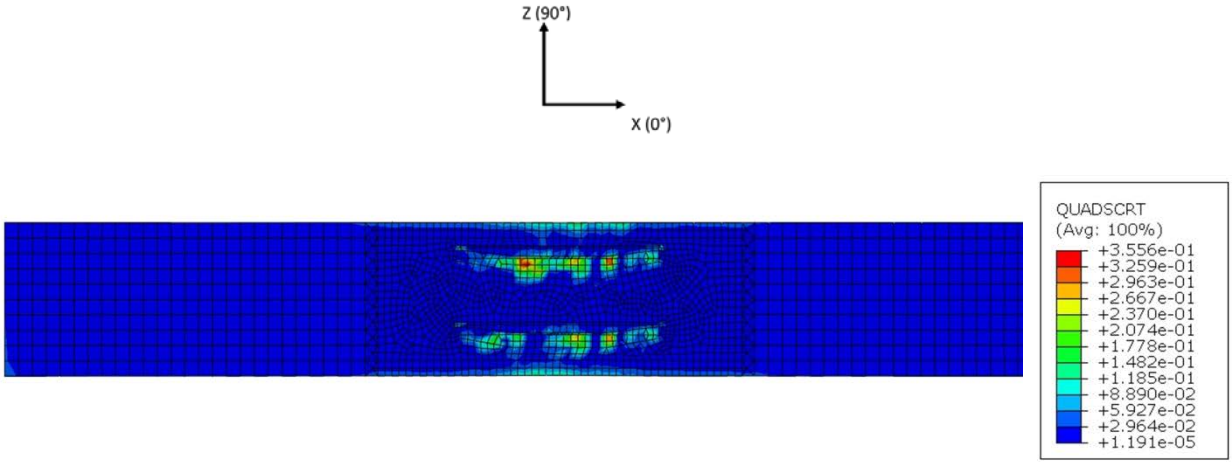

Figure 90 Delamination 10% of the maximum load

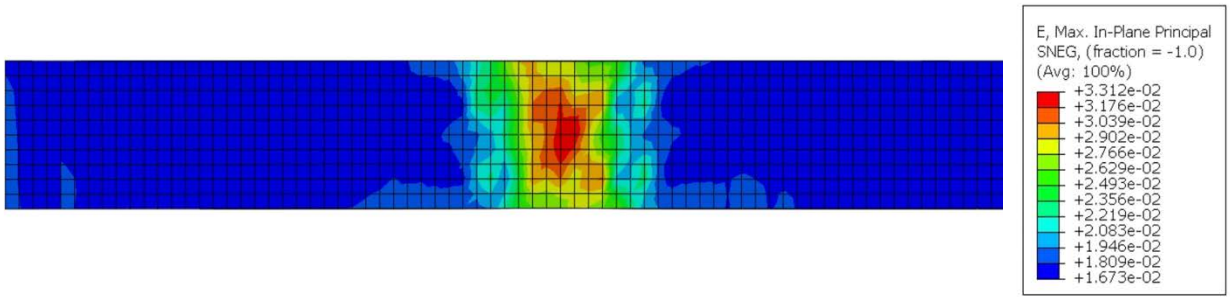

Figure 91 Strain at the outer ply for 0G4.1 at maximum load

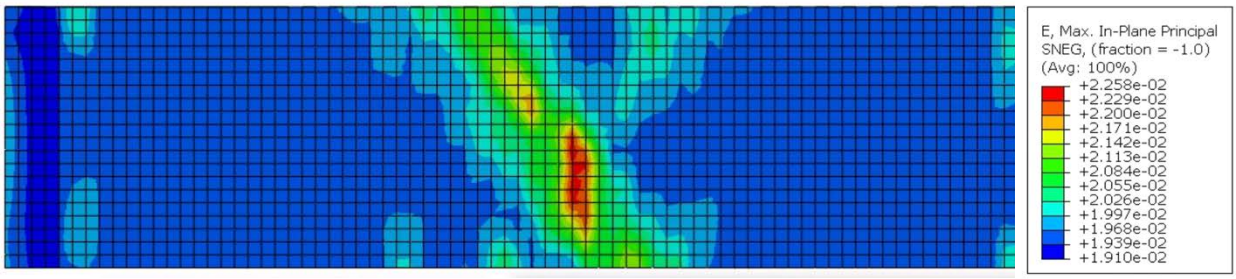

Figure 92 Strain at the outer ply of 45G4.1 at maximum load

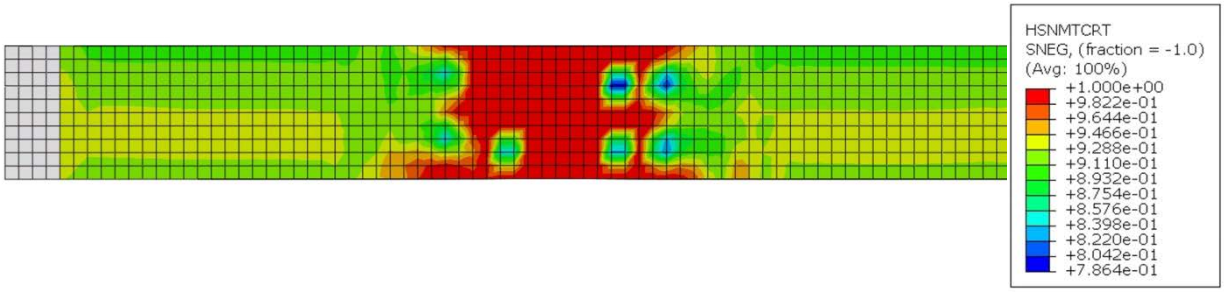

Figure 93 45° 0G4.1: Hashin matrix tension: failure at the location of defects

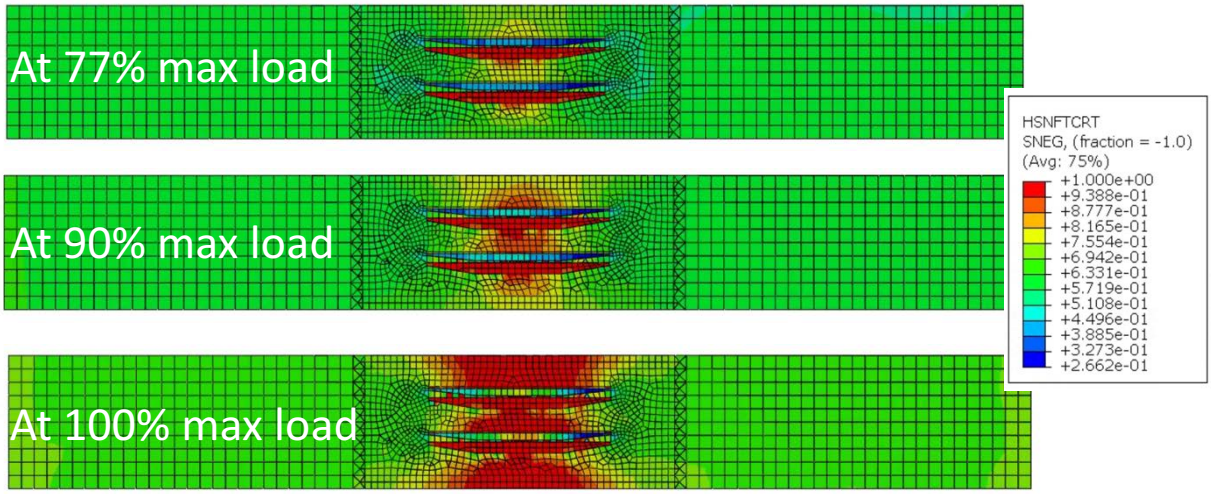

Figure 94 Hashin fibre tension: crack propagation in 0° ply with defect for 0G4.1

7.1.3. Discussion on tensile behaviour

In general, tensile experimental results show a limited effect of embedded defects on the maximum strength of tested specimens compared to the pristine defect-free configuration. Knockdown factors are usually smaller than 5% except for the case of mixed gap orientation and 45G10.05, two extreme cases that will probably never occur in a real structure.

45° and 90° oriented defects configurations behave similarly and their maximum strength decreases when the number of defects increases, while 0° oriented defect configurations have almost no effects. Experimentally, it looks like defects have more effects when they are loaded in the matrix direction. This can be attributed to waviness which is more pronounced in 0° plies when 90° and 45° have defects. Matrix cracking and delamination might be the initiators of the fracture propagation.

The presented FE model does not predict the right mechanical behavior. It seems that waviness is a critical aspect in order to understand the effect of defects and it is not considered in the model. Waviness depends on the location of the plies with embedded defects through-the-thickness and also on the pattern of defects. Due to the chosen stacking sequence, 45° and 90° plies are located more toward the middle of the laminate than 0° plies so the magnitude of waviness might be controlled by the choice of laminate. The magnitude of defect healing could also depend on the stacking sequence and on the orientation of the plies with defects. Healing could explain the difference between modelling results and experiments.

7.2. Compression Tests

7.2.1. Experiments

Compression tests were performed following ASTM D6484 [66]. Coupons were installed in the compression fixture with anti-buckling devices according to the standard. Two sizes of fixtures were used corresponding to the two sizes of coupons: 1.5in (38.1mm) and 3in (76.2mm) wide. However, the smaller fixture corresponding to the configurations pristine and

0° oriented defects was received later in the testing campaign and the larger fixture was used for some of the smaller coupons too. All 1.5in (38.1mm) wide coupons failed at half the expected maximum strength because the fixture was not adequate to prevent buckling. A finite-element modal analysis was performed to confirm the buckling observed. Thus, data for compression of 0° oriented defects was not comparable to the other specimens tested within this thesis. However, some pristine configurations were correctly tested in compression, providing the maximum strength used to normalize the rest of experimental data of 3in (76.2mm) wide coupons.

Stress strain curves obtained in compression from head displacement curves show, for all coupons, only a slight non-linear behavior as shown in Figure 95. A mark on the side of the specimens confirms that there was no slip inside the fixture. No tests were performed with an extensometer because there was no space to place the extensometer due to the small size of the fixture of ASTM D6484 [66] shown in Figure 37. DIC was performed with the same system [81] used for tensile tests, see Figure 96. However, a mistake in the connection of the system was made and the load was not synchronized with the analyzed strain field.

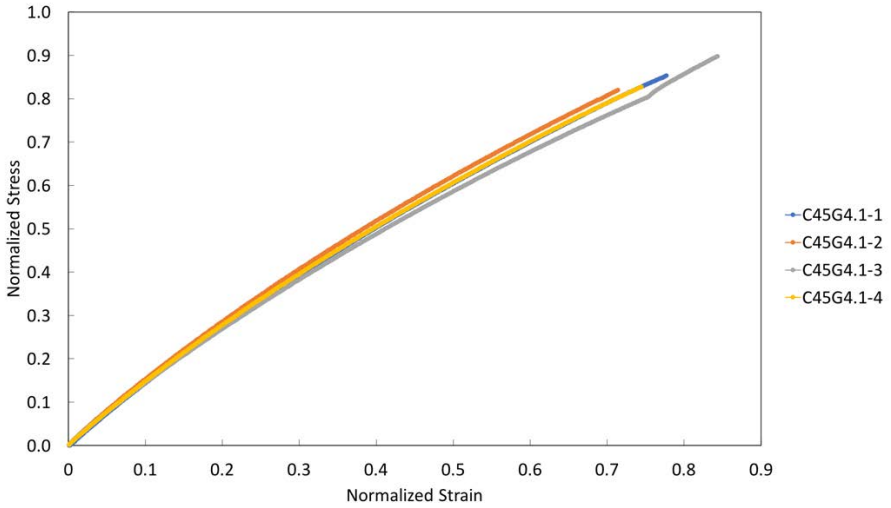

Figure 95 C45G4.1 stress strain curves using head displacement measurement

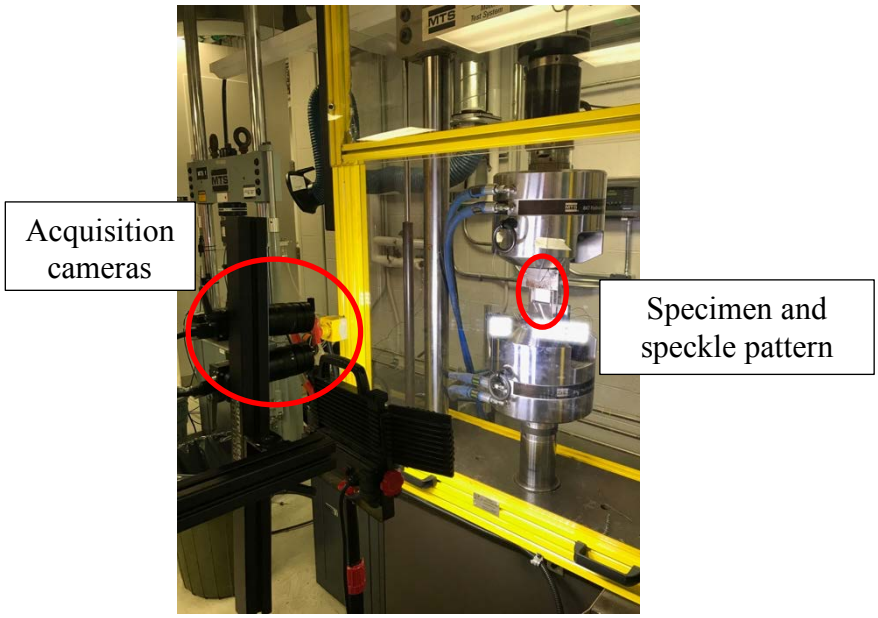

Figure 96 DIC experimental set up

Three specimens of different configurations have been analyzed using DIC techniques. Only a small part of the specimen is visible through the open window of the compression fixture. The window of the 1.5in (1.27mm) wide fixture is so small that too few dark spots from the DIC pattern fit inside the window. Thus, no DIC results were obtained for configuration 0G7.1. However, Figure 97 and Figure 98 show the results for 90G7.05 and 45G7.1 configurations respectively. During the loading, the strain field is homogeneous until the failure where the middle zone shows higher strains, at the location of defects. However, it is not clear if the DIC images reveal the print of the defects themselves since 45° configuration does not show a 45° oriented strain field.

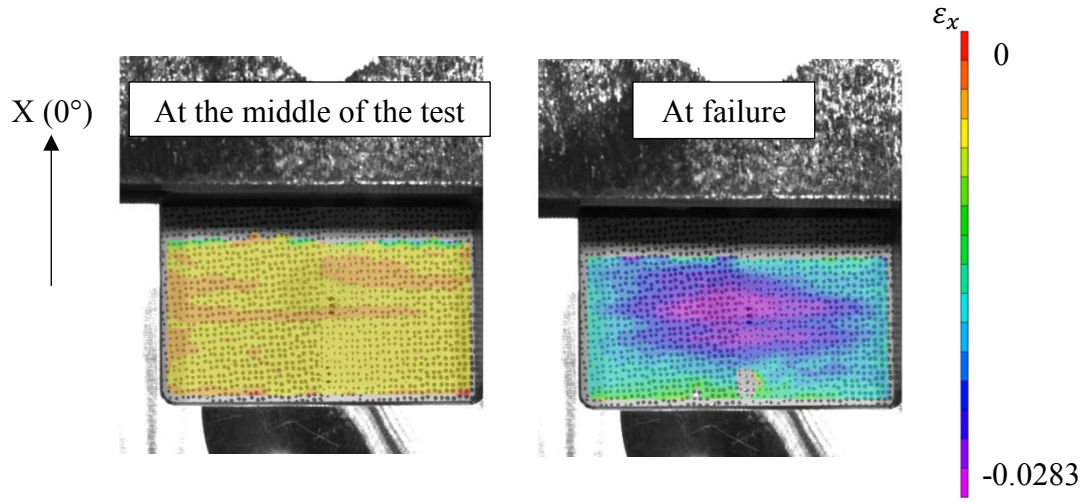

Figure 97 DIC 90G7.05

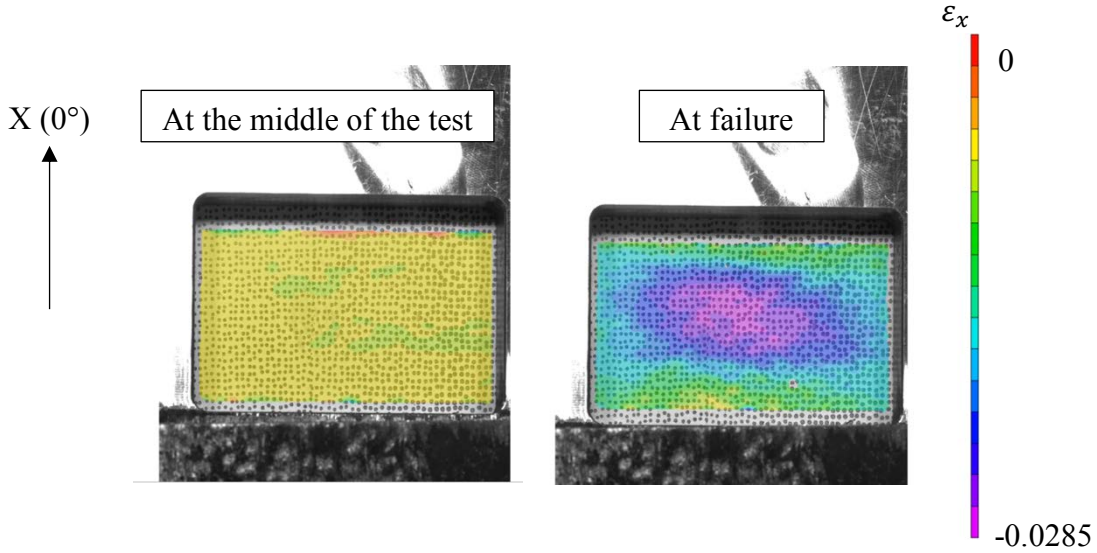

Figure 98 DIC C45G7.1

Two types of fracture indicators emerged: a clear line of crack at the middle of the specimen through the defects, in the window of the fixture as shown in Figure 100, and cracks happening in the grip at the location of friction between the two sides of the fixtures as observed in Figure 99. Each part of the fixture is held in place by the MTS grips. The contact edge between the two has the shape of a triangle. Sometimes the specimens would crack at this location with a clear mark of a triangle shape printed in the composite as shown in Figure 99. This specific crack path probably means that the fixture damaged the coupons because of a problem of alignment between the two sides of the fixture. Late in the compression testing campaign, shims were used, alleviating the problem. However, the compression load reached

by specimens which failed because of fixture misalignment was never too far from the rest of the specimens of same configuration even if the scatter increased. For cases of failure at the middle of the specimen, the crack path is at 45° through-the-thickness as shown in Figure 100, which is characteristic of compression for quasi-isotropic structures.

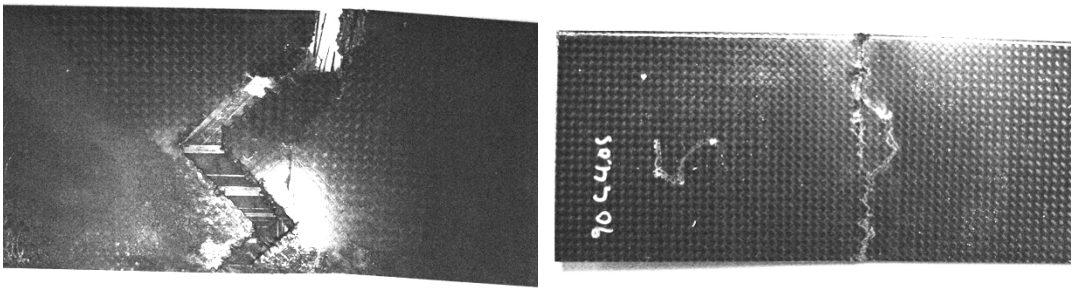

Figure 99 Failure happening due to fixture misalignment

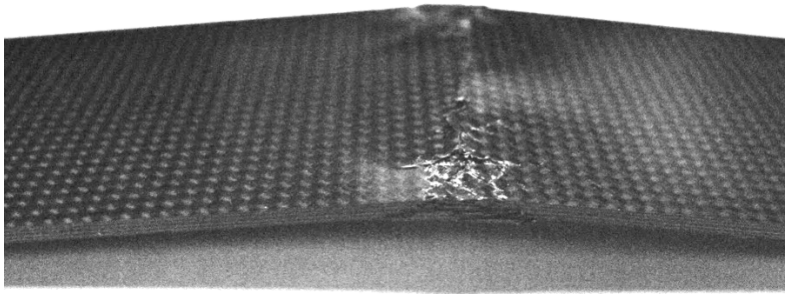

Figure 100 Failure at the middle of the window of the fixture

The knockdown factors obtained for compressive tests are much larger than those obtained from tensile tests. The 45° and 90° configurations behave similarly, see Figure 101: the more defects, the lower the strength. The scatter also increases with the number of defects too. Generally, the coefficient of variation is close to 5% with the exception of 45G10.05 which reaches 16% and 45G7.1 which reaches 9%. The 45° oriented defects configurations plotted in Figure 102 have a from knockdown factor that goes from 20% for 4 defects to 25% for 10 defects. The 90° oriented defects configurations are less than 5% stronger for the same number of defects. Mixed orientation defects configurations have the largest knockdown with only 4 defects, at 28% strength reduction. If more defects had been introduced in mixed orientation it

is expected that larger knockdown factors would have been obtained. The 0° oriented defects configurations data is not available because they all failed in buckling, using the wrong fixture.

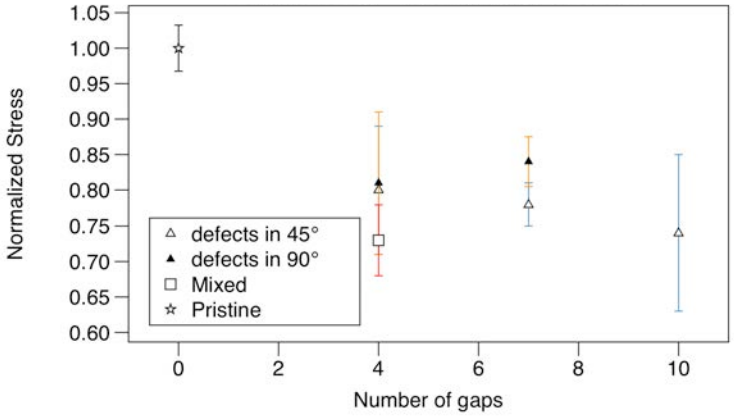

Figure 101 Compression normalized stress at failure - Defects 0.05in (1.27mm) wide

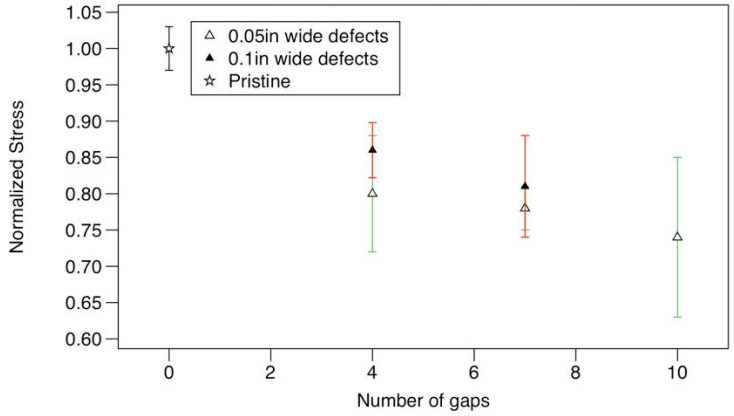

Figure 102 Compression normalized stress at failure - Defects 45° oriented

7.2.2. Modelling of compressive tests

The model is not conservative in compression compared to the test results. The simulations maximum strength is higher than the experimental results for the same configurations. Generally, the predicted knockdown increases with the number of defects which corresponds to experimental trends. For 45° and 90° defect orientation, a plateau seems to appear above 7 defects where the knockdown factors do not increase at the same pace. This behaviour cannot be verified because there is not enough experimental data. For 45° configurations, shown in Figure 104, the difference between modelling and experimental results increases with the number of defects, from 7% to 15%. The predicted knockdown factors for

45° and 90° configurations are about the same while 0° configurations have larger predicted knockdown factors. There is no difference in modelling results between 0.05in (1.27mm) wide and 0.1in (2.54mm) wide defects for 45° and 90° configurations. However, 0° configurations with larger defects have larger knockdown factors as shown in Figure 103.

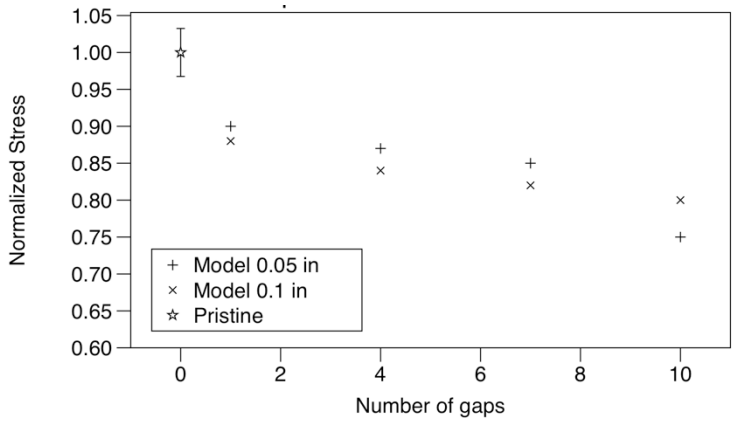

Figure 103 Compression model results 0° oriented defects

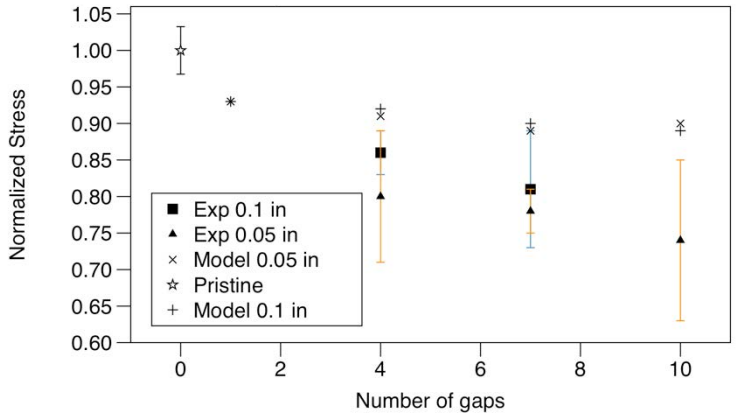

Figure 104 Compression model results 45° oriented defects

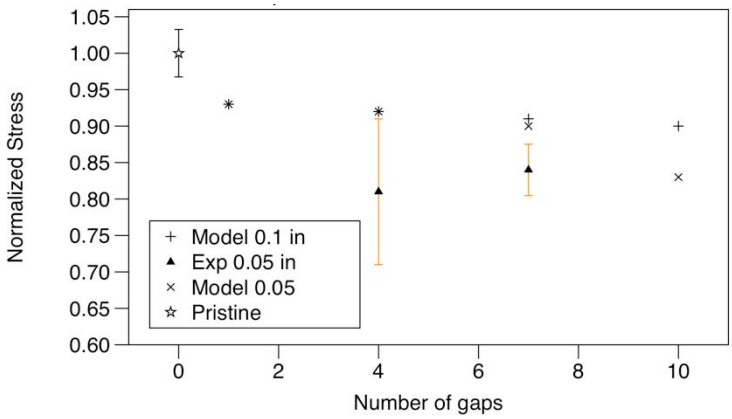

Figure 105 Compression model results 90° oriented defects

The compression model predicts a similar failure initiation and damage propagation than the model in tension. The major difference being there is no delamination on the edges. DIC analysis tend to correlate with this theory because no large strain appears on the edges. This can be explained by the use of the anti-buckling fixture which limits the normal debonding and displacement. However, delamination occurs along the defects, for all orientations, as shown in Figure 106.

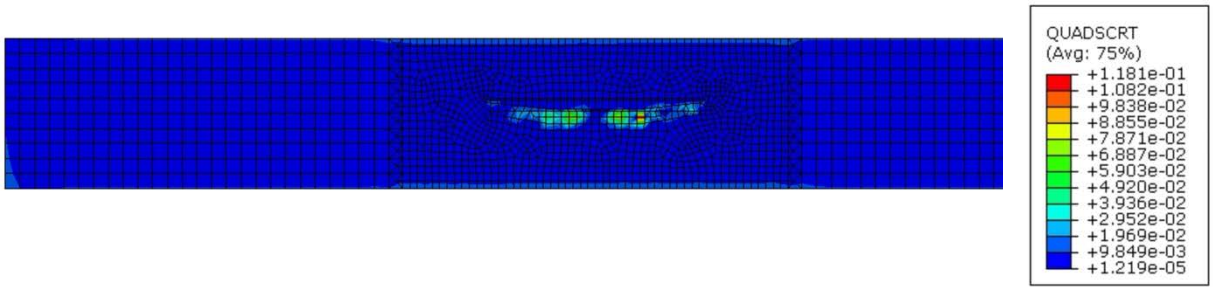

Figure 106 0G4.1: delamination in 0° ply with defects

The overlap fails first because it is a stiff region. The crack propagates from the defect region to the edges, as shown in Figure 107. 0° plies fail in fibre compression while 45° and 90° plies fail in matrix compression, see Figure 108. Even plies without defects fail in the region of defects, at the middle of the laminate, see Figure 109.

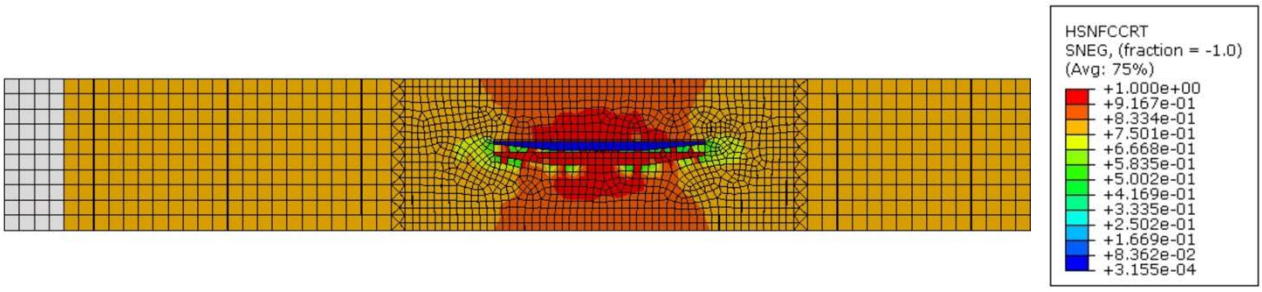

Figure 107 0G4.1: 0G4.1: Hashin fibre compression in 0° ply with defects, at failure

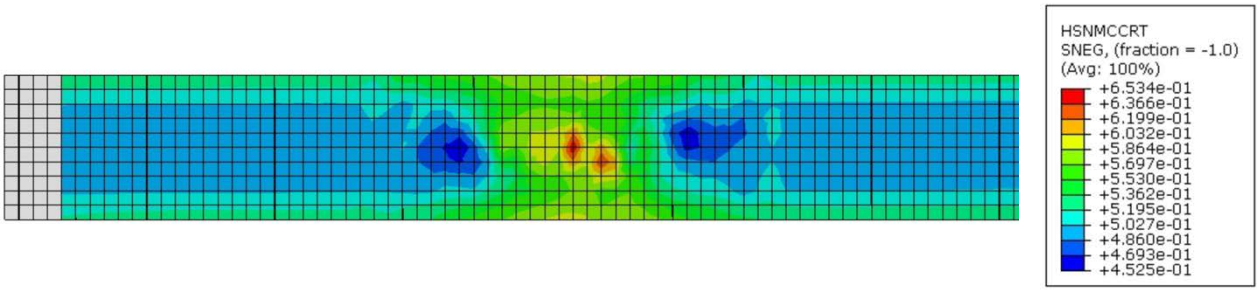

Figure 108 0G4.1: Hashin matrix compression in 45° ply, at failure

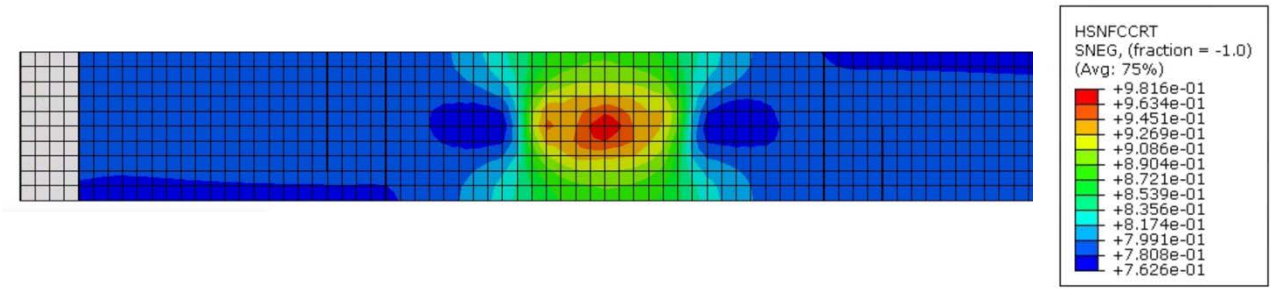

Figure 109 0G4.1: Hashin fibre compression in 0° ply without defects, at failure

Transverse shear is correctly propagated through the thickness of the laminate. 45° and 90° defect orientations are clearly visible even on 0° plies while this was not the case in the model in tension, see Figure 110. The 0° plies still carry most of the load. Defects in 90° and 45° plies have important effects on 0° plies. Large strains appear on the outer ply as shown in Figure 111 but the defect orientation does not emerge, as observed on DIC images.

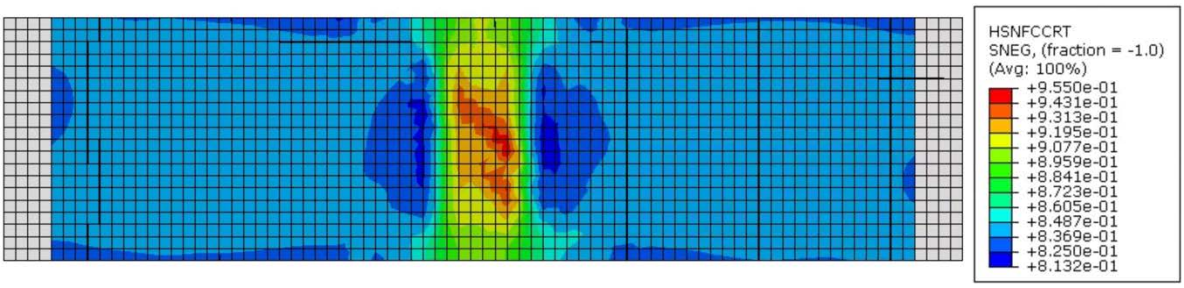

Figure 110 45G4.1: 0° ply Hashin fibre compression, at failure

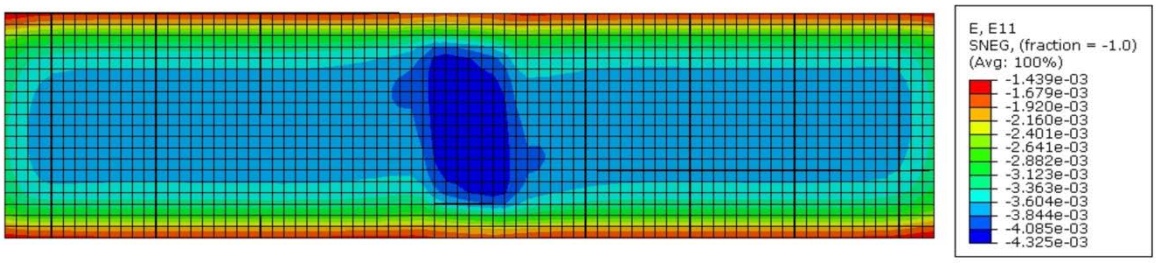

Figure 111 45G4.1: outer ply strain, at failure

As predicted by the laminate theory, 0° plies fail first in fibre compression. When defects are embedded at every orientation, 0° plies fail earlier directly followed by the laminate catastrophic failure. 0° plies attract more load than any other orientation. The role of 0° plies in the laminate is as crucial for the final strength in compression than it is in tension. In the compression model for 0° defects, predicted knockdown factors are not too far away from experimental results. The 0° plies are probably more affected by the asymmetry in the laminate structure introduced by the pattern of embedded defects: high stiffness overlaps and low stiffness gaps.

7.2.3. Discussion on compression modelling

From the experimental measurements, it is shown that compression is more critical than tension with knockdown factors reaching 25% compared to 10% respectively. While the model in tension did not indicate any effect of defects embedded in 45° and 90° plies, the compression model is closer to experimental behaviour but always unconservative. The 45° and 90° configurations both have similar trends, the same in tension and compression: strength decreases when number of defects increases. The size of defects does not seem to have much

effects on the maximum strength of 45° configurations. This observation is highlighted by the model too. More compression experiments are needed especially in 0° configuration to understand the effect of defects on the compressive mechanical behavior of composite laminates. The difference between the experimental results and the model is probably due to waviness, which creates more asymmetry in the laminate structure than the modeled high stiffness (overlaps) and low stiffness (gaps) regions. The 0° plies carry most of the load. They would probably break at lower strength with out-of-plane waviness included in the model. Thus, it looks like waviness is still critical in compression but to another level than it is for tension because the compression model can predict close knockdown factors with the current model assumptions and the post cure geometry of half gap / half overlap defects. It seems that laminates are more dependent on in-plane waviness in compression and more dependent to out-of-plane waviness in tension.

7.3. Fatigue Behaviour

7.3.1. Experiments

During the fatigue life of a specimen, damage accumulates due to the repetitive load application in tension and compression. For industrial applications, the knowledge of the mechanical performance of composite structures under fatigue loading is essential to design safe vehicles with a long life. The single application of any load would not produce any ill effects because the load magnitude is far below the quasi-static maximum stress. Since composite laminates are manufactured with intrinsic acceptable flaws, the laws of fatigue life probably differ from those defined for pristine defect free structures.

Fatigue tests were performed with the same MTS loading machine and the same fixtures that have been used for compression. ASTM D6484 [66] describes loading conditions that have been followed for cycles of tension and compression with stress ratio $R = -1$ which means the

magnitude of tension equals the magnitude of compression (otherwise known as “fully reversed loading”). The loading curve is a sine wave at a frequency of 5Hz. The frequency is an important parameter because if it is too high, the friction in the fixture and in the laminate can increase the temperature thus degrading the material properties too fast. A very low frequency is better to avoid unwanted dynamic effects and sudden energy release but tests would take too long to realize. In the literature, a frequency of 8Hz has been used [82]. The decision to use 5Hz was made because delamination appeared very fast at the beginning of the tests, in the first few cycles. A thermocouple in contact with the specimen kept track of the temperature. No specimens exceeded 32°C which is low compared to the glass transition temperature of the epoxy 3900-2 [72] thus no thermal effects of matrix degradation are expected.

One S-N curve per configuration is obtained. 9 specimens per configuration have been manufactured. One specimen is tested in compression quasi-static to give a failure load of reference per configuration. Considering the 8 other specimens per configuration, different load magnitudes are applied leading to different fatigue lives. All coupons, even pristine defect free specimens, experienced early delamination between the 9^{th} and the 10^{th} plies, exactly as observed in tension. This delamination begins at the middle of the specimens and grows toward the grips. Delamination growth stops because of the pressure of the grips on the specimens, preventing debonding of mode I – normal direction. Without the grips, it is expected that coupons had failed earlier.

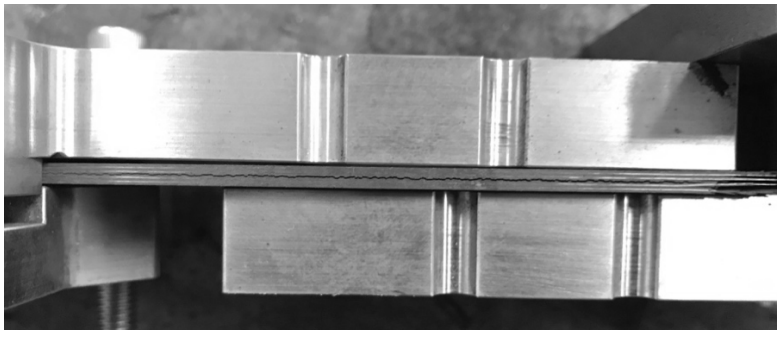

Figure 112 Side view of a coupon in the fixture: delamination in fatigue

All specimens failed in the window of the fixture ASTM D6484. The two fixtures of different sizes were used with shims. The fracture of all specimens occurred in compression and the failure mode looked like what can be observed on Figure 100.

In the following figures, stress has been normalized using the maximum compression stress measured in pristine defect-free configuration. Figure 113 shows all results for all configurations in fatigue, at different applied load levels. An S-N curve follows a linear law between the applied stress and the logarithm of number of cycles. Life between 1000 cycles and 1,000,000 cycles were targeted during testing

.

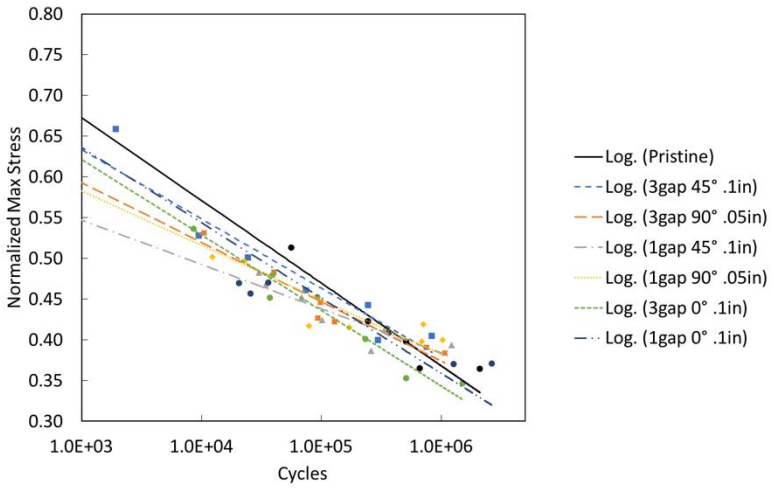

Figure 113 All configuration S-N curves

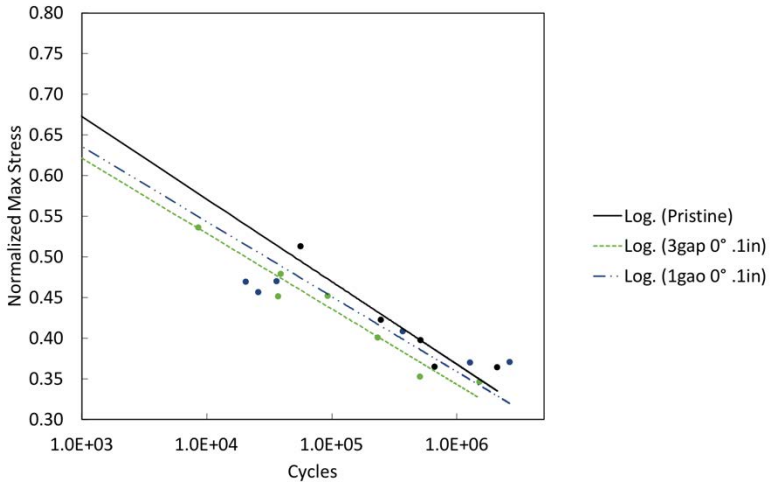

Figure 114 0° configuration S-N curves

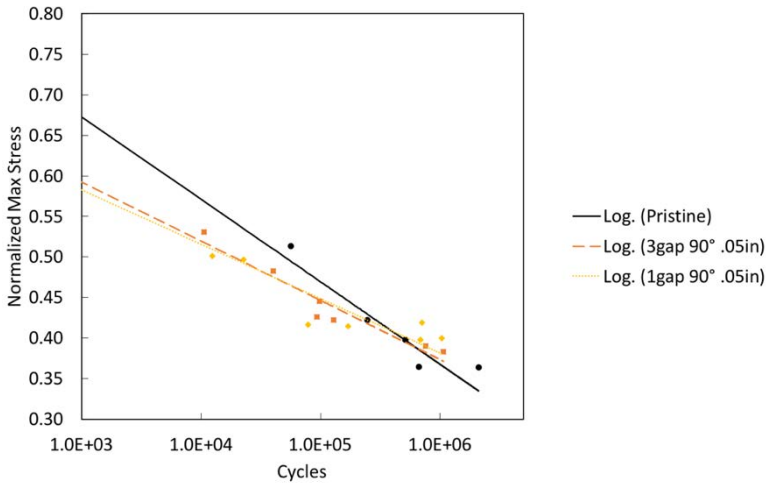

Figure 115 90° configuration S-N curves

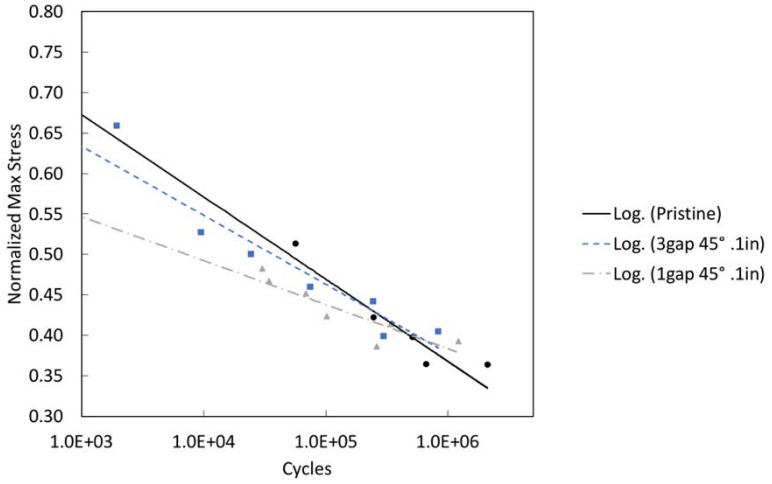

Figure 116 45° configuration S-N curves

Defects appear to have more effects on fatigue life at higher stresses. The 0.05in (1.27mm) wide defects are among the configurations with largest knockdown factors while other configurations with 0.1in (2.54mm) wide defects tend to better resist. There is a threshold of stress below which the effects of defects are close to the pristine defect-free configuration. All defected configurations tend to the pristine configuration at a stress about 60% of the maximum pristine compression stress at 1,000,000 cycles. Figure 114, Figure 115 and Figure 116 emphasize the effect of the number of defects in one orientation and one size. 0° and 90° oriented defects show the same trends for both 1-defect and 3-defects configurations while 45°

oriented defects configurations present the two extremes of all the fatigue results: 45G1.1 is extremely close to the pristine configuration even at high stresses while 45G3.1 presents the largest knockdown factors at high stresses.

7.3.2. Discussion on fatigue results

It was found that at low stress the ability of the material to create damage from embedded defects is reduced. The mechanical behavior is close to pristine defect-free specimens under a certain load threshold estimated at 40% of maximum compression quasi-static strength. This stress threshold corresponds to more than 1,000,000 cycles.

Since measurements were made using the head displacement of the MTS machine, no stiffness analysis was made since the slight slippage of the grip could alter the analysis. It is expected that non-linearity in the stress strain curve emerges because of both matrix cracking and delamination. Specimen collapse is due to fibre breakage according to fracture observations. Early delamination weakens the laminate. It was found that delamination occurred between two 90° plies. Thus, the choice of stacking sequence can have an impact on fatigue life of specimens. Out-of-plane waviness is expected to be as relevant in fatigue than in tension and compression.

8. Conclusion

8.1. Research Contribution

Automated Fibre Placement technology enables efficient manufacturing of large panels, increasing the yield and decreasing the material waste. However, this manufacturing process has its own induced defects. This research was interested in the effects under tension, compression and fatigue of side-to-side half gap / half overlap defects. The influence of several defect parameters was studied in detail. Specimens of different configurations varying size, pattern and orientation of embedded defects have been manufactured and tested. A model for tension and compression quasi-static loading has been developed and the simulation results have been compared to the experimental data.

It is suggested that both out-of-plane waviness and healing process of closing gaps between tows during curing (with caul plates) play a major role on the effect of defects. Healing due to the movement of both fibres and resin under compaction depends on the stacking sequence and on the plies in which defects are embedded. Increasing the defect width does not necessarily decreases the maximum strength.

Compression is more critical than tension and the largest strength knockdown factors reach 25% compared to 10% respectively. However, these results correspond to worst case scenario configurations that would likely not be acceptable in manufacturing flightworthy parts. In general, the tension average knockdown factor is about 5% and the compression average knockdown factor is close to 20% for all configurations. The 45° and 90° configurations behave similarly in both compression and tension: their strength decreases when the number of defects increases. Mixed defect orientations configurations are expected to have even worse performance but it would have to be confirmed with further tests.

0° oriented defects configurations are predicted by the developed model to have the largest knockdown factors in tension while those defects barely had any effects in experiments. Thus, the model in tension does not predict this configuration properly. Waviness is thought to play an important role in the mechanical behaviour of the defect and it is not considered in the model, thus explaining the difference. In compression, the model is closer to experimental results but always unconservative. The post-cure geometry of 0° oriented defects needs to be better represented because it seems the healing process during the cure cycle might be very efficient for 0° configurations.

In fatigue, configurations have been tested under tension-compression $R = -1$ cycles. Defected configurations have larger knockdown factors at high stresses but a threshold exists under which their performance is very close to the pristine defect-free configuration. The 45° configurations are very sensitive to the number of defects while it does not appear to have any effect on 90° configurations. It is suspected that the stacking sequence, therefore the position through-the-thickness of each ply orientation, might have an effect on the magnitude of waviness and healing of embedded defects.

The certification of composite structures manufactured with AFP requires an understanding of the failure mechanism of the laminates too. In tension and fatigue, delamination propagates along the defects toward the edges, leading to matrix cracking in 90° and 45° plies. Without the support of the grips during testing, it is expected that laminates had failed earlier. However, due to the presence of the grips to prevent further delamination, specimens were still able to carry load. The failure is due to fibre breakage in 0° plies which carry most of the load in both tension and compression.

8.2. Future Work

The outcome to AFP manufacturing techniques in the aircraft/rotorcraft industry can be tremendous if used at their full capacity. More work is however required to understand the effects of defects on the mechanical properties of the parts under complex loading and for various laminate configurations. Due to testing mistakes, 0° configurations data is missing for some defect configurations. In general, a new set of configurations should be designed to complete the test matrix presented in this thesis.

Different stacking sequences should be added in the test matrix to understand the generation of waviness and the healing process when defects are embedded in different orientations but at the same location through-the-thickness of the laminate.

Defects could be analyzed with CT-Scan to precisely measure out-of-plane waviness and fibre volume content to create better models which have to represent waviness in the future.

In tension experimental tests, an extensometer should always be used. In fatigue and compression, the evolution of stiffness during the specimen life should be analyzed with a DIC system.

References

1. Lukaszewicz, D.H.J.A., C. Ward, and K.D. Potter, *The engineering aspects of automated prepreg layup: History, present and future.* Composites Part B: Engineering, 2012. **43**(3): p. 997-1009.
2. Chen, J., et al. *Manufacturing of composite helicopter tailboom using afp process*. in *70th American Helicopter Society International Annual Forum 2014, May 20, 2014 - May 22, 2014*. 2014. Montreal, QC, Canada: American Helicopter Society.
3. Abdi, F., et al. *Certification modelling of composites fuselage, considering effect of defects from fiber placement manufacturing processes*. in *55th AIAA Aerospace Sciences Meeting, January 9, 2017 - January 13, 2017*. 2017. Grapevine, TX, United states: American Institute of Aeronautics and Astronautics Inc.
4. Rossi, D.D., *Effect of Half Gap/Overlap Defects on the Strength of Composite Structures Fabricated with Automated Fiber Placement Methods*, in *Mechanical Engineering*. 2018, McGill Univeristy: Montreal.
5. Juarez, P.D., K.E. Cramer, and J.P. Seebo. *Advances in in situ inspection of automated fiber placement systems*. in *Thermosense: Thermal Infrared Applications XXXVIII, April 18, 2016 - April 21, 2016*. 2016. Baltimore, MD, United states: SPIE.
6. Lan, M., *Etude de l'influence des singularités créées par la technique de placement de fibres automatisé sur les performances des matériaux composite*. 2016, Université Bretagne Loire.
7. Croft, K., et al., *Experimental study of the effect of automated fiber placement induced defects on performance of composite laminates.* Composites Part A: Applied Science and Manufacturing, 2011. **42**(5): p. 484-491.
8. Fayazbakhsh, K., et al. *The effect of gaps and overlaps on the in-plane stiffness and buckling load of variable stiffness laminates made by automated fiber placement*. in *15th European Conference on Composite Materials: Composites at Venice, ECCM 2012, June 24, 2012 - June 28, 2012*. 2012. Venice, Italy: European Conference on Composite Materials, ECCM.
9. Flight, B. https://www.bellflight.com. 2019.
10. Ashby, M.F. and D. Cebon. *Materials selection in mechanical design*. in *Proceedings of the 3rd European Conference on Advanced Materials and Processes. Part 1 (of 3), June 8, 1993 - June 10, 1993*. 1993. Paris, Fr: Publ by Editions de Physique.
11. Visweswaraiah, S.B., *Mechanical Characterization and Modelling of Hybrid Fibre Architectures of Randomly Oriented Strand Composites*, in *Mechanical Engineering*. 2018, McGill University: Montreal.
12. Belnoue, J.P.H., et al., *Understanding and predicting defect formation in automated fibre placement pre-preg laminates.* Composites Part A: Applied Science and Manufacturing, 2017. **102**: p. 196-206.
13. Li, X., S.R. Hallett, and M.R. Wisnom, *Modelling the effect of gaps and overlaps in automated fibre placement (AFP)-manufactured laminates.* Science and Engineering of Composite Materials, 2015. **22**(2): p. 115-129.
14. Grimshaw, M.N., C.G. Grant, and J.M.L. Diaz. *Advanced technology tape laying for affordable manufacturing of large composite structures*. in *46th International SAMPE Symposium and Exhibition -2001 a Materials and Processes Odyssey, May 6, 2001 - May 10, 2001*. 2001. Long Beach, CA, United states: Soc. for the Advancement of Material and Process Engineering.
15. Evans, D.O., *Fiber placement.* 1998. **Peters S.T. (eds) Handbook of Composites**.
16. Krolewski, S. and T. Gutowski. *Economic comparison of advanced composite fabrication technologies*. in *34th International SAMPE Symposium and Exhibition -*

Tomorrow's Materials: Today, May 8, 1989 - May 11, 1989. 1989. Reno, NV, USA: Publ by SAMPE.
17. Krolewski, S. and T. Gutowski, *EFFECT OF THE AUTOMATION OF ADVANCED COMPOSITE FABRICATION PROCESSES ON PART COST*. SAMPE Journal, 1987. **23**(3): p. 21-26.
18. Postier, R.A., *FACTORY AUTOMATION FOR COMPOSITE STRUCTURES MANUFACTURING*. S.A.M.P.E. quarterly, 1985. **16**(3): p. 45-49.
19. Oromiehie, E., et al., *Automated fibre placement based composite structures: Review on the defects, impacts and inspections techniques.* Composite Structures, 2019. **224**.
20. Kim, B.C., P.M. Weaver, and K. Potter, *Manufacturing characteristics of the continuous tow shearing method for manufacturing of variable angle tow composites.* Composites Part A: Applied Science and Manufacturing, 2014. **61**: p. 141-151.
21. Kim, B.C., P.M. Weaver, and K. Potter, *Computer aided modelling of variable angle tow composites manufactured by continuous tow shearing.* Composite Structures, 2015. **129**: p. 256-267.
22. Henneberg, A., P. Samann, and M. Sinapius. *Consolidated fiber placement - Cutting of consolidated fiber tapes*. in *SAMPE Long Beach 2016 Conference and Exhibition, May 23, 2016 - May 26, 2016*. 2016. Long Beach, CA, United states: Soc. for the Advancement of Material and Process Engineering.
23. Dodwell, T.J., R. Butler, and A.T. Rhead, *Optimum fiber steering of composite plates for buckling and manufacturability.* AIAA Journal, 2016. **54**(3): p. 1139-1142.
24. Akbarzadeh, A.H., M. Arian Nik, and D. Pasini, *The role of shear deformation in laminated plates with curvilinear fiber paths and embedded defects.* Composite Structures, 2014. **118**(1): p. 217-227.
25. *SA2GE Project*, in *Composite Fuselage Structures*. 2015, Bell Helicopter Textron Canada Limited.
26. Falco, O., et al., *Variable-stiffness composite panels: Defect tolerance under in-plane tensile loading.* Composites Part A: Applied Science and Manufacturing, 2014. **63**: p. 21-31.
27. Falco, O., et al., *Effect of tow-drop gaps on the damage resistance and tolerance of Variable-Stiffness Panels.* Composite Structures, 2014. **116**(1): p. 94-103.
28. Fayazbakhsh, K., et al. *A study of the influence of gaps and overlaps on the strength of composite panels made by automated fiber placement*. in *26th Annual Technical Conference of the American Society for Composites 2011 and the 2nd Joint US-Canada Conference on Composites, September 26, 2011 - September 28, 2011*. 2011. Montreal, QC, Canada: DEStech Publications Inc.
29. Fayazbakhsh, K., et al., *Defect layer method to capture effect of gaps and overlaps in variable stiffness laminates made by Automated Fiber Placement.* Composite Structures, 2013. **97**: p. 245-251.
30. Schmidt, C., et al. *Thermal Image-based Monitoring for the Automated Fiber Placement Process*. in *10th CIRP Conference on Intelligent Computation in Manufacturing Engineering - CIRP ICME 2016, July 20, 2016 - July 22, 2016*. 2017. Ischia, Italy: Elsevier B.V.
31. Yassin, K. and M. Hojjati, *Processing of thermoplastic matrix composites through automated fiber placement and tape laying methods: A review.* Journal of Thermoplastic Composite Materials, 2018. **31**(12): p. 1676-1725.
32. Woigk, W., et al., *Experimental investigation of the effect of defects in Automated Fibre Placement produced composite laminates.* Composite Structures, 2018. **201**: p. 1004-1017.

33. Li, X., S.R. Hallett, and M.R. Wisnom, *A finite element based statistical model for progressive tensile fibre failure in composite laminates.* Composites Part B: Engineering, 2013. **45**(1): p. 433-439.
34. Debout, P., H. Chanal, and E. Duc, *Tool path smoothing of a redundant machine: Application to Automated Fiber Placement.* CAD Computer Aided Design, 2011. **43**(2): p. 122-132.
35. Helenon, F., et al. *Modelling slit tape deposition during automated fibre placement*. in *19th International Conference on Composite Materials, ICCM 2013, July 28, 2013 - August 2, 2013*. 2013. Montreal, QC, Canada: International Committee on Composite Materials.
36. SAS, A. *Boeing 787 – lessons learnt*. 2008.
37. Sawicki, A.J. and P.J. Minguet. *Effect of intraply overlaps and gaps upon the compression strength of composite laminates*. in *Proceedings of the 1998 39th AIAA/ASME/ASCE/AHS/ASC Structures, Structural Dynamics, and Materials Conference and Exhibit and AIAA/ASME/AHS Adaptive Structures Forum. Part 1 (of 4), April 20, 1998 - April 23, 1998*. 1998. Long Beach, CA, USA: AIAA.
38. Turoski, L., *Effects of Manufacturing Defects on the Strength of Toughened Carbon/Epoxy Prepreg Composites*. 2000, Montana State University.
39. Hsiao, H.M. and I.M. Daniel, *Elastic properties of composites with fiber waviness.* Composites Part A: Applied Science and Manufacturing, 1996. **27**(10): p. 931-941.
40. Zhao, C., et al., *An Experimental Study of the Influence of in-Plane Fiber Waviness on Unidirectional Laminates Tensile Properties.* Applied Composite Materials, 2017. **24**(6): p. 1321-1337.
41. Mandell, J.F., D.D. Samborsky, and L. Wang. *Effects of fiber waviness on composites for wind turbine blades*. in *Advancing Materials in the Global Economy - Applications, Emerging Markets and Evolving Technologies, May 11, 2003 - May 15, 2003*. 2003. Long Beach, CA, United states: Soc. for the Advancement of Material and Process Engineering.
42. Lan, M., et al., *Microstructure and tensile properties of carbon-epoxy laminates produced by automated fibre placement: Influence of a caul plate on the effects of gap and overlap embedded defects.* Composites Part A: Applied Science and Manufacturing, 2015. **78**: p. 124-134.
43. Lan, M., et al., *Influence of embedded gap and overlap fiber placement defects on the microstructure and shear and compression properties of carbon-epoxy laminates.* Composites Part A: Applied Science and Manufacturing, 2016. **82**: p. 198-207.
44. Marouene, A., P. Legay, and R. Boukhili, *Experimental and numerical investigation on the open-hole compressive strength of AFP composites containing gaps and overlaps.* Journal of Composite Materials, 2017. **51**(26): p. 3631-3646.
45. Blom, A.W., et al., *A theoretical model to study the influence of tow-drop areas on the stiffness and strength of variable-stiffness laminates.* Journal of Composite Materials, 2009. **43**(5): p. 403-425.
46. Heinecke, F., W. Van Den Brink, and T. Wille. *Assessing the structural response of automated fibre placement composite structures with gaps and overlaps by means of numerical approaches*. in *20th International Conference on Composite Materials, ICCM 2015, July 19, 2015 - July 24, 2015*. 2015. Copenhagen, Denmark: International Committee on Composite Materials.
47. Marrouze, J.P., J. Housner, and F. Abdi. *The 19th international conference on composite materials effect of manufacturing defects and their uncertainties on strength and stability of stiffened panels*. in *19th International Conference on*

Composite Materials, ICCM 2013, July 28, 2013 - August 2, 2013. 2013. Montreal, QC, Canada: International Committee on Composite Materials.
48. Wisnom, M.R. and J.W. Atkinson, *Reduction in tensile and flexural strength of unidirectional glass fibre-epoxy with increasing specimen size.* Composite Structures, 1997. **38**(1-4): p. 405-411.
49. Wisnom, M.R., *Relationship between strength variability and size effect in unidirectional carbon fibre/epoxy.* Composites, 1991. **22**(1): p. 47-52.
50. Elsherbini, Y. and S.V. Hoa. *Fatigue behavior of unidirectional carbon/epoxy AFP laminates containing gaps*. in *31st Annual Technical Conference of the American Society for Composites, ASC 2016, September 19, 2016 - September 21, 2016*. 2016. Williamsburg, VA, United states: DEStech Publications Inc.
51. Elsherbini, Y.M. and S.V. Hoa, *Fatigue threshold-stress determination in AFP laminates containing gaps using IR thermography.* Composites Science and Technology, 2017. **146**: p. 49-58.
52. Talreja, R., *FATIGUE OF COMPOSITE MATERIALS: DAMAGE MECHANISMS AND FATIGUE-LIFE DIAGRAMS.* Proceedings of The Royal Society of London, Series A: Mathematical and Physical Sciences, 1981. **378**(1775): p. 461-475.
53. Kobayashi, S. and N. Takeda, *Experimental and analytical characterization of transverse cracking behavior in carbon/bismaleimide cross-ply laminates under mechanical fatigue loading.* Composites Part B: Engineering, 2002. **33**(6): p. 471-478.
54. Kawai, M., et al., *High-temperature off-axis fatigue behaviour of unidirectional carbon-fiber-reinforced composites with different resin matrices.* Composites Science and Technology, 2001. **61**(9): p. 1285-1302.
55. Jen, M.-H.R., et al., *Fatigue response of APC-2 composite laminates at elevated temperatures.* Composites Part B: Engineering, 2008. **39**(7-8): p. 1142-1146.
56. Mandell, J.F. and U. Meier. *EFFECTS OF STRESS RATIO, FREQUENCY, AND LOADING TIME ON THE TENSILE FATIGUE OF GLASS-REINFORCED EPOXY*. in *Long-Term Behavior of Composites, Symposium.* 1983. Williamsburg, VA, USA: ASTM.
57. Curtis, P.T. and B.B. Moore, *COMPARISON OF THE FATIGUE PERFORMANCE OF WOVEN AND NON-WOVEN CFRP LAMINATES IN REVERSED AXIAL LOADING.* International Journal of Fatigue, 1987. **9**(2): p. 67-78.
58. Colombo, C. and L. Vergani, *Influence of delamination on fatigue properties of a fibreglass composite.* Composite Structures, 2014. **107**(1): p. 325-333.
59. *ASTM D3039*, in *Standard Test Method for Tensile Properties of Polymer Matrix Composite Materials*. 2014, West Conshohocken, PA: American Society for Testing and Materials.
60. Elsherbini, Y.M. and S.V. Hoa, *Experimental and numerical investigation of the effect of gaps on fatigue behavior of unidirectional carbon/epoxy automated fiber placement laminates.* Journal of Composite Materials, 2017. **51**(6): p. 759-772.
61. Meneghetti, G., et al. *Fatigue limit evaluation of a stainless steel using thermal data analysis*. in *14th International Conference on Fracture, ICF 2017, June 18, 2017 - June 20, 2017*. 2017. Rhodes, Greece: International Conference on Fracture.
62. Risitano, A., et al., *Fatigue assessment by energy approach during tensile tests on AISI 304 steel.* Frattura ed Integrita Strutturale, 2017. **11**(39): p. 202-215.
63. Risitano, A. and G. Risitano, *Determining fatigue limits with thermal analysis of static traction tests.* Fatigue and Fracture of Engineering Materials and Structures, 2013. **36**(7): p. 631-639.

64. *ASTM D3518*, in *Standard Test Method for In-Plane Shear Response of Polymer Matrix Composite Materials by Tensile Test of a ±45° Laminate*. 2013, West Conshohocken, PA: American Society for Testing and Materials.
65. Zhao, C., B. Wang, and J. Xiao, *Macroscopic characterization of fiber micro-buckling and its influence on composites tensile performance.* Journal of Reinforced Plastics and Composites, 2017. **36**(3): p. 196-205.
66. *ASTM D6484*, in *Standard Test Method for Open-Hole Compressive Strength of Polymer Matrix Composite Laminates*. 2014, American Society for Testing and Materials: West Conshohocken, PA.
67. Wisnom, M.R., *Size effects in the testing of fibre-composite materials.* Composites Science and Technology, 1999. **59**(13): p. 1937-1957.
68. Lessard, L.B., A.S. Schmidt, and M.M. Shokrieh, *Three-dimensional stress analysis of free-edge effects in a simple composite cross-ply laminate.* International Journal of Solids and Structures, 1996. **33**(15): p. 2243-2259.
69. Becker, W., *Closed-form solution for the free-edge effect in cross-ply laminates.* Composite Structures, 1993. **26**(1-2): p. 39-45.
70. Kassapoglou, C. and P.A. Lagace, *CLOSED FORM SOLUTIONS FOR THE INTERLAMINAR STRESS FIELD IN ANGLE-PLY AND CROSS-PLY LAMINATES.* Journal of Composite Materials, 1987. **21**(4): p. 292-308.
71. Pipes, R.B. and N.J. Pagano, *Interlaminar Stresses in Composite Laminates Under Uniform Axial Extension.* Journal of Composite Materials, 1970. **4**(4): p. 538-548.
72. Toray. *Resin system 3900-2*. 2019.
73. Ibrahim, M.E., *Nondestructive evaluation of thick-section composites and sandwich structures: A review.* Composites Part A: Applied Science and Manufacturing, 2014. **64**: p. 36-48.
74. Montanini, R. and F. Freni, *Non-destructive evaluation of thick glass fiber-reinforced composites by means of optically excited lock-in thermography.* Composites Part A: Applied Science and Manufacturing, 2012. **43**(11): p. 2075-2082.
75. Pan, Y.P., et al. *Detection of defects in commercial C/C composites using infrared thermography*. in *SEM Annual Conference and Exposition on Experimental and Applied Mechanics 2009, June 1, 2009 - June 4, 2009*. 2009. Albuquerque, NM, United states: Society for Experimental Mechanics Inc.
76. Yurgartis, S.W., *Techniques for the quantification of composite mesostructure.* Composites Science and Technology, 1995. **53**(2): p. 145-154.
77. Blanc, R., et al., *Fiber orientation measurements in composite materials.* Composites Part A: Applied Science and Manufacturing, 2006. **37**(2): p. 197-206.
78. Krumenacker, N., *Experimental study of variability and defects in vacuum-bag-only corner laminates*, in *Mechanical Engineering*. 2018, McGill University: Montréal.
79. *Polymer matrix composite guidelines for characterization of structural materials*. MIL-HDBK-17-1F ed. Vol. 1. 2002, Washington, DC, USA: US Department of Defense.
80. Documentation, A.O., *Cohesive Elements Traction Separation Definition* https://www.sharcnet.ca/Software/Abaqus610/Documentation/docs/v6.10/books/usb/default.htm?startat=pt06ch29s05abo27.html.
81. Solutions, C. *VIC-3D 8 System* https://www.correlatedsolutions.com/vic-3d/.
82. Elsherbini, Y., *Fatigue behavior of carbon/epoxy AFP laminates containing gaps*, in *Mechanical Engineering*. 2017, Concordia University: Montreal.